Integrated Fieldwork 2021

WP 1: (Final Report)
Three-Dimensional Reference Frame via GNSS Observations

Supervisor

Ron Schlesinger

Team Member

Jiaxin Liu

Lingke Wang

Bingwang Chen

Miao Peng

Epiphanie Imanimfashe

Contents

1. Introduction

The aims of WP1 are to establish the fundamental network in the integrated field work area and determine new surveying points at the Hysolar building. PF 4, PF 7 and PF 10 are known points, the final coordinates of the static network points FP 1,2,7,9 and UTM coordinates with heights in DHHN2016 needs to be measured and calculated. The network adjustment provides 3D-coordinates up to mm-accuracy in the global system.

2. Problems or mistakes made by the students

- Some groups did not start measuring at the same time, although complete synchronization is not strictly required. However too much difference will reduce the available data because we need the data that are measured at the same time.
- Due to lack of experience, some teams spent too much time to transfer or install and set up the instrument, so that the measurement time is less than one hour, such as only 40 minutes.
- Wrong setting: antenna type (AS10/GS15) and equipment (tripod/pillar)
- Wrong point name: for example, write PF7 as FP7

3. Results

Coordinates of new network points in ETRS89_UTM32

Point No.	$\boldsymbol{X}$ $[\boldsymbol{m}]$	$\boldsymbol{Y}$ $[\boldsymbol{m}]$	$\boldsymbol{Latitude}$ [° ′ ″]	$\boldsymbol{Longtitude}$ [° ′ ″]	$\boldsymbol{H_{Ellp.}}$ $[\boldsymbol{m}]$
$FP1$	32507140.303	5398883.586	48° 44′ 34.54370"	9° 05′ 49.64258"	506.306
$FP2$	32506980.664	5398922.892	48° 44′ 35.82316"	9° 05′ 41.82783"	501.123
$FP7$	32507095.352	5398980.042	48° 44′ 37.66934"	9° 05′ 47.44739"	502.693
$FP9$	32506964.520	5398761.215	48° 44′ 30.58781"	9° 05′ 41.02748"	503.700

Tab. 1: Results of all measurements after adjustment with fixed control points PF4,7&10

Accuracy of new points

Point No.	$\boldsymbol{Latitude}$ $\boldsymbol{Sd}$ $[\boldsymbol{m}]$	$\boldsymbol{Longitude}$ $\boldsymbol{Sd}$ $[\boldsymbol{m}]$	$\boldsymbol{Height}$ $\boldsymbol{Sd}$ $[\boldsymbol{m}]$	$\boldsymbol{Position\ 3D}$ $\boldsymbol{Sd}$ $[\boldsymbol{m}]$
$FP1$	0.0053	0.0050	0.0073	0,0072
$FP2$	0.0052	0.0049	0.0073	0,0072
$FP7$	0.0054	0.0050	0.0077	0,0074
$FP9$	0.0057	0.0053	0.0078	0,0078

Tab. 2: Results of all accuracy after adjustment with fixed control points PF4,7&10

According to the accuracy above, we can find that the accuracy of the new points is about 8mm compared to the Reference points.

To get the geoid Undulation of each point we could use the online transformation tool of *Bundesamt für Kartographie und Geodäsie (BKG)*:

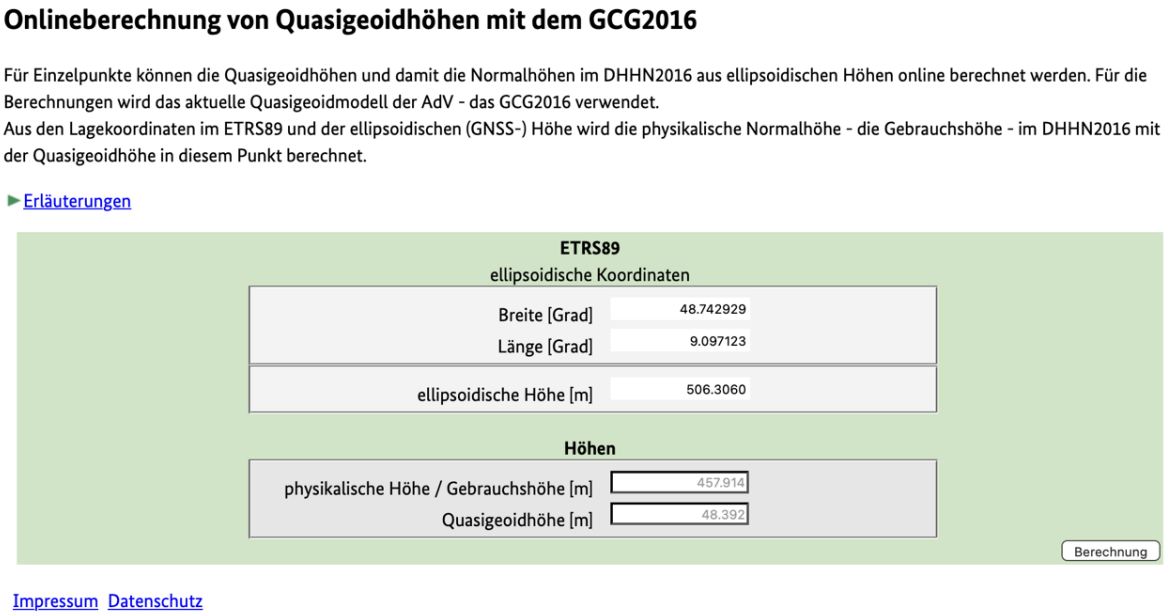

Figure 1: source : http://gibs.bkg.bund.de/geoid/gscomp.php?p=g

Ellipsoidal heights (ETRS89) transformed into DHHN2016 - system

$$H_{DHHN2016} = h_{ETRS} - \zeta_{GCG2016}$$

Point Nr.	DHHN2016 [m]	Quasigeoidheight [m]
$FP1$	457.914	48.392
$FP2$	452.728	48.395
$FP7$	454.301	48.392
$FP9$	455.304	48.396
$PF4$	425.751	48.407
$PF7$	426.063	48.403
$PF10$	441.375	48.389

Tab. 3: Results of all points in ellipsoidal heights (ETRS89) transformed into DHHN2016-system

Compare with results in WP3

Point Nr.	$\boldsymbol{H_{Niv}}$ $[\boldsymbol{m}]$	$\boldsymbol{H_{DHHN}}$ $[\boldsymbol{m}]$	$\boldsymbol{\Delta H}$ $[\boldsymbol{m}]$
$FP1$	457.9800	457.914	0.0660
$FP2$	452.7891	452.728	0.0611
$FP7$	454.3704	454.301	0.0694

Tab. 4: Comparison with results in WP3 Levelling Measurement

Compare the elevation we got with the elevation measured in WP3, we can find that the error is between 6.1-6.9cm.

Since the German Combined QuasiGeoid 2016 (GCG2016) should be better than 1cm in plain areas and 2cm in high-mountain areas (see: https://www.bkg.bund.de/DE/Ueber-das-BKG/Geodaesie/Integrierter-Raumbezug/Hoehenbezugsflaeche/hoehenbezug.html), this error (offset) rather refer to input coordinates with accuracy not better than 6cm.

4. Adjustment and analyze

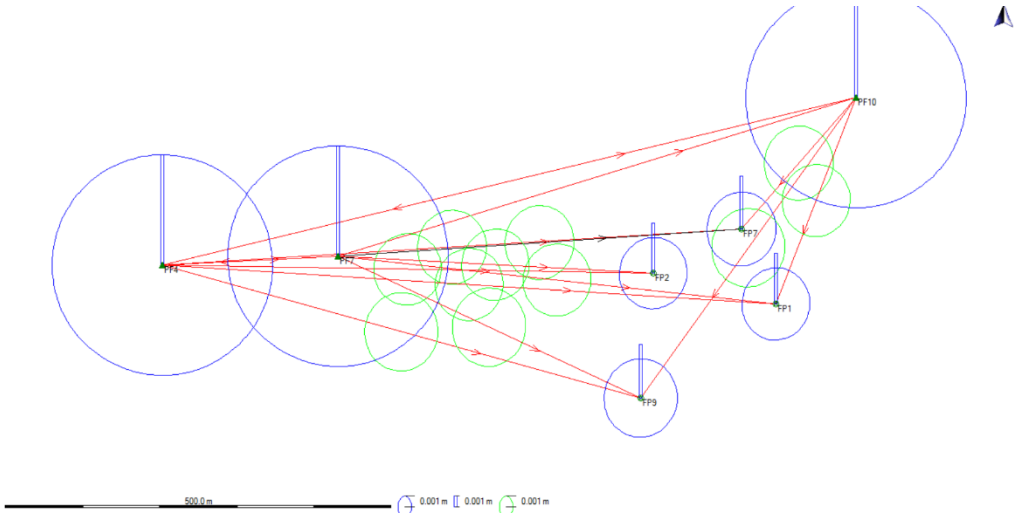

Figure 2: Error Ellipse (Known points as reference)

The above figure shows the error ellipse of these new network points, but only the known points are set as reference. The height accuracy in GNSS measurements is always about 1.5 times as good as the positional accuracy, that could result from the geometry of the satellite constellation. Besides, because of high building or tree, the accuracy in z-axis is also affected, although it is not the only reason for the bad accuracy.

Since the given coordinate list 'Coordinates of the pillars_ETRS89.txt' did not contain any accuracy information, we simply set the accuracy of the 'Control'point to 0.01m.

Since the data we measured this time are relatively good, we did not discard any data, so we have a relatively good internal accuracy. (Observations: 117, Unknowns: 21, Degree of freedom: 96).

Stations	
Number of (partly) known stations:	3
Number of unknown stations:	4
Total:	7
Observations	
GPS coordinate differences:	108 (36 baselines)
Known coordinates:	9
Total:	117
Unknowns	
Coordinates:	21
Total:	21
Degrees of freedom:	96

However, for better/consistent network between new points, new points should also be set as reference, because the adjustment would be done on baselines which are 'directly' observed between new points.

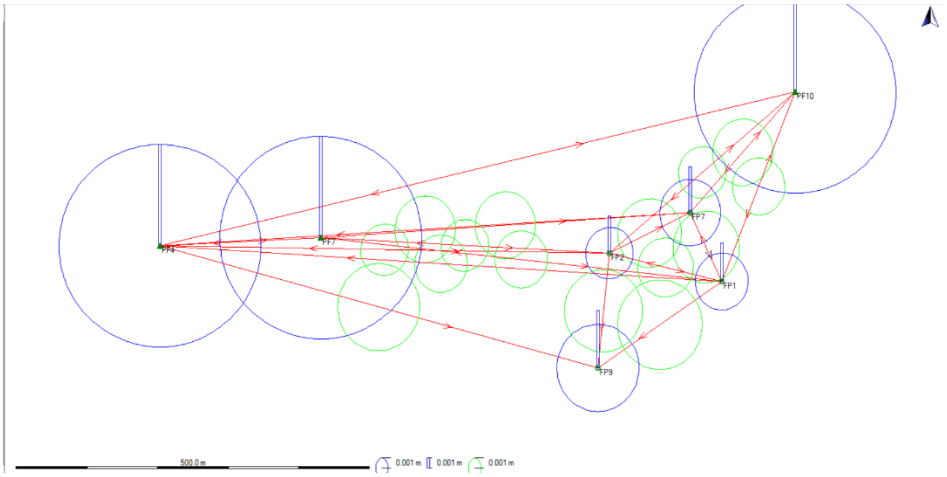

Figure 3: Error Ellipse (new points also as reference)

We can now find that there are baselines between the new points in the figure, when the new point is also set as reference.

Compared with the first case, there are just submillimeter changes in the coordinates after the adjustment.

Integrated Fieldwork 2021

WP 2: Creation of a 3D Network by Total Station

Supervisor

Gabriel Kerekes

Team Member

Zhan Li

Dennis Müller

Roland Ullmann

Sven Wagner

University of Stuttgart
Germany

Contents

1. Introduction

High redundant 3D geodetic network frame is essential for the Integrated Fieldwork, which is one of the main goals of the second working package. We are using the robotic total station (Leica TS30) to establish the network, which is suited for tasks that imply repetitive measurements. For integrating the network in an absolute coordinate system, UTM-coordinates are also needed. These are provided to all other groups later. In order to achieve these goals, the following steps are required:

1. Marking network points
   Network points are marked with metal bolts in accessible and stable areas to make sure that the locations of the network points are stable and the free line-of-sight can be realized.
2. Measuring the network
   Method based on free stationing is need. The position of the total station could be chosen freely. Each new point must be measured at least from two station points with three sets. Also, two Adjacent stations should have at least two identical measurement points.
3. Processing the data
   First, all the information for the local network adjustment is gathered. And we use the data before to solve the datum problem. All coordinates are transformed to global network frame.
4. Network adjustment (JAG3D) and transformation in UTM.
   The network adjustment under the requirement of the network quality will be implied. The network will be conducted in three versions: First, freely eliminate the problem of the original measurement. Then add constraints to see how the network fits the given data. Finally, fix it when fixing certain points in the adjustment.

2. Input/Output

As a secondary objective, detailed points will be measured and coordinates will be delivered to WP5, WP6 and WP8. We process the GNSS-Coordinates from WP1 for FP1, FP2, FP7 and FP9, as well as precise heights from WP3 for FP1, FP2 and FP7. Finally, UTM-Coordinates of all Fixpoints will be provided to WP5 and UTM-Coordinates of grid points for WP7 and WP8.

3. Measurement Teams

During the fieldwork, nine teams measured new points around the Hysolar Building, the student accommodations and around the climbing tower at the university campus in Vaihingen.

Total Station measurements:

Seven teams measured different sections of fix points.

Team	Station Points	Sets	Observations	Fix Points
A	4	4	104	FP1, FP2, FP6, FP7, FP8
B	5	4	120	FP2, FP3, FP4, FP5, FP6, FP7
C	5	3-4	161	FP1, FP6, FP7, FP8, FP9, FP10, FP11
D	3	4	112	FP1, FP2, FP6, FP7, FP8, FP11
E	6	4	136	FP2, FP3, FP4, FP5, FP6, FP11
G	5	4	126	FP3, FP3, FP4, FP5, FP6
I	5	4	144	FP2, FP6, FP8, FP9, FP10, FP11

Table 1: Statistics of the measurement teams

Figure 1: Overview of the Fix Points

Polar measurements:

Team F measured grid points for WP8 (Profile Measurements by Gravimetry) around the climbing Tower near the sports field.

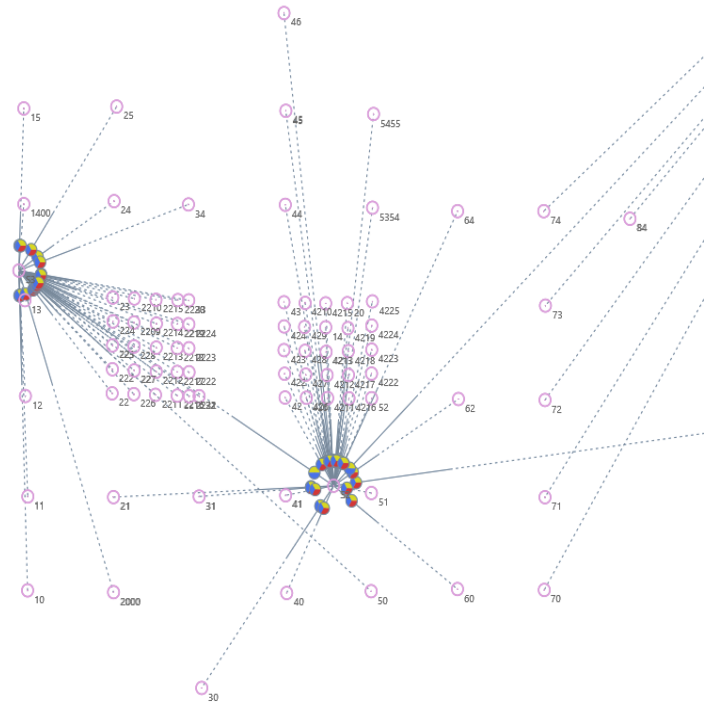

Figure 2: Adjusted Network around the climbing tower

Team H measured grid points for WP7 (GNSS Availability Check) near the Hysolar-Building

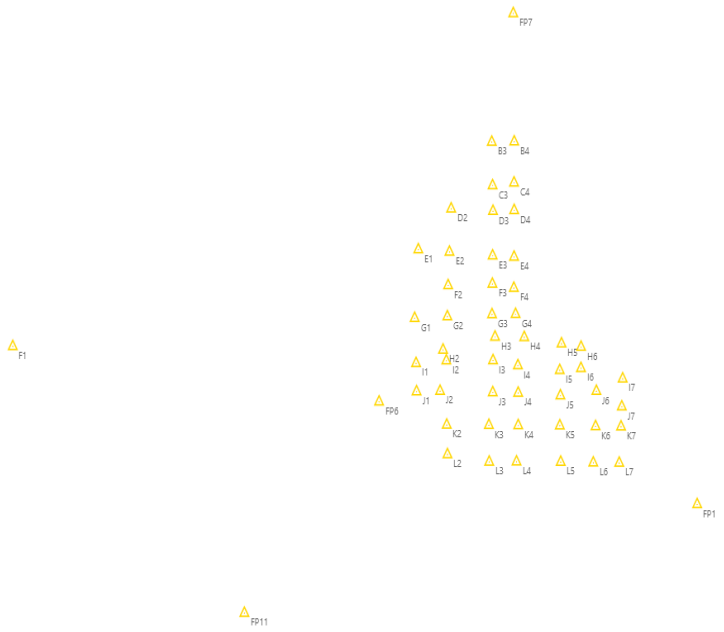

Figure 3: Adjusted Network around the Hysolar-Building

4. Network adjustment

For adjusting the network, transforming and projecting it onto a UTM coordinate system, we used the OS-Software “JAG3D”. In order to read the raw input data, formatting was done before. It took multiple steps to reach the desired result.

First of all, we had to process the data. Since we receive several data sets that contain only a section of the network, we decided to adjust all of them individually, before merging them all together into the finished network.

The first step in adjusting the data, was to create a text file with comma-separated values (CSV) out of the received report files from the total station. This had to be done for each group. While doing this, we had to separate the multiple station points and organize the different values and measurements in such a fashion, that we could easily import these into the software. Once the values are imported and organized within JAG3D, we have to determine approximate values for the coordinates in the local network. Then we start the local adjustment of the small network segments, that each group has surveyed. The final step for this part is to reduce the set measurements based on single observations. This allows us to group and average similar observations, which have the same unmoved position, instrument height and reflector height. Before doing this, we examine the data and exclude outliers. Afterwards we readjust the network.

After all of this is done, we have finished adjusting local networks for all the individual groups. The next step is to take the adjusted data and merge it into a complete network covering the area of interest. Now one last adjustment will take place and the result is an adjusted local network, where all the individual measurements from all groups are together in one place.

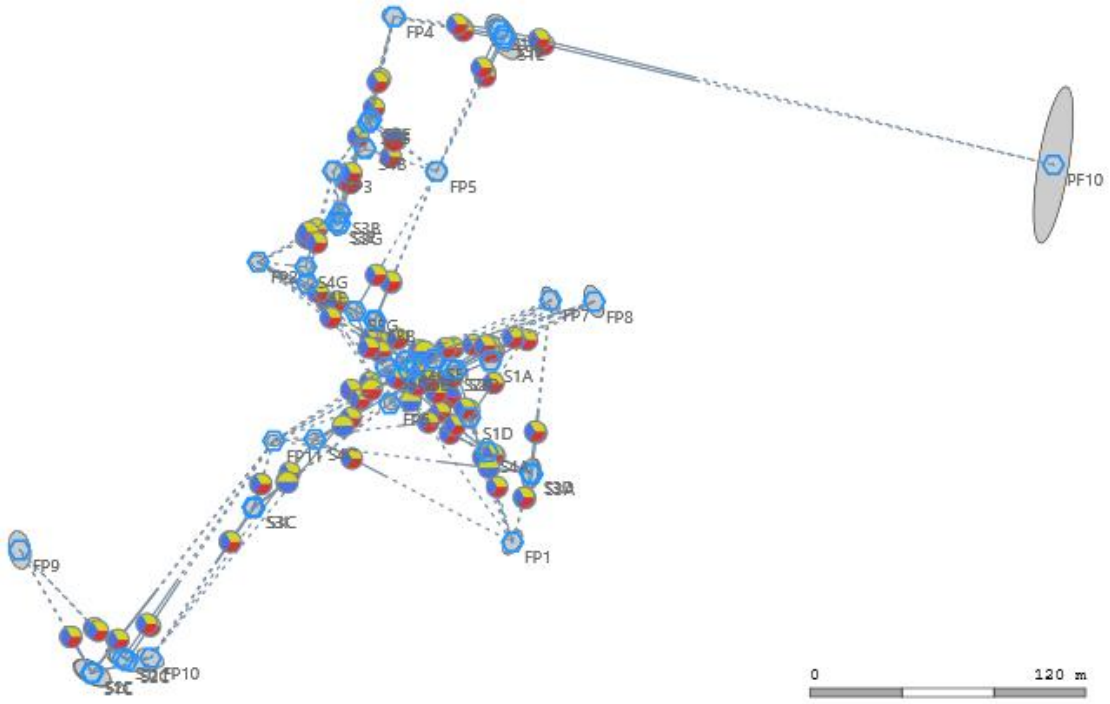

Figure 4: Adjusted local network

When looking at *Figure 1*, you can see that the shape of the network and the results, considering the proportions of the confidence ellipses compared to each other, are as expected. For example, the confidence ellipse for the point "PF10" is larger in the width than length. This is to be expected, given the network geometry and number of observations towards that point.

[mm]	FP **1**	FP **2**	FP **3**	FP **4**	FP **5**	FP **6**	FP **7**	FP **8**	FP **9**	FP **10**	FP **11**
σ_y	2.5	1.9	1.9	3.0	2.7	1.5	2.2	2.5	2.8	3.3	1.7
σ_x	3.0	1.7	2.1	2.2	2.2	1.6	3.4	4.0	4.7	2.4	1.4
σ_z	0.9	0.7	0.8	1.0	0.9	0.5	0.9	1.2	1.8	1.4	0.9

Table 2: Standard deviations for the adjusted local network

When looking at *Table 1*, we see that the standard deviations range from 0.5 mm up to 4.7 mm, but standard deviations of less than 1mm for heights are lower than expected, since this is a network in local cartesian coordinates without height data.

The next goal was to obtain UTM coordinates for all fixed points from the network adjustment. This required UTM coordinates and elevations for certain fixed points from other work packages. WP 1 provided us the coordinates for the fixed points FP 1,2,7 and 9. Precise heights

for FP 1,2 and 7 were delivered by WP 3. Following the acquisition of these values, we entered them for the fixpoints and started adjusting. The result is the following 3D-Network projected onto a UTM coordinate system:

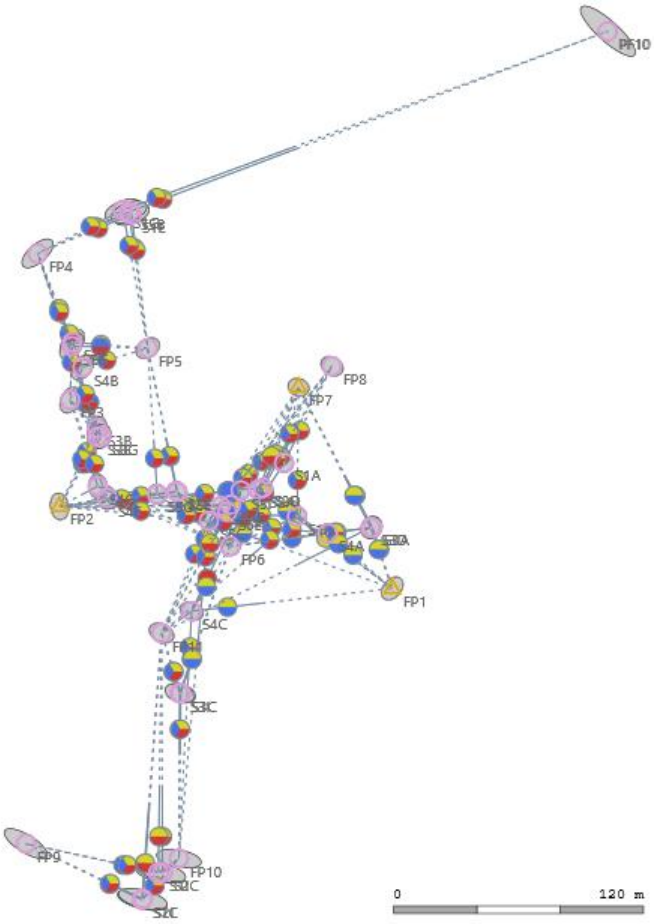

Figure 5: Adjusted global network

When inspecting *Figure 2*, we can immediately see that the network has been rotated and resembles the on-site orientation with regard to the north direction. The shape of the ellipses and their proportions towards each other haven't changed much.

[mm]	FP **1**	FP **2**	FP **3**	FP **4**	FP **5**	FP **6**	FP **7**	FP **8**	FP **9**	FP **10**	FP **11**
σ_y	15.1	12.9	14.3	21.9	16.5	13.7	14.6	15.5	30.3	31.3	17.1
σ_x	16.1	18.7	18.1	20.1	14.4	12.1	12.5	13.6	21.0	13.3	13.8
σ_z	2.1	1.5	1.6	1.7	1.7	1.5	1.5	1.7	2.1	1.9	1.7

Table 3: Standard deviations for the adjusted global network

When taking a look at *Table 2* we see that the standard deviations in the direction of the x- and y-Axis are now in the range of 1.2 to about 3.1 cm. This means that in some cases the deviations have increased almost tenfold. An accuracy of almost the same magnitude is present, when comparing the standard deviations of both networks.

The global network was then used for transforming the coordinates of the measured points by WP 7 and 8. It was also used for the correct positioning of the poles with the checkerboards for WP 5, so they can calculate the position of the stational laser scanner.

Figure 3 shows the adjusted network and the positions of the rover during the GNSS-availability measurements, Figure 2 for the gravimeter measurements. The idea for these measurements was to find out the UTM-coordinates as well as their position relative to each other.

5. Summary

In summary, it can be said that the measurements ran smoothly, the teams collected and provided the required data, but also some difficulties with the measurements occurred. One was the ATR of the Leica TS30, which has difficulties differentiating targets that are in nearly the same line of sight. This leads to rough errors which means that the measurement must be eliminated in order to assure the whole network quality. Furthermore, because the members of the workpackage 2 were not present during all the measurements the evaluation of the data was not always transparent. A sketch for each measurement would be a nice addition to help avoiding such ambiguities. After processing the data form the measurements the adjustment begins. The Software used for this step is the OS -Software JAG3D. For each measurement team a local adjustment is set up to eliminate unsuitable data from the project before merging it into one, because a rough error (e.g., measuring the wrong target) can significantly worsen the entire network. For the adjustment process the stochastic model (instrument accuracies) needs to be known and iteratively verified in the adjustment. After the stochastic model fits the adjustment the local coordinates can be transformed into UTM. After the adjustment and transformation, the 3D Network by Total Station is successfully created, and UTM-Coordinates can be delivered to other workpackages.

6. Conclusion

In conclusion to this fieldwork, it can be said that the communication between the WPs worked well and the objectives of this workpackage which were to create a 3D-Network by Total Station and to deliver UTM-Coordinates to WP5, WP7 and WP8 were achieved. An alternative way would have possibly been a hybrid adjustment where the WPs 1,2 and 3 would have worked closer together and provided a Network with GNSS measurements and precise heights together - that maybe would have increased the precision of the whole Network.

This Workpackage has delivered a 3D-Network by Total Station (Leica TS30) with 11 Fixpoints and 33 Stationpoints. These points are around the Hysolar building, the sport field and the student's accommodations in Vaihingen with local- and UTM-Coordinates for every point. Accuracies of the network points range from 12.9mm to 31.3mm in y, 12.1mm to 21.0mm in x and 1.5mm to 2.1mm in z. Furthermore UTM-Coordinates for 2 separate Polar measurements were delivered, around the climbing tower near the sport field for WP8 and around the Hysolar building for WP 7.

7. Work distribution:

Brief Description:

Introduction……...– Zhan Li

Measurement during fieldwork …….– Roland Ullmann

– Sven Wagner

Equipment List……. – Dennis Müller

Data-processing:

Data preparation……... – Roland Ullmann

Network adjustment (JAG3D).…….– Zhan Li

– Roland Ullmann

– Dennis Müller

– Sven Wagner

WP-Communication……. – Sven Wagner

Scientific report:

Introduction, Input/Output……– Zhan Li

Measurement Teams……. – Dennis Müller

Network adjustment……. – Roland Ullmann

Summary, Conclusion, Work distribution… – Sven Wagner

Integrated Fieldwork 2021

WP 3: Precision Leveling

Supervisor

Dr.-Ing. Martin Metzner

Team Member

Yu-Hao Chiang

Ni Li

Felix Mayerle

Jingyi Bao

Richard Ertmann

University of Stuttgart
Germany

Contents

1. Introduction

Leveling is the process of determining the relative height of each point on the surface of the earth, and calculating the absolute height of other points through the absolute height of the benchmarks and the relative height of other points relative to the benchmarks.

The main goal of WP3 is to get the absolute height information in" Deutsches Haupthöhennetz 2012" (DHHN 12) for points by the precise leveling and finally delivering the height information for WP1 and WP2. The following tasks need to be done, firstly, determine from WP1 and WP2, where elevation points are needed and with which quality; secondly, measurement planning for the leveling sessions loops and establishment of intermediate leveling points if necessary; thirdly, measurement realization, results analysis, and loop adjustment; finally, delivery of height information to WP1 and WP2.

2. Progress

For the precise levelling, 7 fixed points are measured. The Figure1 below shows the measurement area, the selected measurement points, and the measurement route.

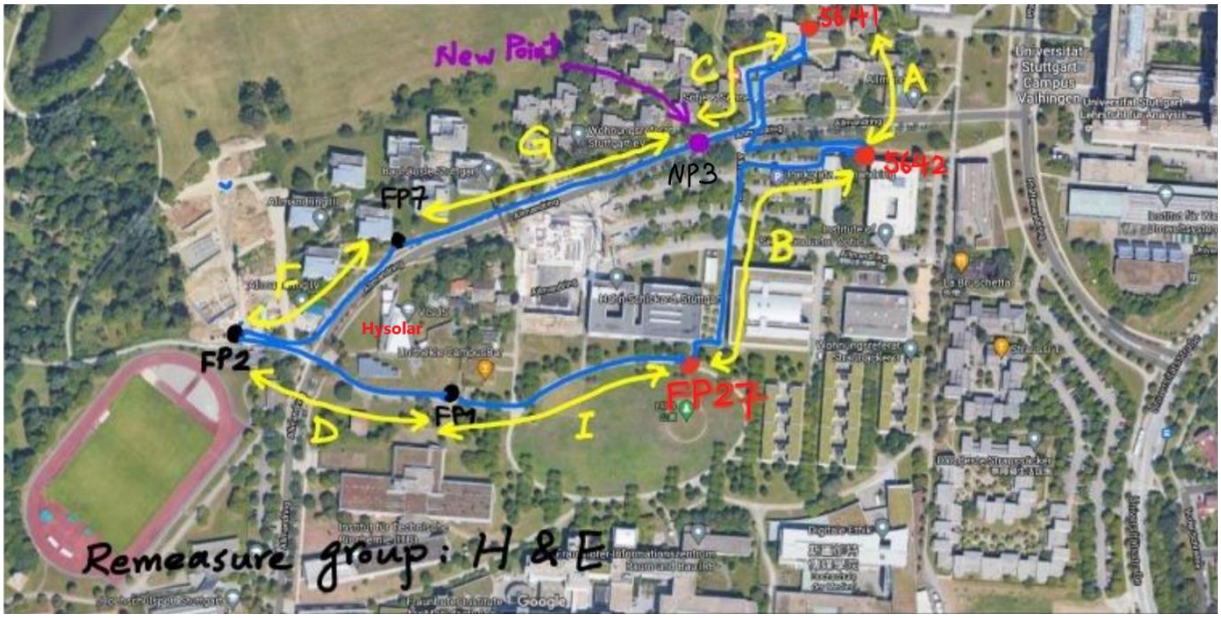

Figure 1 Measurement area, measurement points and the measurement routes

As shown in Figure 1, the measurement area is around the Hysolar Building and datum points 5641, 5642 located at the Vaihingen Campus of the University of Stuttgart. Points 5641, 5642, FP27, FP1, FP2, FP7, NP3 are the 7 fixed points need to measure. Among them, 5641, 5642 are

given benchmarks, and FP1, FP2, FP7 are the same measurement points as WP1 and WP2, NP3 is the intermediate leveling points established by WP3.

This field work has a total of 9 measurement groups, comprehensively considering the measuring area, the reliability of the results, and the number of measurement groups, we have set up 7 measurement sections. Each of 7 of the measurement groups is responsible for measuring a section, and the remaining two groups are responsible for remeasuring sections with unsatisfactory results.

Each measurement group needs to perform round-trip measurements on the measurement section. During the measurement process, we chose the BFFB (backward-forward-forward-backward) measurement mode and set the accuracy regarding back- and foresight $(B1-F1)-(B2-F2) < 0.07mm$ since our group realized that the accuracy 0.1mm was too low during the initial test phase. In the testing phase before the start of the measurement, our group found that a standard deviation of σ <1mm/km is difficult to achieve, so the standard deviation was set as σ <1.5mm/km.

Table 1 is the route for each group, this table shows the measurement process. Each group has carried out measurement on each road section. In the measurement process, whether the data is qualified or not is verified according to whether the closing error exceeds the limit (the standard deviation σ is 1.5mm/km). The closure error of group D is over the limits, also group G has very bad results due to heavy rain, so these two sets of data are discarded and remeasured by another two groups. It can be seen in Table1 that the remeasured results are pretty good.

Table 1 The route for each group

Team	Route	Distance[m]	Closing error[mm]	Closing error limits[mm]
A	5641 - 5642 - 5641	477.60	0.19	0.72
B	5642 - FP27 - 5642	521.26	0.47	0.78
I	FP27 - FP1 - FP27	390.25	0.43	0.59
D	FP1 - FP2 - FP1	337.02	0.74	0.51
F	FP2 - FP7- FP2	291.8	0.03	0.44
G	FP7 - NP3 - FP7	Data too bad for heavy rain		
C	NP3 - 5641 - NP3	200.56	0.16	0.30
H	Remeasure FP1 - FP2 - FP1	338.17	0.06	0.51
E	Remeasure FP7 - NP3 - FP7	506.46	0.05	0.76

3. Results and analysis of the measurements

3.1. Measurements' results check

After the measurement, all the data are analyzed, and it's been found that the result of route 5641-5642-5641 had a big problem. 5641 was used as the height starting point in this route to calculate the height of 5642, and the calculated result is very different from the real value given by 5642, which is beyond the difference limits 0.00036m a lot, which can be seen in Table 2, the data for this route was discarded. Since all the routes carried out round-trip measurements for each measurement section, the remaining data can still be adjusted.

Table 2 Benchmark 5642's calculated height in route 5641-5642-5641

Calculated height[m]	Given height[m]	Distance between 5641-5642[m]	Height difference[m]	Height difference limits[m]
455,353	454,672	239.10	0.681	0.00036

After measurements' results check, the routes available for adjustment were sorted out. The number of stations, distance, closing error in each available route are shown in Table 3. In order to analysis, the data of team D is also added in Table 3.

Table 3 Number of stations, distance, closing error in each route

Team	Route	Number of stations	Distance[m]	closing error[mm]
B	5642 - FP27 - 5642	20	521.26	0.47
I	FP27 - FP1 - FP27	12	390.25	0.43
H	FP1 - FP2 - FP1	12	338.17	0.06
D	FP1 - FP2 - FP1	8	337.02	0.74
F	FP2 - FP7- FP2	12	291.80	0.03
E	FP7 - NP3 - FP7	16	506.46	0.05
C	NP3 - 5641 - NP3	12	200.56	0.16

Usually, in the adjustment, the distance or the number of stations will be used to assign the weight of the closure error.

$$\Delta\hat{h} = \Delta h + \delta \times (-1) \times L_i/L \qquad \text{(eq.1)}$$

or

$$\Delta\hat{h} = \Delta h + \delta \times (-1) \times n_i/n \qquad \text{(eq.2)}$$

$\Delta\hat{h}$: adjustment height difference; Δh: actual measured height difference; δ: total closing error; L_i, n_i: distance, number of stations of this section; L, n: total length of distance, total number of stations.

But in Table 3, the data of team I and H show that the number of stations of the two routes both are 12, and the total length of the two routes is similar. Theoretically, their closure errors should also be similar, but the closure differences of their measurement results are very different, so here it's not a good choice for us to use distance to assign weights.

Comparing the data of team H and D in Table 3, they are the same route with almost the same route length, and the number of stations of team H is 1.5 times that of team D. Theoretically, the closing error of team H should bigger than that of team D, but the measurement result is opposite to the theoretical value. so here it's also not a good choice for us to use the number of stations to assign weights.

Analyzing all the measurement results, the most important influence on the measurement accuracy is the operation of the surveying personnel and the weather problems. When the sunlight is very strong, the accuracy will be reduced. At this time, you must use an umbrella for the level. When measuring the route FP7 to NP3, the weather was very bad and heavy rain made the measurement difficult, and the final measurement results were also very unsatisfactory. Fortunately, two remeasuring groups were arranged when planning the routes and remeasured this section.

Considering both the operation of the surveyor and the weather problem, the closing error was used as the weight of the adjustment.

3.2. Estimated results (before adjustment)

Table 4 is the estimated results of height before adjustment, which used 5642 as the height starting point, calculated the height of 5641 through the height transfer.

Table 4 Estimated results (before adjustment)

Results of each point before adjustment			
point	Mean height difference[m]	Measuring distance[m]	Height[m]
5642			454.6720
	4.3749	260.80	
FP27			459.0467
	-1.0660	195.03	
FP1			457.9809
	-5.1909	169.02	
FP2			452.7900
	1.5816	146.17	
FP7			454.3716
	-2.4046	253.21	
NP3			451.9670
	-3.5488	100.88	
5641			**448.4184**

Table 5 is the heights of known level benchmark

Table 5 Heights of known level benchmark

Point name	**Known height (DHHN 12) [m]**
5641	**448.4170**
5642	454.6720

Table 4 shows that the calculated height value of 5641 is 448.4184m, and from Table 5, it can be seen that the actual value of 5641 given is 448.4170m, the difference between the two values is 1.4mm, which is within the tolerance 1.69mm, so these data are qualified and can be used for subsequent adjustment。

3.3. Conditional adjustment of level network

1. mathematical model

   1) Conditional equation:

$$\boldsymbol{AV + W = 0} \qquad \text{(eq.3)}$$

In (eq.3), A is the coefficient matrix of V; V is the correction number vector; W is the closing error vector.

2) Correction number equation:

$$\boldsymbol{V} = \boldsymbol{Q}\boldsymbol{A}^{\mathrm{T}}\boldsymbol{K} \qquad \text{(eq.4)}$$

In (eq.4), Q is the cofactor matrix; K is the connection number vector.

3) Set $\mathbf{N}_{\mathrm{aa}} = \boldsymbol{A}\boldsymbol{Q}\boldsymbol{A}^{\mathrm{T}}$, list the normal equations:

$$\boldsymbol{N}_{\mathrm{aa}}\boldsymbol{K} + \boldsymbol{W} = \mathbf{0} \qquad \text{(eq.5)}$$

Find the value of the connection number vector K.

4) Substitute K into the correction number equation to find the value of V, and find the value of observation adjustment $\hat{L}$

$$\hat{\boldsymbol{L}} = \boldsymbol{L} + \boldsymbol{V} \qquad \text{(eq.6)}$$

In (eq.6), L is the vector of observations

2. Heights of each point after adjustment

The programming language Matlab was used to perform adjustment calculations. After calculation, the height and standard deviation of each point are obtained:

Table 6 Results of each point after adjustment

Results of each point after adjustment					
point	Mean height difference[m]	Measuring distance[m]	Height correction[mm]	Corrected height difference[m]	Height[m]
5642					454.6720
	4.3749	260.80	0.4393	4.3744	
FP27					459.0464
	-1.0660	195.03	0.4019	-1.0664	
FP1					457.9800
	-5.1909	169.02	−0.0039	-5.1909	
FP2					452.7891
	1.5816	146.17	0.2991	1.5813	
FP7					454.3704
	-2.4046	253.21	−0.0033	-2.4046	
NP3					451.9658
	-3.5488	100.88	−0.0105	-3.5488	
5641					448.4170

Table 7 Heights and the standard deviations of each point

Point	Heights[m]	The standard deviations[mm]
5642	454.6720	0.04319
FP27	459.0464	0.17742
FP1	457.9800	0.18618
FP2	452.7891	0.18246
FP7	454.3704	0.13590
NP3	451.9658	0.12251
5641	448.4170	0.043190

From Table 7, it can be found that the results are good for the standard deviations are small.

3.4. Compared with last year's results

To perfect data assessment, the results of this precision leveling are also compared with the height information derived from last year in Table 8. But unfortunately, according to the route planes, only point FP27 can be compared. The height difference between the two years in point FP27 is just 1mm, further verify the reliability of our results.

Table 8 Comparison of two-year results

Point	Height of this year[m]	Height of last year[m]	Height difference[mm]
FP27	459.0464	459.0454	1

4. The problems and suggestions for measuring

1) Be sure to use an umbrella when the sun is strong, otherwise, the accuracy regarding back- and foresight (B1−F1) − (B2−F2) will be difficult to reach 0.07mm.
2) During the measurement, it was found that the electronic level is more sensitive to vibration, so during the measurement process, the fewer people standing next to the instrument, the better, and the people next to the instrument should not move as much as possible. When measuring on the roadside, if there is a car passing by, wait for the car to pass before starting the measurement.
3) During the measurement, it is necessary to check whether the level bubble has been centered.
4) When measuring slopes with large elevation differences, the viewing distance should be short as possible, 3-10m is a better choice.
5) When planning a route, choose a route with fewer slopes and low gradients to reduce

errors in the process of height transmission.

6) Before planning a route, it is necessary to survey and select points on the spot because some existing fixed points are not suitable for putting leveling staff and cannot be used for leveling.
7) Avoid bad weather, such as heavy rain.

5. Conclusion

Before planning a route, it is very important to survey on-site for selecting points and choosing routes, choose available points, and avoid steeply sloped routes. Therefore, after the start of the fieldwork, it's necessary to communicate with WP1 and WP2 in time to know what fixed points they measure in common and choose 3 points that are suitable for putting leveling staff and are convenient for route planning from their common measurement points. If they change the measurement points, it's also needed to adjust the precision leveling measurement plan in time.

By analyzing the measurement data of all groups, the operations of the surveying personnel and weather problems have the greatest impact on the measurement accuracy. Therefore, during the measurement process, the measurement personnel must strictly follow the specifications and avoid measuring in bad weather (such as strong wind and heavy rain).

For the group whose closing error exceeds the limit, it is necessary to analyze the problem in time, find the cause of the over limit, precautions, and solutions, and promptly inform the subsequent measurement group of the precautions and solutions in time.

Through this field work, it can be found that digital level measurement has more advantages than optical measurement. Its convenient operation method and automatic data acquisition and processing process reduces the labor intensity of the operators and reduces the influence of human factors on the measurement work, and ensures the security, reliability, and accuracy of the data.

Integrated Fieldwork 2021

WP 4: Navigation Routes/Paths near Hysolar

Supervisor

Clemens Sonnleitner

Team Member

Yang Li

Roland Lintz

Xiaohan Liu

Peiwei Pan

Paula Peitschat

Zhiya Yang

Shuhua Yu

University of Stuttgart
Germany

Contents

1. Introduction

In this WP, coordinates and height profiles around the area of the Integrated Field Work are measured by using GNSS in a kinematic survey. There are three main tasks in this WP. Firstly, measure the fix points from WP1 and WP2. Secondly, measure the marked paths, paths around UFO, paths around Hysolar Building and streets around new student accommodation buildings. Thirdly, get the height profile of areas by driving a route near the Hysolar Building chaotically or in a certain pattern.

A remote-controlled car with a mobile multi-band RTK GNSS receiver and a multi-band RTK reference GNSS station is used to measure. At the same time, a laptop is used to monitor the actual position. We use laptop to connect base station via WIFI and set the positioning mode, GNSS select, update rate, elevation mask angle, SNR mask, coordinates input mode, correction, position out and settings of Raw data. Then, the raw data will be processed using the RTKLIB and we get the point cloud and document the location of the surveyed objects. In the end, we analyse the results and come to a conclusion.

2. Point measurements

2.1 Positions and standard deviations of WP4

For static point measurements, we measured 10 fixed points, some of which were measured with the fan off to determine if the fan and other electrical devices are affecting the GNSS signals, which are electromagnetic waves. We did the post processing in static mode and got the position files of each point. When processing point measurements, we set the elevation mask as 15°. This is because the atmosphere and multi-path effects have larger influence on signals with low elevation angle. We set the SNR mask as 35 dBHz for the rover and the base station to reduce the influence of signal noise. At first, we used the observations from GPS, GLONASS, Galileo and BEIDOU. However, this way the ‘fix’ percentage of most points were 0%. It can be helpful to exclude individual satellites or an entire system with high residuals to achieve better results. For example, in our evaluation GLONASS satellites were often eliminated if they had high residuals. Through this setting the ‘fix’ percentage was greatly improved. Table 1 shows the position of each point in ETRS89_UTM32 with height in DHHN 2016. Table 2 shows the standard deviation of the position in east, north and upward

directions and the percentage of 'fix' solution. From the table below it's obvious that most points have very high precision. It is because the static mode and combined filter were used, so that the filter tries to calculate the point as statically as possible during processing. If you choose the kinematic mode and the forward filter, the standard deviation increases into the centimeter level. However, we noticed that the measurements of Group C have a low precision due to the usage of a single frequency antenna because of a broken adapter. The last point marked in orange background reached centimeter precision and the 'fix' percentage is not 100%. From Figure 1 it can be seen that FP6 is under the tree and it is the closest point to the solar photovoltaic panels, which has an impact on the GNSS signals. We didn't see much difference between points measured with fan on and off. So, we assume that the electronic parts of the devices do not have a noticeable effect on signal receiving.

Point Nr.	X [m]	Y [m]	Normal height [m]
GrB_FP1	507140.299597	5398883.608991	457.938
GrE_FP1_off	507140.305970	5398883.569314	457.935
GrE_FP1	507140.302069	5398883.573089	457.944
GrG_FP2	506980.638956	5398922.889435	452.704
GrC_FP3	506988.001922	5398977.760401	446.092
GrF_FP3	506985.773699	5398973.981503	447.525
GrC_FP4	506971.280003	5399045.668053	437.296
GrF_FP4	506970.149472	5399044.248573	435.793
GrI_FP4	506970.133700	5399044.221875	435.843
GrI_FP6	507062.573282	5398903.702663	455.126
GrA_FP7	507095.414372	5398980.053351	454.330
GrA_FP8	507111.437826	5398990.152916	454.154
GrH_FP9	506964.511282	5398761.176756	455.323
GrE_FP11	507029.654967	5398862.231109	455.533
GrG_FP11	507029.640173	5398862.245097	455.506
GrG_FP11_off	507029.636044	5398862.253985	455.515
GrH_FP11	507029.621102	5398862.209835	455.525
GrB_FP27	507326.101177	5398902.510790	459.023
GrG_FP27	507326.118188	5398902.489247	459.039

Table 1: Point positions in UTM coordinates

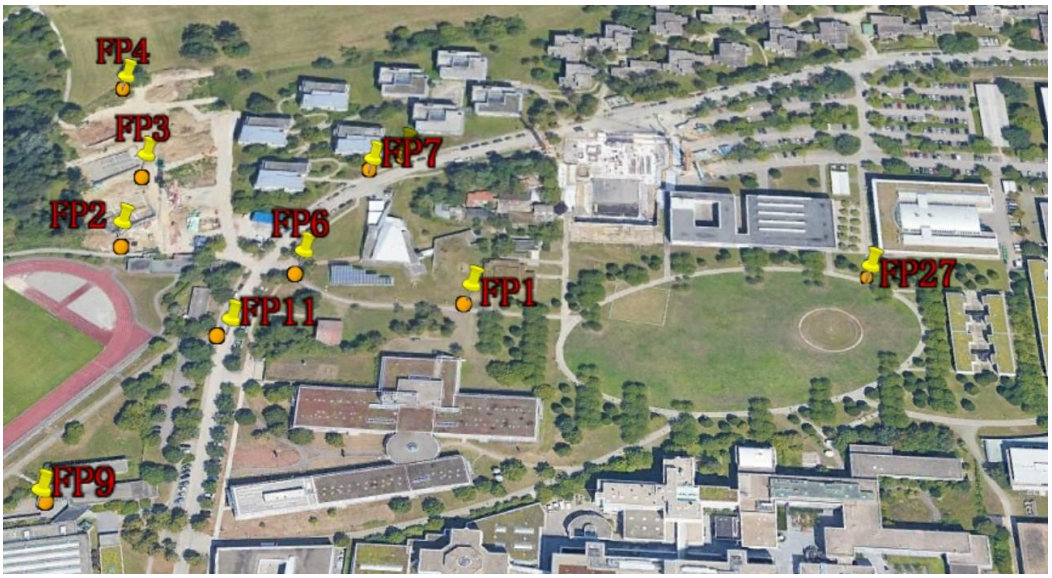

Figure 1: Position of the points

Point Nr.	std.E [m]	std.N [m]	std.U [m]	fix percentage
GrB_FP1	0.0002	0.0002	0.0006	100.00%
GrE_FP1_off	0.0000	0.0001	0.0005	100.00%
GrE_FP1	0.0001	0.0001	0.0001	100.00%
GrG_FP2	0.0001	0.0002	0.0002	100.00%
GrC_FP3	0.1826	0.4445	0.2411	32.80%
GrF_FP3	0.0013	0.0012	0.0042	100.00%
GrC_FP4	0.6831	0.5263	0.3369	46.70%
GrF_FP4	0.0001	0.0001	0.0002	100.00%
GrI_FP4	0.0004	0.0011	0.0004	100.00%
GrI_FP6	0.0433	0.0744	0.0927	94.50%
GrA_FP7	0.0000	0.0001	0.0002	100.00%
GrA_FP8	0.0000	0.0001	0.0002	100.00%
GrH_FP9	0.0001	0.0001	0.0001	100.00%
GrE_FP11	0.0008	0.0003	0.0022	100.00%
GrG_FP11	0.0001	0.0002	0.0004	100.00%
GrG_FP11_off	0.0002	0.0002	0.0005	100.00%
GrH_FP11	0.0002	0.0001	0.0004	100.00%
GrB_FP27	0.0003	0.0002	0.0005	100.00%
GrG_FP27	0.0006	0.0004	0.0006	100.00%

Table 2: Standard deviation and fix percentage

2.2 Comparisons with other WPs

We also compared our positioning results to other working packages.

Point Nr.	dev.X [m]	dev.Y [m]	dev.Nh [m]
GrB_FP1	-0.0043	0.0223	0.0240
GrE_FP1_off	0.0021	0.0173	0.0210
GrE_FP1	-0.0018	0.0136	0.0300
GrG_FP2	-0.0251	0.0030	-0.0240
GrA_FP7	0.0623	0.0106	0.0290
GrH_FP9	-0.0093	0.0390	0.0190

Table 3: Difference between WP4 and WP1 in UTM coordinates

In WP1, the fundamental network in the area of the Integrated Field Work is established and new surveying points at the Hysolar building are determined with their coordinates. This is realised by measurements with expensive GNSS receivers and several observations of the network points of a duration of 1 hour. Table 3 shows the difference between the point positions from WP4 and WP1 in UTM coordinates. From the table we can see that the point positions are close to the results of WP1. The difference varies from several millimeters to several centimeters. In general, deviations also occur in the static point measurements due to inaccuracies in the placement of the car above the point.

Point Nr.	dev.X [m]	dev.Y [m]	dev.Nh [m]
GrB_FP1	-0.042503	0.046091	0.0479
GrE_FP1_off	-0.036130	0.006414	0.0449
GrE_FP1	-0.040031	0.010189	0.0539
GrG_FP2	0.011056	0.003935	-0.0845
GrC_FP3	2.296522	3.776101	-1.5227
GrF_FP3	0.068299	-0.002797	-0.0897
GrC_FP4	1.179803	1.380253	1.4713
GrF_FP4	0.049272	-0.039227	-0.0317
GrI_FP4	0.033500	-0.065925	0.0183
GrF_FP4	0.049272	-0.039227	-0.0317
GrI_FP6	0.020982	-0.028537	-0.0655
GrA_FP7	0.050572	-0.018549	-0.0408
GrA_FP8	-0.001074	-0.074684	-0.0387
GrH_FP9	0.046282	0.029656	-0.0372
GrG_FP11	0.036473	0.052597	-0.0459
GrG_FP11_off	0.032344	0.061485	-0.0369
GrH_FP11	0.017402	0.017335	-0.0269

Table 4: Difference between WP4 and WP2 in UTM coordinates

WP2 established a high redundant 3D geodetic network frame by using robotic total stations and measured detailed points. Table 4 shows the difference between the point positions from WP4 and WP2 in UTM coordinates. From the table we can see that the difference of most points is several centimeters. We also noticed that points from the single-frequency GNSS antenna have much bigger difference than other points.

Point Nr.	dev.Nh [m]
GrE_FP1_off	-0.0450
GrE_FP1	-0.0360
GrG_FP2	-0.0851
GrA_FP7	-0.0404
GrB_FP27	-0.0234
GrG_FP27	-0.0074

Table 5: Difference between WP4 and WP3 in DHHN 2016

WP3 delivers the height information for the interest points using precision levelling. Table 5 shows the normal height difference between WP4 and WP3. We can see that the normal height difference between WP4 and WP3 is several centimeters, which corresponds to the height difference in Table 3 and 4.

3. Paths

Depending on the areas from which a height profile has been created, the accuracy of the solutions varies significantly. This depends on whether a ‘fix‘, ‘float‘ or ‘single‘ solution is achieved. Especially multipath propagations and signal interruptions prevent a ‘fix‘ solution.

This effect can be seen well in the trajectory where group D was chased by the mobile laser scanner. In the following figures the ‘fix‘ solutions with an accuracy of centimeter level are shown in green. ‘float‘ solutions with an accuracy of submeter level are shown in yellow and ‘single‘ with the lowest accuracy of meter level in red. Especially between the buildings and under trees there is a lot of multipath propagation and signal loss, so that only a float or SPP solution can be calculated.

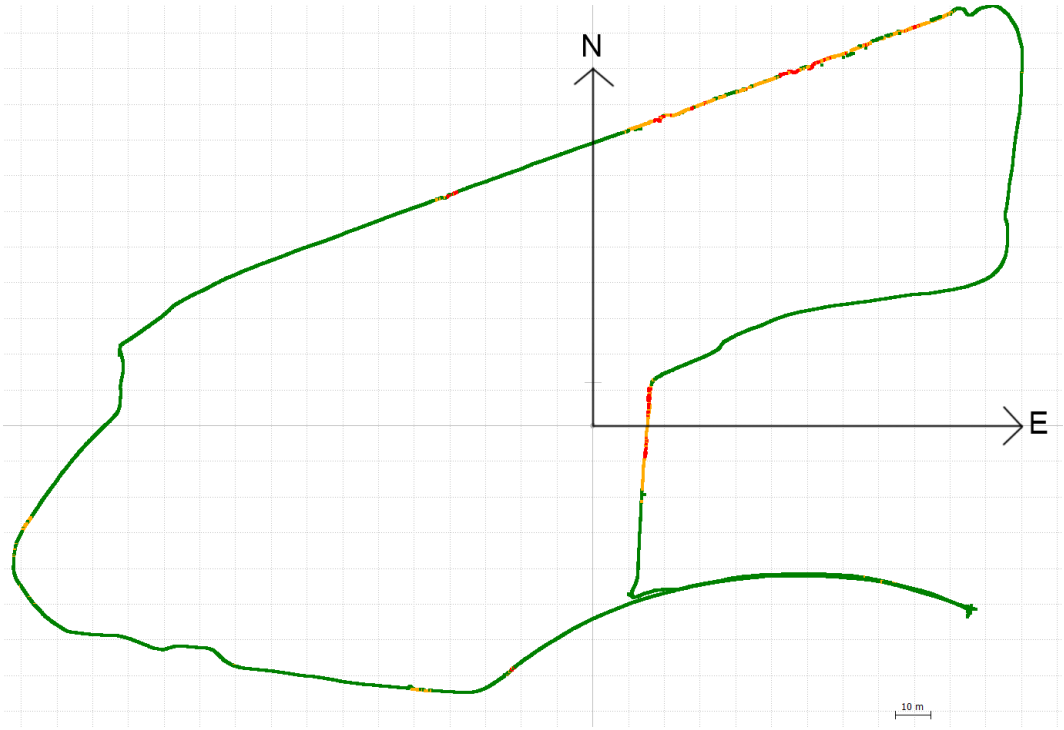

Figure 2: RTKPOST laser route of group D

Figure 3: laser route of group D in google earth

To increase accuracy by trying to obtain more ‘fixed‘ solutions, the evaluation in RTKLIB can be analyzed to exclude satellites with a low SNR from the following recalculation.

On the following pages the driven paths are displayed in Google Earth. We should note that the satellite picture of Figure 6 is old and there are buildings nowadays.

Figure 4: Paths of UFO (Group A)

Figure 5: Paths of Hysolar building (Group E)

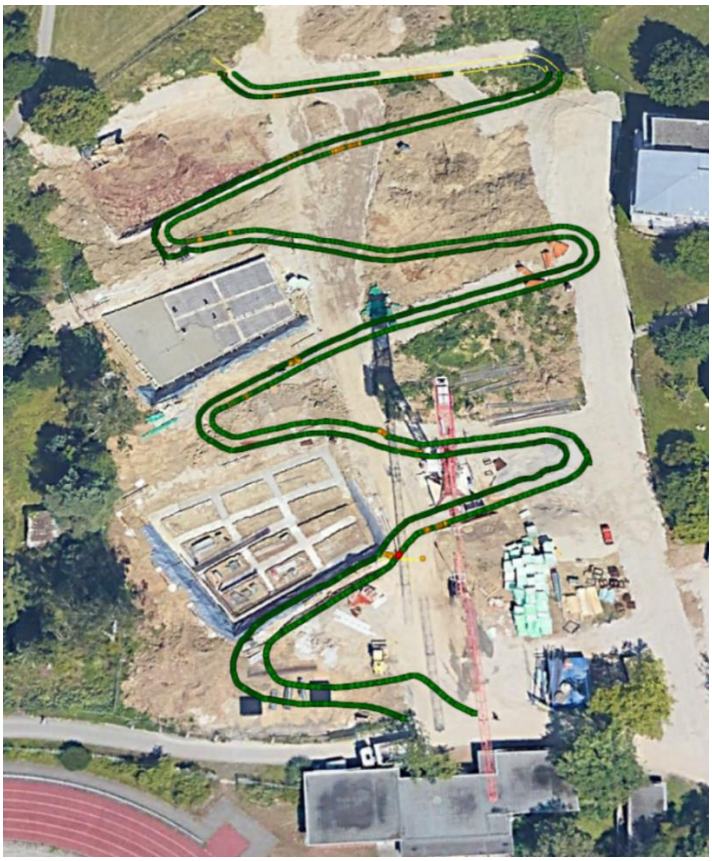

Figure 6: Paths of student accommodation (Group F)

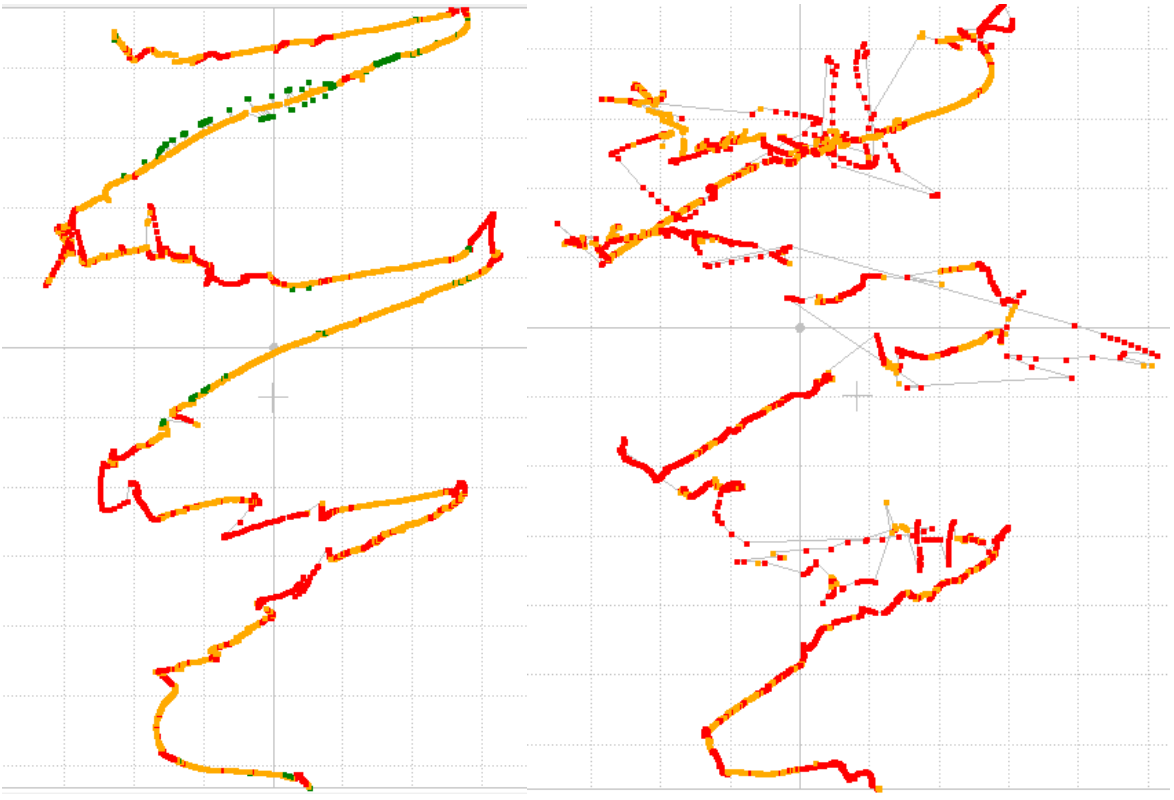

Figure 7: Group C student accommodation

Figure 7 shows the result of Group C. We can see from the picture that the most point solutions are float and single. This is because of the usage of the single-frequency GNSS antenna.

The road widths were measured for comparison with the calculated road widths. However, for routes of Hysolar building and student accommodation, it's difficult to define the start point and end point, and the road width varies along the route. So, we decided to calculate the road width of the UFO route. For each point on the small ellipse, a function finds the point on the big ellipse, which has the shortest distance to the point on the small one. We calculated the mean of the distances and consider it as the road width. The results are shown in the Table 6. From the table we can see that the differences of Group A and Group D are around 8 centimeters, while the difference of Group G is more than 20 centimeters. This might be because the RC car couldn't be controlled exactly on the defined path from which the width was measured. Also for Group A and Group D, the 'fix' percentage is around 90% while Group G only has around 60% of 'fix' solution.

	width_measured [m]	width_calculated [m]
GrA_path	2.4000	2.3204
GrD_path	2.4075	2.3250
GrG_path	2.4000	2.6200

Table 6: Measured road width and calculated road width

4. Height profiles

As already described in the last section, signal loss and multipath propagation occur due to blocking by objects. One of the elevation profiles is another illustrative example. Below is the evaluation of the journey of group H in google earth. The solution is colour-coded as before. In such areas, the positioning using GNSS is not very accurate. Under the trees no fixed solution is achieved.

Figure 8: height profile group H

All areas that have been surveyed by car can be used to represent the height profile. Some paths were driven systematically according to a certain pattern. You can also achieve good results with a ‘chaotic‘ driving pattern. However, the latter is less efficient because the points are not evenly spread and perhaps areas are not covered at all. Furthermore, linear interpolation is used to achieve a continuous surface between the measured points. Only points with a ‘fixed‘ solution were used to minimize the number of outliers that would distort the surface.

In the following figure the surface next to the Hysolar building is shown, which was composed of two different height measurements (group E and I). The measurement of the path was also added, while using one side of each path from group E and B.

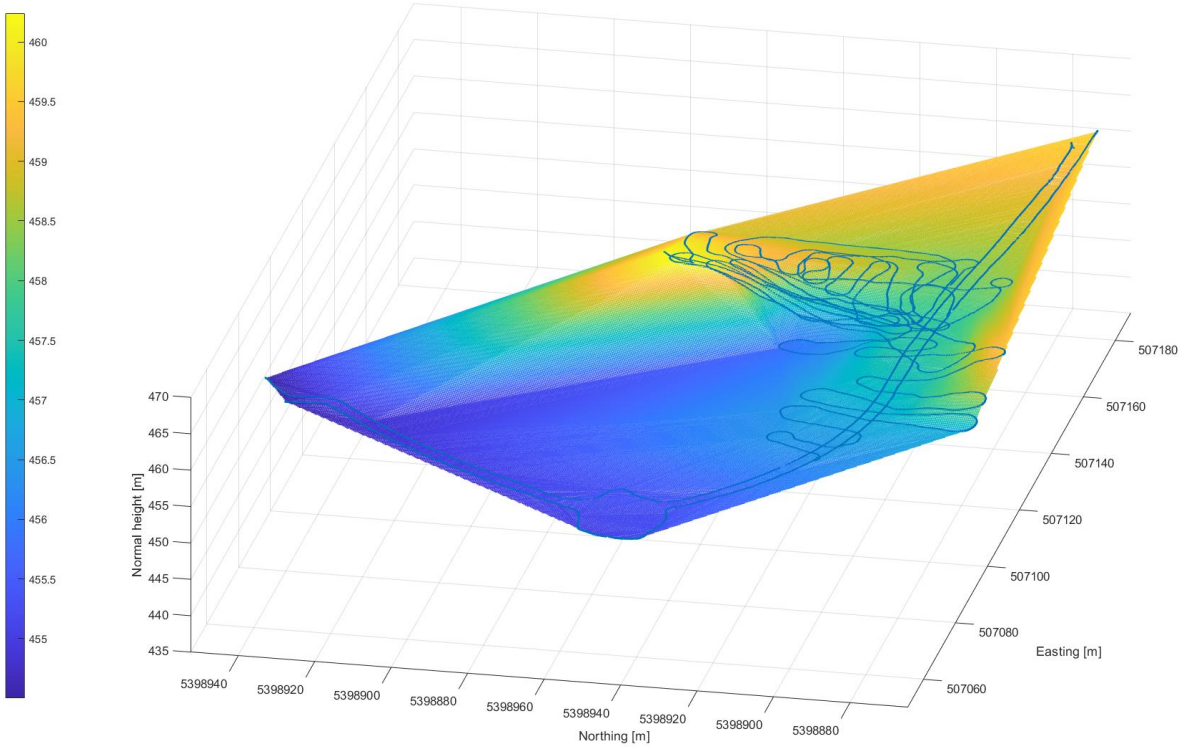

Figure 9: height profiles near Hysolar

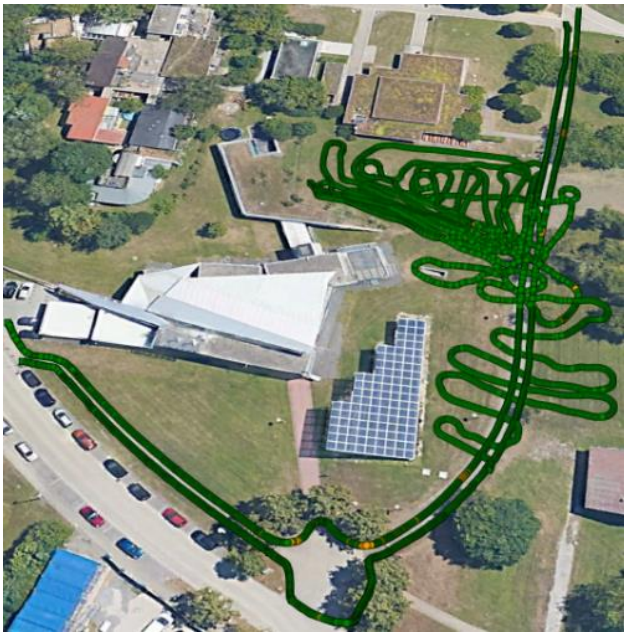

You can see that the data sets fit together and the area can be approximated. On the left you can also see the routes in google earth. Below is a close-up of the area with higher point density.

Figure 10: routes near Hysolar in google earth

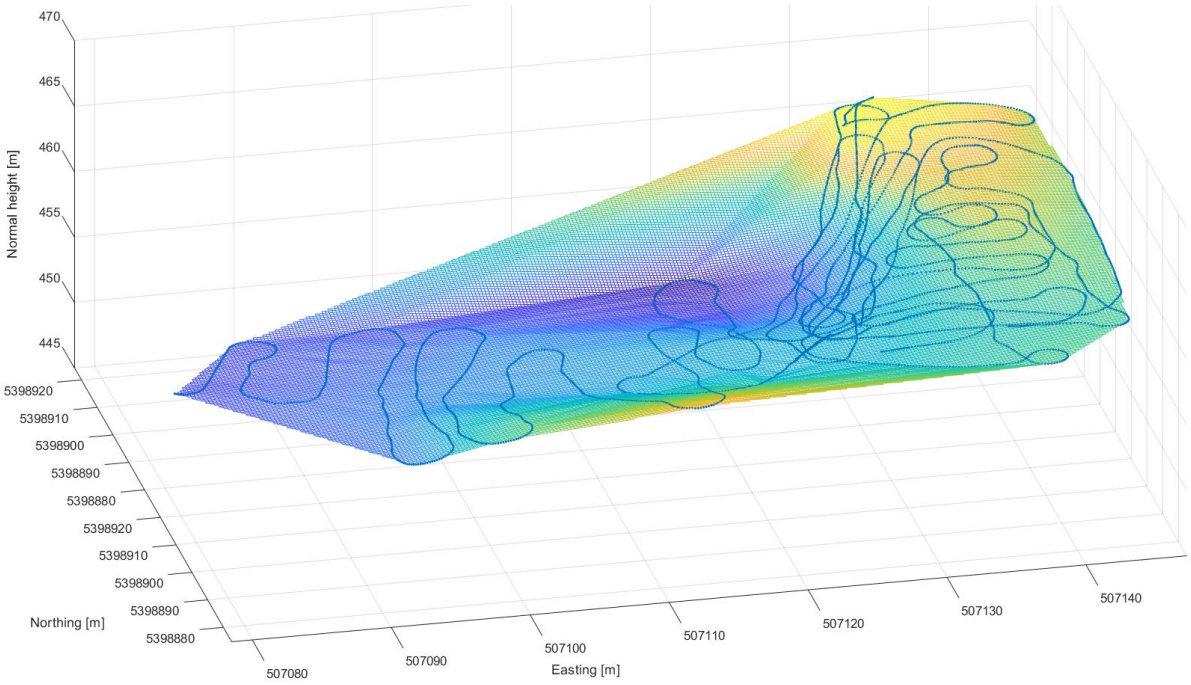

Figure 11: close-up of height profile near Hysolar

The following figure shows the UFO and the path around it. Since no measurements were made between the UFO and the path, the interpolated heights are probably not correct.

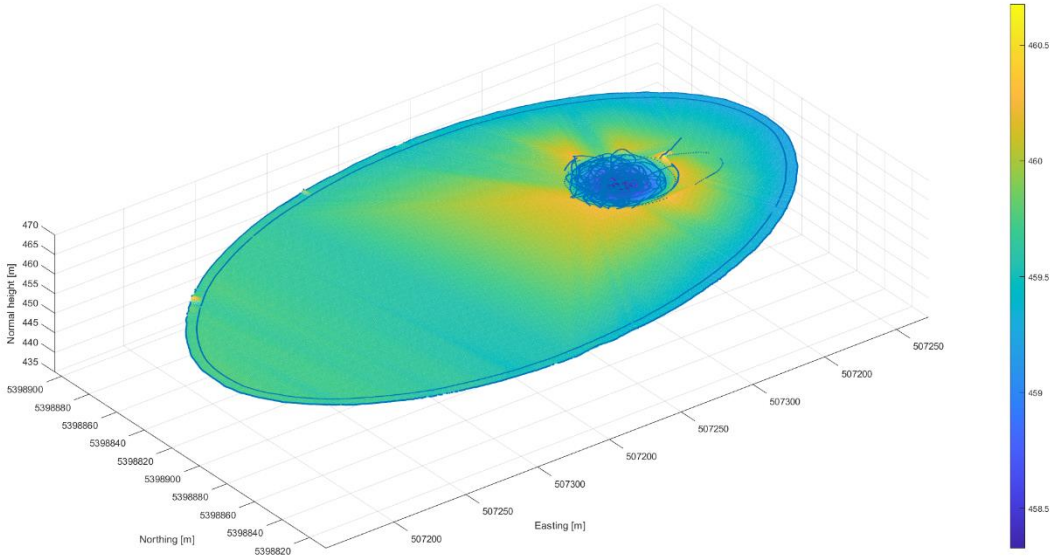

Figure 12: height profile around UFO

In this area, the data sets of groups A, B and F were used for the height profiles in the UFO and the data sets of group A for the path around.

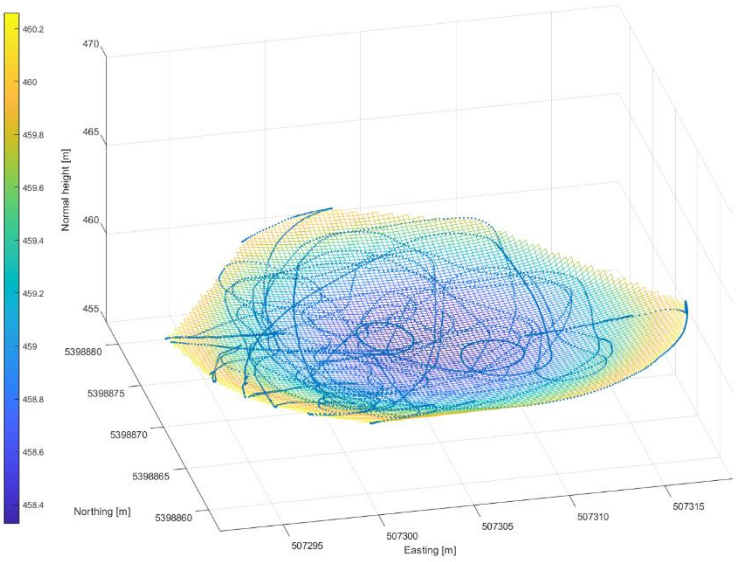

Here you can see a close-up of the inside of the UFO, using only the data from group A. You can see that the group did not record the height profile in any particular pattern, but chaotically. Consequently, some areas are covered more densely than others and are therefore better represented.

Figure 13: close-up of height profile of UFO

The following figure shows the height profile in the area of the student accommodations. The data sets of group I were used for interpolating the surface.

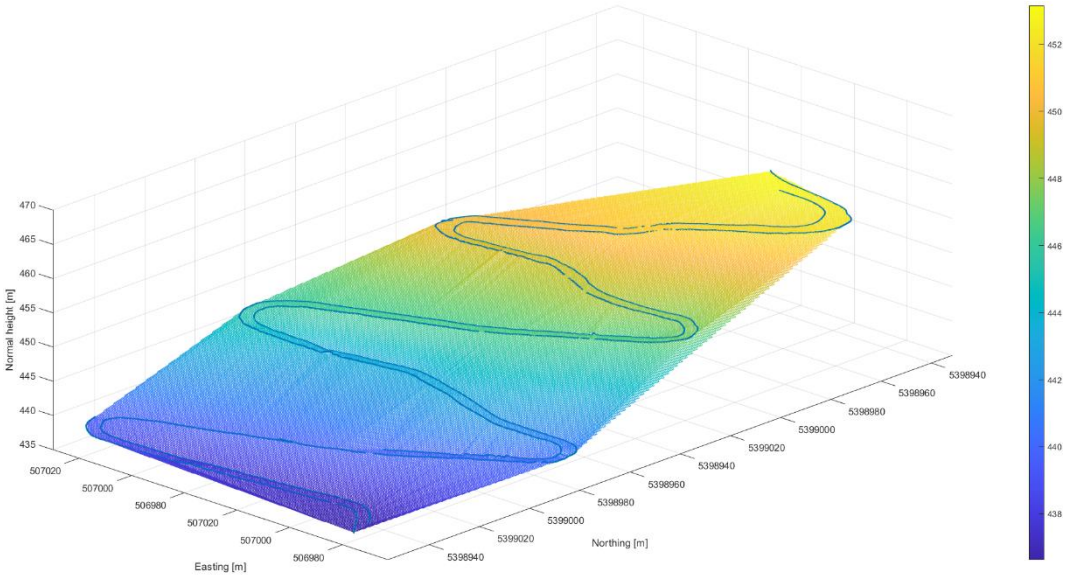

Figure 14: height profile near student accommodations

You can see that the paths are interrupted. This is due to the fact that only ‘fix‘ solutions were used to create the height profiles and, as explained earlier, a lower rate of ‘fix‘ was achieved between the student accommodations.

In the final figure all the height profiles, all the measurements during the scans with the mobile laser scanner and the path measurements were combined.

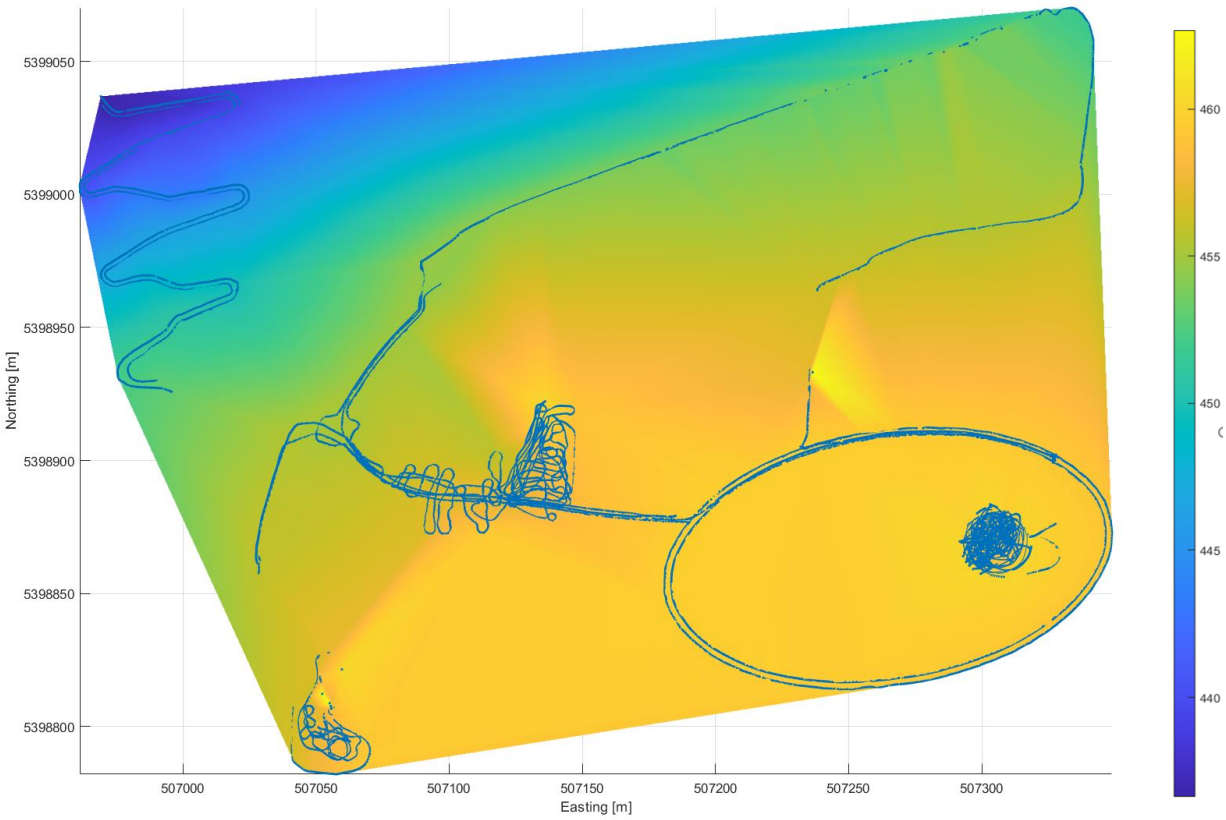

Figure 15: height profile with all driven paths

5. Difficulties in the evaluation process

So that the gathered data fits together, it must be ensured that the absolute coordinates of the measurements are correct. At the beginning of the evaluation this was not the case and for example the height profiles differed in height. This led us to check the RINEX headers to see if the data there was correct. In addition to false antenna heights, the base coordinates in the header were also incorrect. We then corrected the data manually by referring to the field books. Unfortunately, there were not always enough decimal digits for the latitude and longitude. Therefore, we had to find another method to get accurate base coordinates. One alternative was to use the data from a virtual SAPOS reference station as the base and calculate an RTK position for the base using the actual base as the rover. The other alternative was to calculate an RTK solution for the base using the recorded base correction data.

6. Conclusion

According to the results and analysis, we can see that the most important factor affecting accuracy is the environment, such as buildings and trees. When the car travels under shelter, like trees, or is close to buildings, there will be signal reflection, signal loss and multi-path. The accuracy of position and height will be higher when the car travels in a wide, unsheltered area.

In addition, comparing the result gained from the Group C with other groups, it can be concluded that measurements on multiple frequencies are more accurate. This makes the measurements robust, especially in difficult environments, e.g. partially covered sky view.

Moreover, comparing the static results with kinematic results, the static method has a higher accuracy, because the static measurement is more redundant.

The comparison with WP1 is particularly interesting. In WP1, high cost receivers were used, while in our work package low cost receivers were used. Acceptable accuracies have been achieved for low cost receivers. From the comparisons, it can be concluded that for certain applications with lower accuracy requirements, low cost GNSS receivers are an alternative to consider, as they are cheaper and more time efficient.

Integrated Fieldwork 2021

WP 5: Complementary 3D Object Reconstruction using Close-range Photogrammetry and Terrestrial Laser Scanning

Supervisor

Norbert Haala

Philipp Schneider

Michael Kölle

Team Member

Pauline Speidel

Anna Hettich

Lu Chen

Jonathan Rößle

Elias Veser

YEN-TEH LI

Valentin Schmitt

University of Stuttgart
Germany

Contents

1. Introduction

Nowadays there is a hit trend that people are willing to obtain the information about objects of interest by a combination of two or more methods. In order to acquire the 3D model of the Hysolar building and its surroundings such at the sports field, the combination of Photogrammetric capturing and laser scanning (Figure 1) is applied into the measurement. In terms of photogrammetry, the reconstruction 3D mode relies on the intersecting rays defined by measurement of tie points in images. Meanwhile, the laser scanner can obtain the distance of a point by measuring the time of flight of an emitted pulse.

Figure 1: DJI Phantom 4 RTK and Leica P20 TLS

Several approaches are used in the data processing. While Cyclone (Leica) is used in the processing whose data captured by laser scanner, the photogrammetric data is processed by Metashape (Agisoft). In addition, CloudCompare is used in the processing. These photogrammetric acquisitions aim to get colored dense 3D point cloud which can be derived into a Mesh version. All models will be georeferenced using identical targets ensuring their alignment with respect to others. These common targets will be set upon points with known coordinates. In addition, detailed evaluation of both acquisition methods is acquired in the final results.

2. Processing

2.1 UAV

For the photogrammetry part, we made 2 attempts: separated dataset from different days and all photos from different days all processed together. We also included target information given by WP2 in the processing. Therefore, after we finished the processing, the coordinates information of the objects of interest can be determined, with respect to the WGS84 coordinate system. In addition, we yielded some products such as dense point cloud, Mesh, DEM and Orthophoto. Sections 2.1.1 to 2.1.5 present the results derived.

2.1.1 Initial processing

We have chosen to present the complete dataset process (2 flight days). We aligned them with tie points. When we imported the data into the software, we had to set RTK camera coordinates accuracy, which can be chosen as 0.1 meters. The figure 2 presents the tie point 3D coordinates after this first bundle adjustment.

Figure 2: Thin point cloud of Hysolar Building (UAV)

Secondly, we have created markers on the targets as manual tie points and processed all again. Hence, we got coordinates of these markers. Because we split these targets per flight day, we found that the same target often had consistent X and Y coordinates but the Z component was different. However, it turned out that the height differences of computed Z for the same target

were very large compared the data from field sheet. We concluded that there were some mistakes in the field book measurements which we corrected by adding the target offset. Nevertheless, there are also points whose coordinates in the horizontal plane differ significantly between the days, such as FP7 (see figure 3).

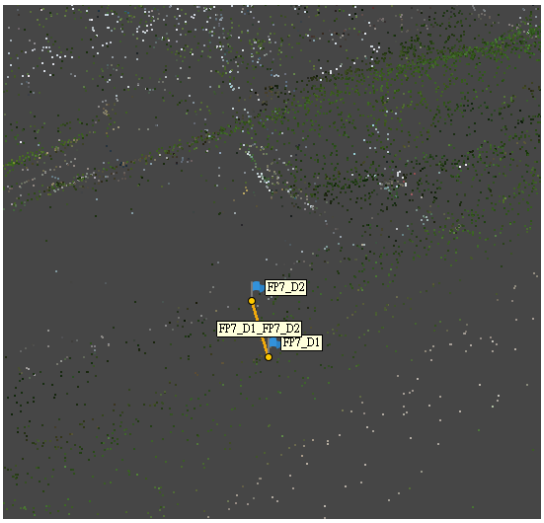

Figure 3: Difference of FP7 from the flights of the 2 days

Hence, we did not use the height differences from the field sheet between day 1 and day 2 as a constrains. We trusted more the RTK GNSS coordinates. Therefore, we could not use the WP2 coordinates because these vertical shifts were uncertain.

However, we used the perspective central positions from GNSS data, and we also did iteratively optimization for the cameras, introducing further distortion parameters, except K4 which was a Fish-eye coefficient. The selected settings can be seen in Figure 4. The final projection errors were smaller than 0.5 for all tie points.

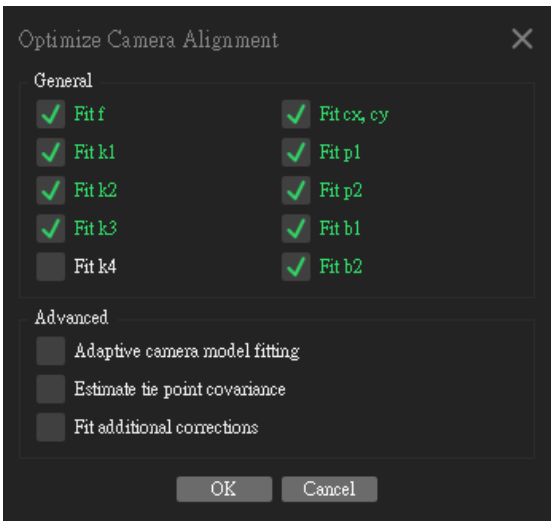

Figure 4: Distortion parameters for alignment (Metashape)

2.1.2 Dense image matching

We have created dense point cloud with dense image matching for the Hysolar building (Figure 5) and the sport field. The Hysolar model is one of the deliveries for the WP6.

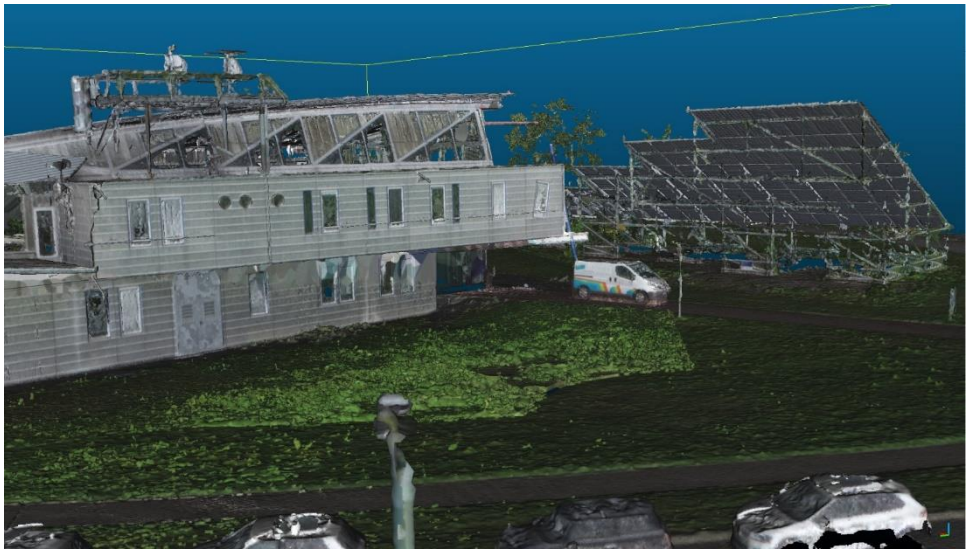

Figure 5: Dense Cloud of the Hysolar Building (UAV)

2.1.3 Build Mesh and Texture

From that point cloud, the mesh model was built. It contains texture from images projected to the 3D mesh geometry. As we can see in the following figure 6, the solar panel part was difficult to triangulate because only few points were describing it. We finally succeeded to reconstruct it by increasing the octree division in CloudCompare. This octree division is a 3D space division used for computation purpose avoiding the full cloud load into the RAM. Therefore, a larger octree depth requires more RAM but is includes more neighbors points.

Figure 6: Mesh (solar panels)

2.1.4 Build DSM

From the previous work, we have built the DSM product of the sport field (Figure 8) for the WP8. We used Metashpae to rasterize the mesh model into a grid. In addition, we created a DSM of the Hysolar building and the terrain around it, which can be seen in Figure 7.

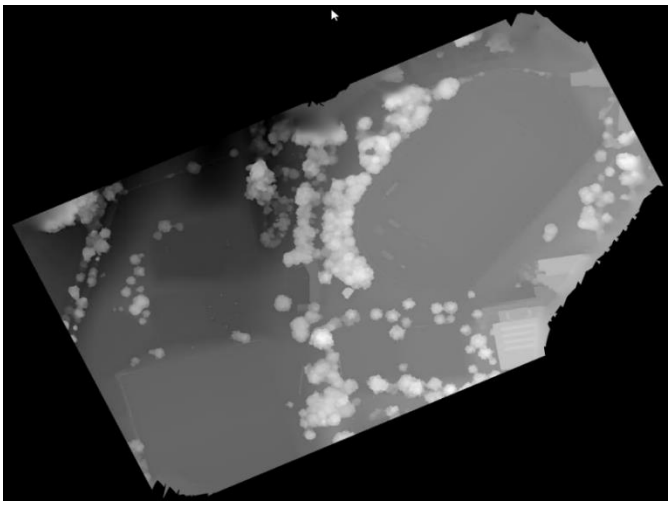

Figure 8: DSM of the sports field

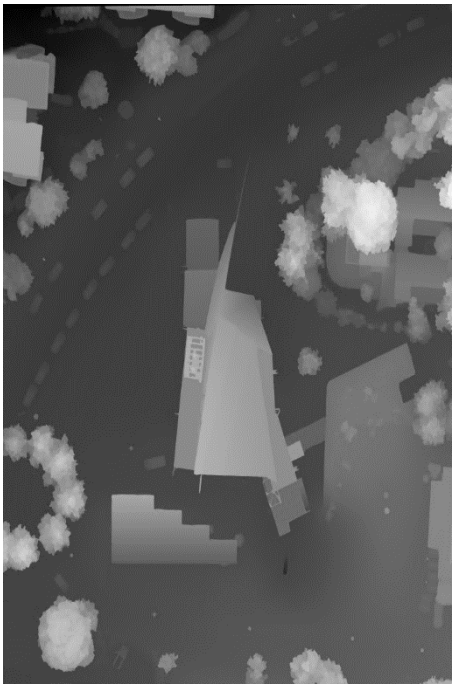

Figure 7: DSM of the Hysolar Building

2.1.5 Generate Orthophoto

In the final step, the Orthophoto was generated from DSM products we have done in the previous step. It was also a delivery to the WP8.

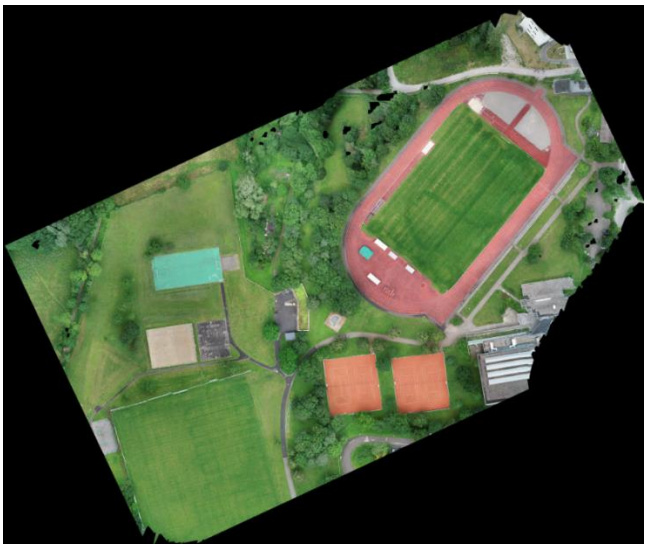

Figure 10: Orthophoto of the sport field

Figure 9: Orthophoto of the Hysolar Building

2.2 Terrestrial Laser Scanner (TLS)

A TLS instrument measures laser points and it can also capture images which will colorize the point cloud (for example in Figure 12). However, the image acquisition was not active for all stations and we cannot create a colored model from every scan. Normally, the colors of a LiDAR point cloud, as shown in Figure 11, indicate the intensity of the reflection.

Figure 12: Colored Point Cloud

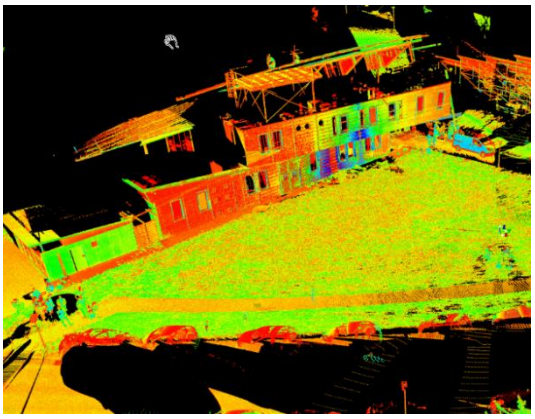

Figure 11: Point Cloud in Cyclone (Intensity)

The TLS processing aims to find the 3D transformation between scan stations. That coordinate transformation is used at the last step to convert the measurements in the local coordinate system into the global coordinate system. From the step, we can get the true coordinates of points.

First of all, we made an independent registration for each measurement day. It makes uses of common targets (3 with absolute coordinates at least if we use only such constraint) which can be sphere or B&W reflector. It is a straightforward processing because everything is assumed to be constant in one day: sphere position, B&W target heights, etc. Hence, we had 3 registrations, one per day, using respective targets and returning around 5 mm residuals. For example, Figure 13 shows the results of the Day 3 registration. A relative registration between stations around 5 mm is a good result because it includes the measurement accuracy (millimeters), target detection and registration constraints.

```
Constraints
Constraint ID  ScanWorld                        ScanWorld                        Type
                 Status  Weight  Error    Error Vector                 Horz     Vert

b2             Station-001: SW-001 (Leveled)  Station-002: SW-002 (Leveled)  Coincident:
Sphere - Sphere  On      1.0000  0.006 m  (-0.004, -0.005,  0.001) m  0.006 m   0.001 m

FP1            Station-001: SW-001 (Leveled)  Station-002: SW-002 (Leveled)  Coincident:
Vertex - Vertex  On      1.0000  0.004 m  ( 0.000,  0.003,  0.001) m  0.003 m   0.001 m

FP1            Station-001: SW-001 (Leveled)  Marker Day 3.txt (Leveled)     Coincident:
Vertex - Vertex  On      1.0000  0.005 m  ( 0.000,  0.003,  0.004) m  0.003 m   0.004 m

FP6            Station-001: SW-001 (Leveled)  Marker Day 3.txt (Leveled)     Coincident:
Vertex - Vertex  On      1.0000  0.006 m  ( 0.000, -0.002, -0.006) m  0.002 m  -0.006 m

b1             Station-001: SW-001 (Leveled)  Station-002: SW-002 (Leveled)  Coincident:
Sphere - Sphere  On      1.0000  0.004 m  ( 0.004,  0.000,  0.000) m  0.004 m   0.000 m

FP1            Station-002: SW-002 (Leveled)  Marker Day 3.txt (Leveled)     Coincident:
Vertex - Vertex  On      1.0000  0.002 m  ( 0.000, -0.001,  0.002) m  0.001 m   0.002 m
```

Figure 13: Registration Report Day 3

The following step would have been to make a larger registration gathering the 3 days and introduce true coordinate to transform the model to the proper coordinate system. However, it did not succeed. Some changes had been done to distinguish different targets using the same ID (spheres and B&W targets). Then, the main issue was the B&W target height, and thus FP1 visible on day 1 is not the same than FP1 on day 2. That issue could have been overtaken whether the target height was known precisely, including the offset. We found larger error than 10 cm, and we decided to not pursue that way. Hence, we did not register a full model and relied on daily registration only.

Each daily registration has been brought to a common coordinate system using target coordinates from the UAV model of day 1 and day 2. It allowed us to avoid usage of target heights written on the field sheet. These coordinates are close enough to true positions thanks to RTK GNSS in the UAV. We could expect an accuracy a bit larger than 2cm due to RTK GNSS accuracy around 1 cm (X,Y) and 2 cm (Z) and the matching accuracy. After comparison between the UAV part and WP2 coordinates, we found an average accuracy of 2.43 cm. A final comparison to true coordinate from WP2 shall present the final accuracy. However, not enough targets were visible in day 1 and day 3, so the model could only be exported in station coordinates.

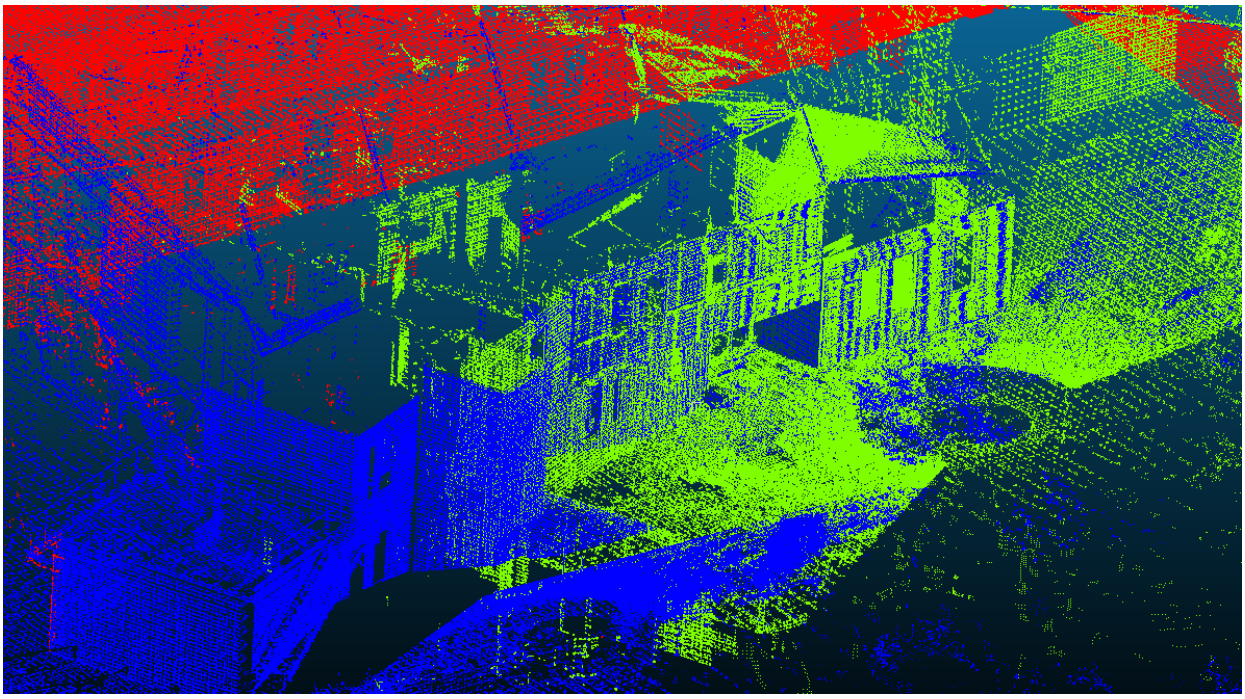

Figure 14: Point cloud of 3 different days

Finally, we moved day 1 and 3 models to the reference day 2 model by choosing 4-5 identical points in both clouds and aligning it. The result can be seen in Figure 14. The different colors represent the different days or point clouds that are assembled. This returned a maximum of 2 cm residuals. A final registration to the UAV point cloud shall provide the difference in-between.

We discovered lately the actual meaning of WP2 coordinates, including the UTM zone in front of the X coordinates. That explained why the target registration was not returning consistent model.

3. Comparison of the Point Clouds

On one hand, there is our UAV model/mesh with point color:

Figure 15: Mesh (UAV)

On the other hand, there is the TLS full model with mixed color:

Figure 16: Colored point cloud (TLS)

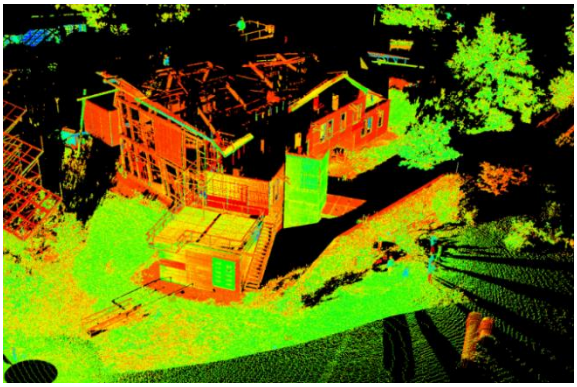

Figure 17: Point Cloud with intensity (TLS)

Both models are in the same coordinate system and complement each other as displayed hereafter.

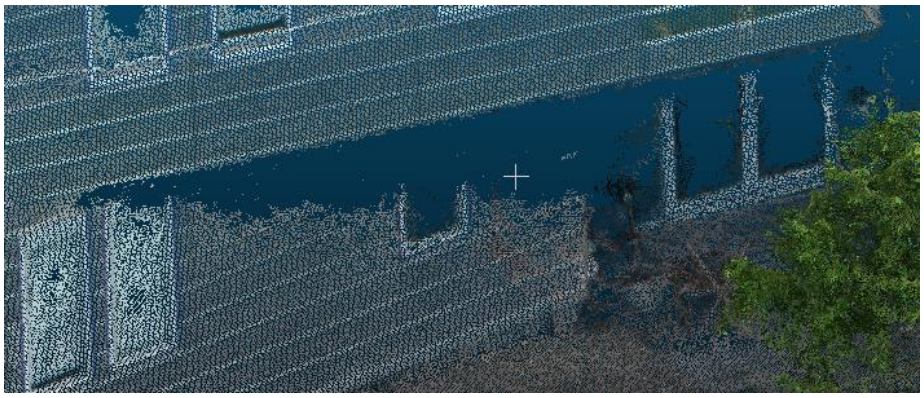

Figure 18: Point Cloud (UAV)

Figure 19: Point cloud (UAV+TLS)

Hereafter is the final point cloud (Figure 20) including UAV and TLS measurements. The day 1 area is grey, because the image acquisition was not used. On day 2 and day 3, the building color comes from the photo acquisition with the TLS. Only for the grass the image acquisition of TLS failed, which gave it a yellow color.

Figure 20: Dense cloud (UAV and TLS combined)

4. Statistical Comparison

Camera Calibration:

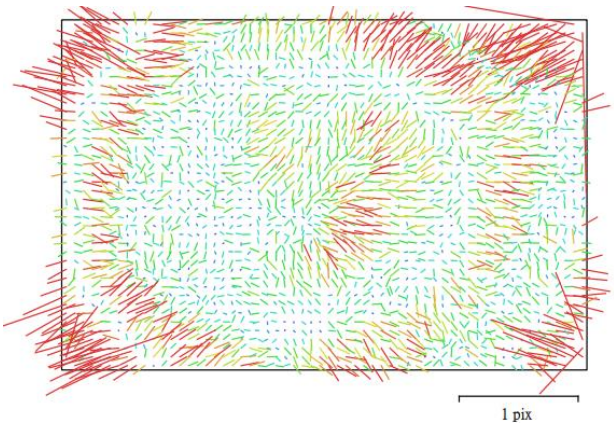

Figure 22: Image residuals (Day 1)

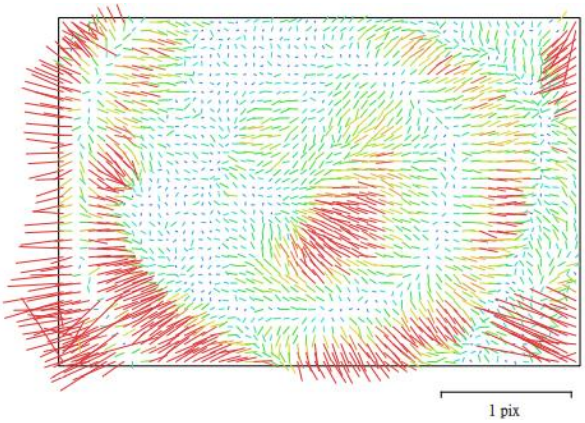

Figure 21: Image residuals (Day 2)

The vectors, as shown in Figures 21 and 22, are usually smaller than one pixel. It is noticeable that the residuals are worse especially in the edge region. This could indicate that the camera calibration and linking did not work so well there, especially because fewer tie points are probably found there.

Total errors of points (UAV):

	X error (cm)	Y error (cm)	Z error (cm)	Total (cm)
Total	0.426157	0.776699	2.26481	2.43192

The error in x and y direction is in a good range of less than 1 cm. In the Z direction it is significantly larger at 2,26 cm. This is also to be expected, because the height can be determined worse in the normal case.

5. Modelling

From the full and complete model as point cloud, we can also yield a mesh product. Both will be the delivery to the WP6 for the visualization in CESIUM.

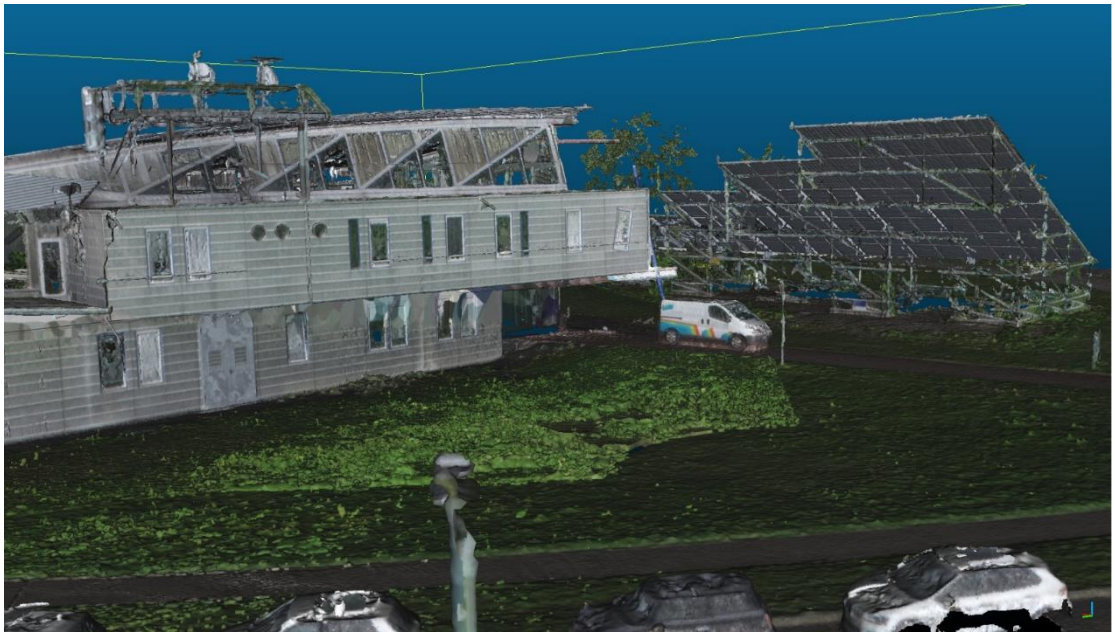

Figure 23: Mesh (UAV and TLS combined)

Integrated Fieldwork 2021

WP 6: Mobile Laser Scanning and Visualization of Multiple Point Clouds

Supervisor

Norbert Haala

Philipp Schneider

Michael Kölle

Team Member

Cindy Chun

Tzu-Hsuan Lai

Nadine Sprügel

Yihan Tao

Xuanxuan Wang

Contents

1. Introduction

Mobile laser scanning is a technique applied for 3D mapping. In this task, we will apply Geoslam's handheld Zeb sensor for capturing the Hysolar building inside and outside and sports field and then obtain a point cloud of the respective areas. The measurement is conducted based on the ground control points in order to reduce the loop closing errors and for georeferencing. The point clouds products will be prepared based on the georeference results provided by WP2. In addition, visualization of the point clouds of the concerning area will be achieved by the Cesium framework and hosted on the website. The designed website will allow the 3D presentation of the main products of WP 5 and 6 as well as the trajectory of WP 4.

2. Data Processing

2.1 Raw Data and Data Processing

The collected raw data contains the scanning data of the Hysolar building (inside and outside) and the climbing tower in the sports field as well as the trajectory of each scan.

During the data processing we divided the cloud products into three segments and focused on the respective areas which we have interests in. The targeted data sets are processed in GeoSLAM. In addition, the point clouds are demanded to process based on georeference information in the UTM system. The georeferencing of the point clouds was done in GeoSLAM. Plus, in comparison with the trajectory from WP 4, a georeferencing trajectory is generated by raw data which was obtained from the scanner with the assistance of Python. By importing the raw data into MATLAB, the corresponding time for the control points are determined. And the georeferencing was accomplished by a Python script with the time and coordinates. Because the route started at PF27 (near the UFO) which was not georeferenced by the other WPs, the coordinates of the PF27 are determined with the help of a map on the internet.

2.2 Hysolar Building outdoors

The point clouds after processing for hysolar building outdoors (see Figure 2.1-2.3) are

displayed in the figures as follows:

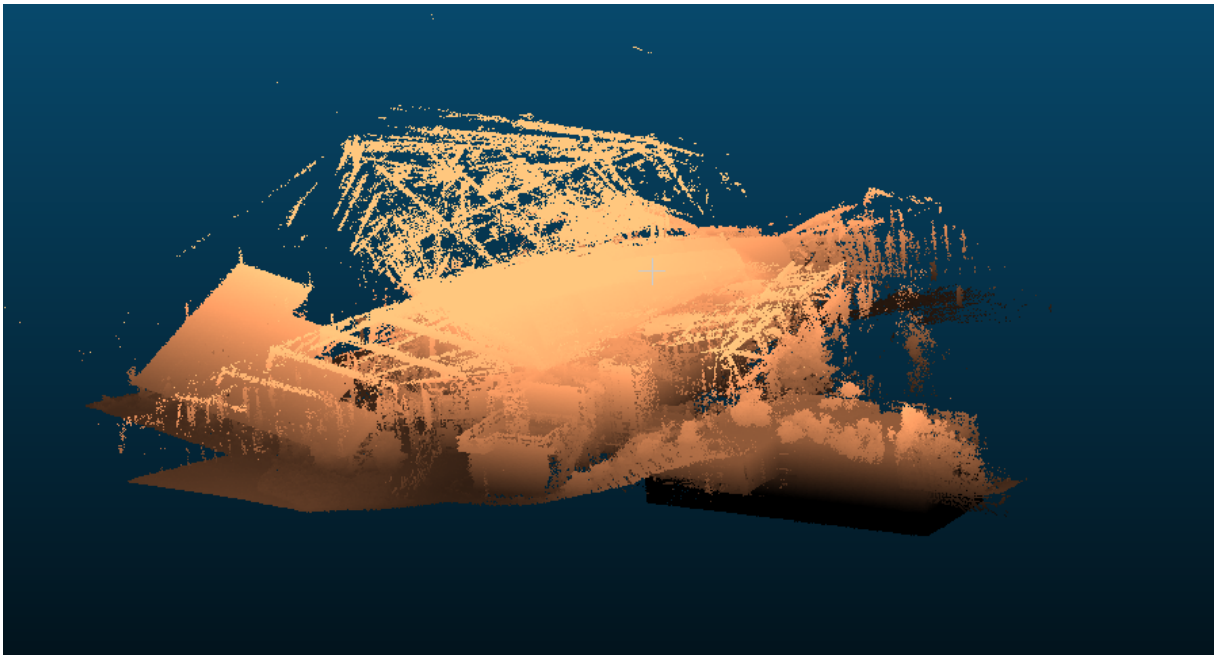

Fig 2.1 The point cloud for Hysolar building outdoors (North-East direction)

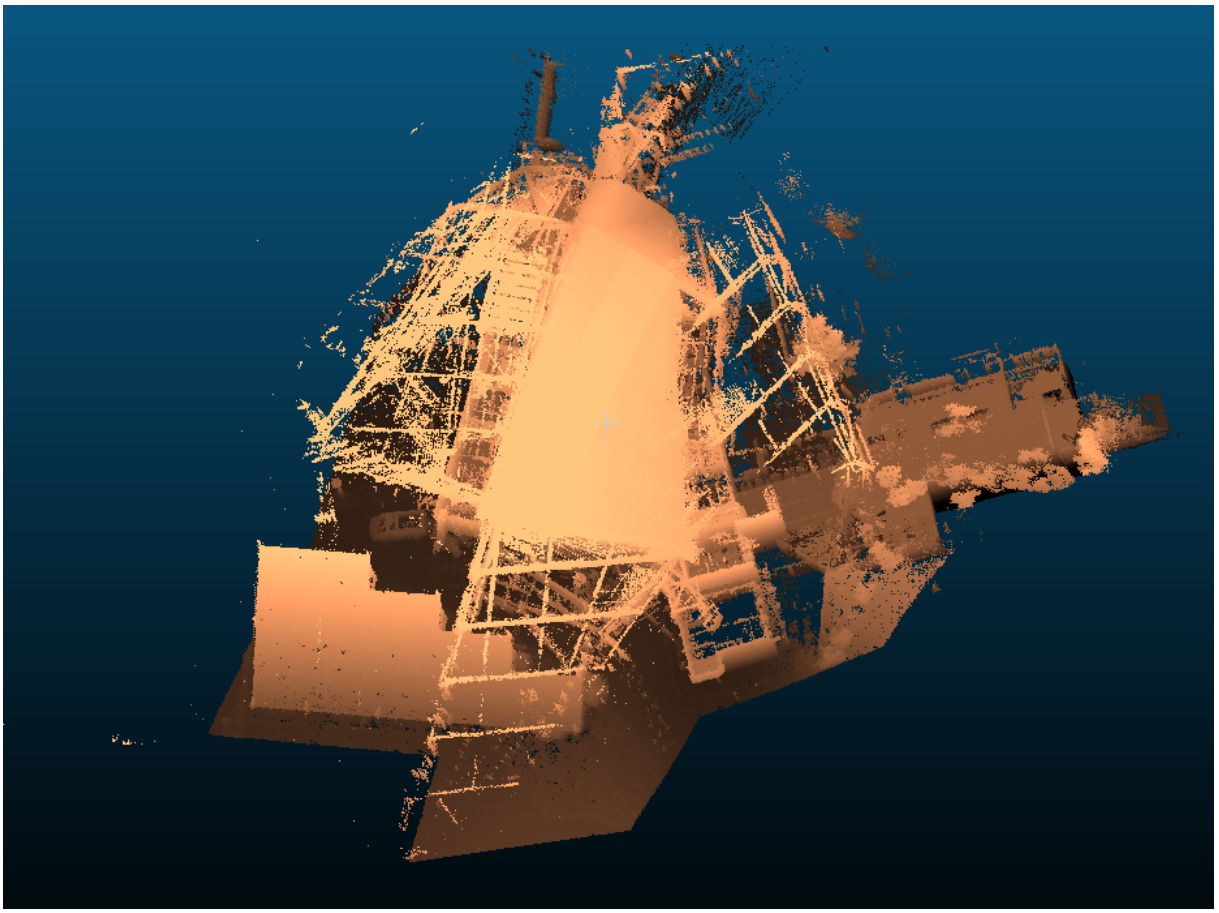

Fig 2.2 The point cloud for Hysolar building outdoors (North direction)

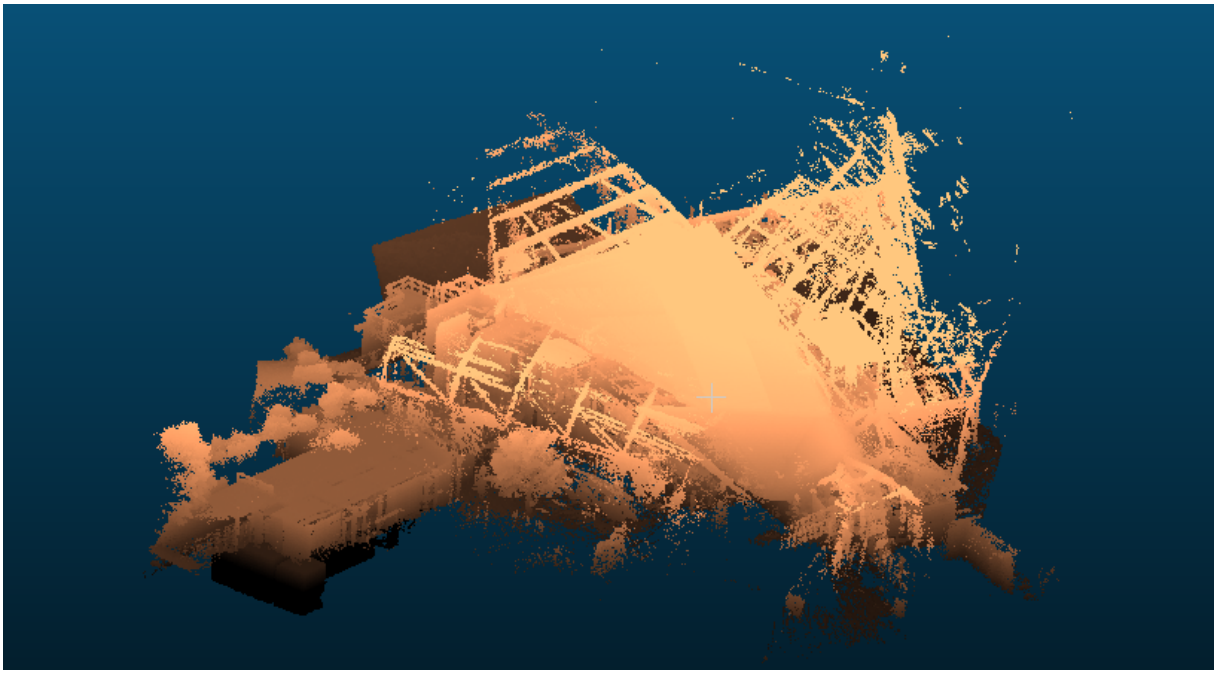

Fig 2.3 The point cloud for Hysolar building outdoors (South-West direction)

2.3 Hysolar Building indoors

The point clouds for Hysolar building indoors (see Figure 2.4-2.5) are presented as follows:

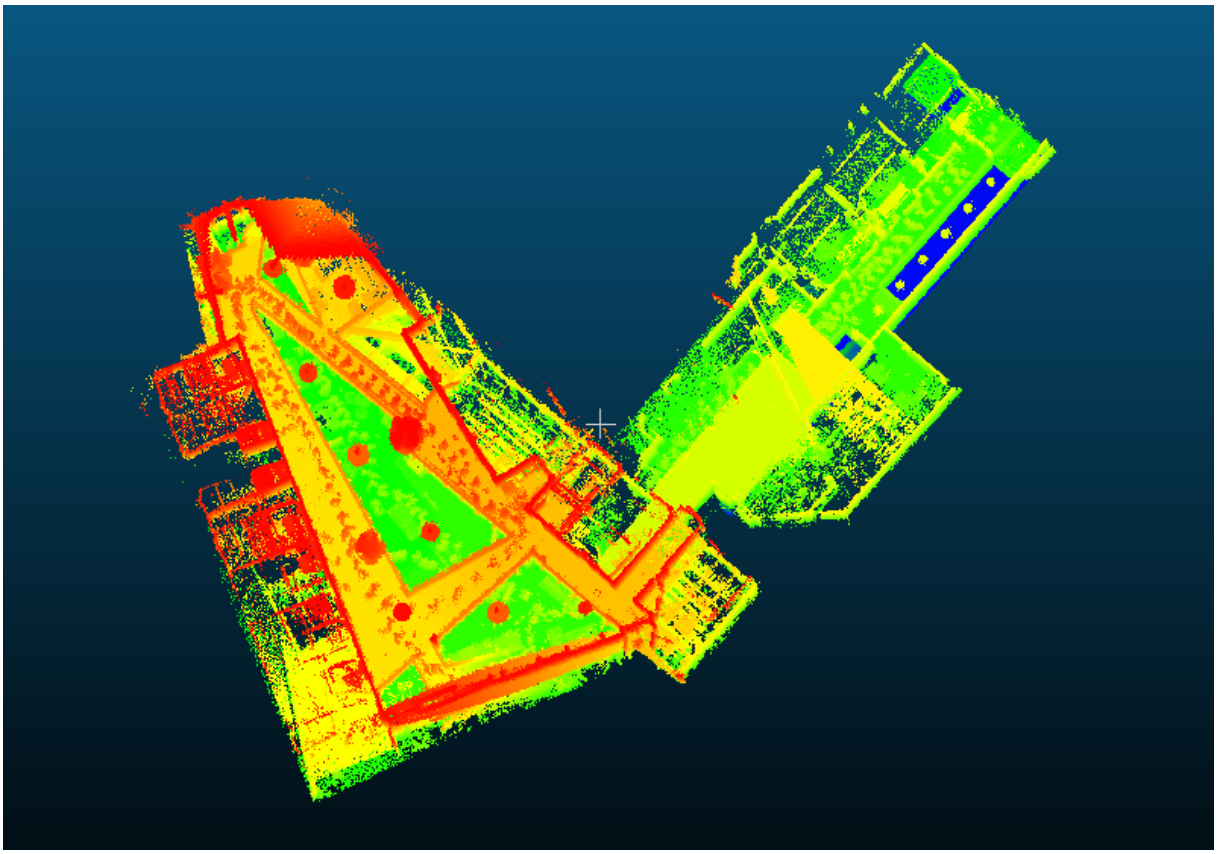

Fig 2.4 The point cloud for Hysolar building indoors (Top view)

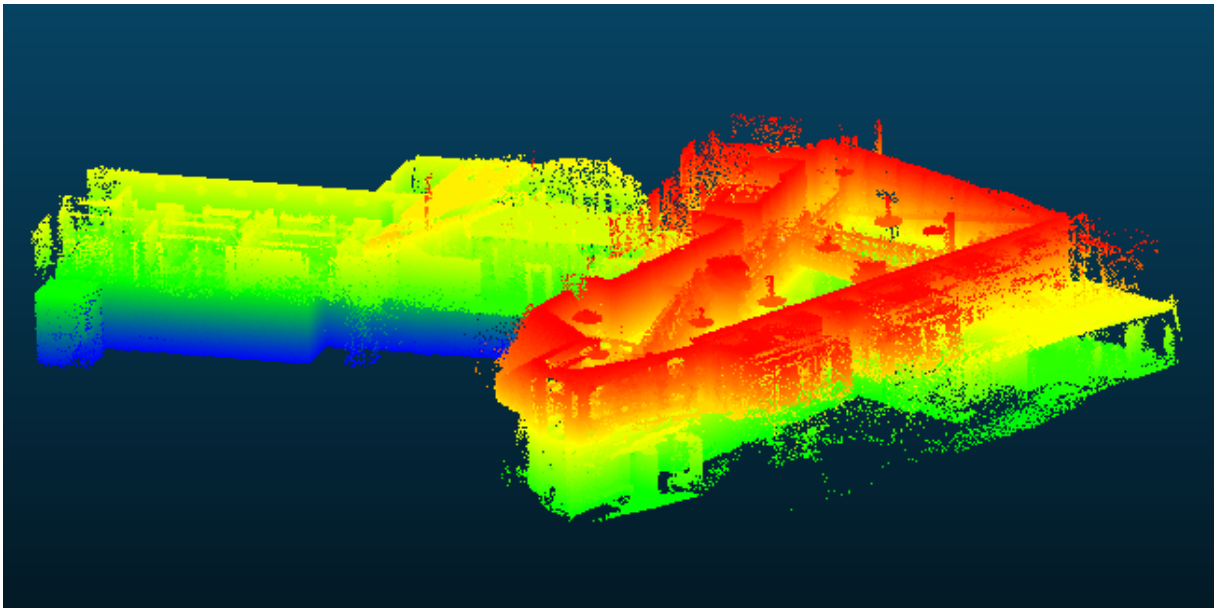

Fig 2.5 The point cloud for Hysolar building indoors (Side view)

2.4 Climbing Tower (Sports field)

The point cloud for climbing tower (see Figure 2.6) are shown as follows:

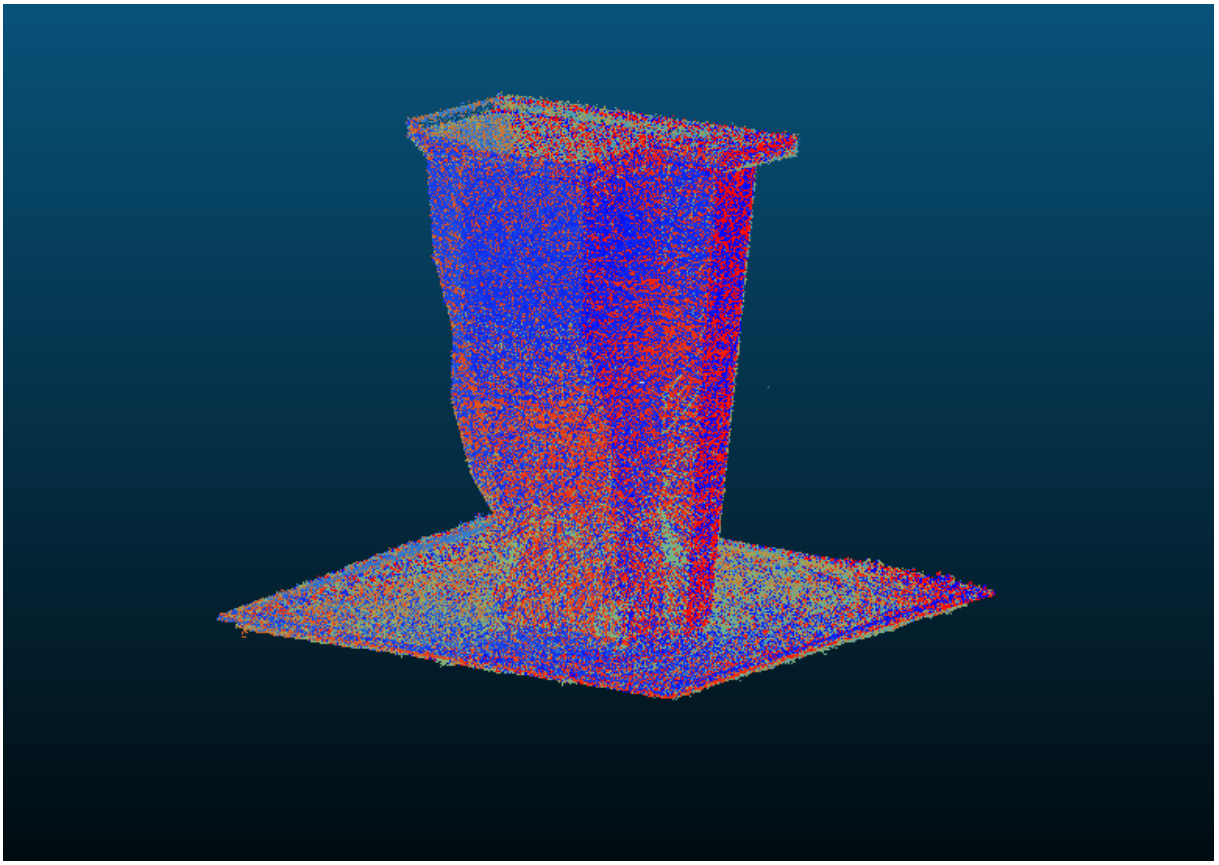

Fig 2.6 The point cloud for climbing tower

2.5 The Trajectory Along the Path outside Hysolar Building

The point clouds and trajectories (see Figure 2.7) are shown as follows:

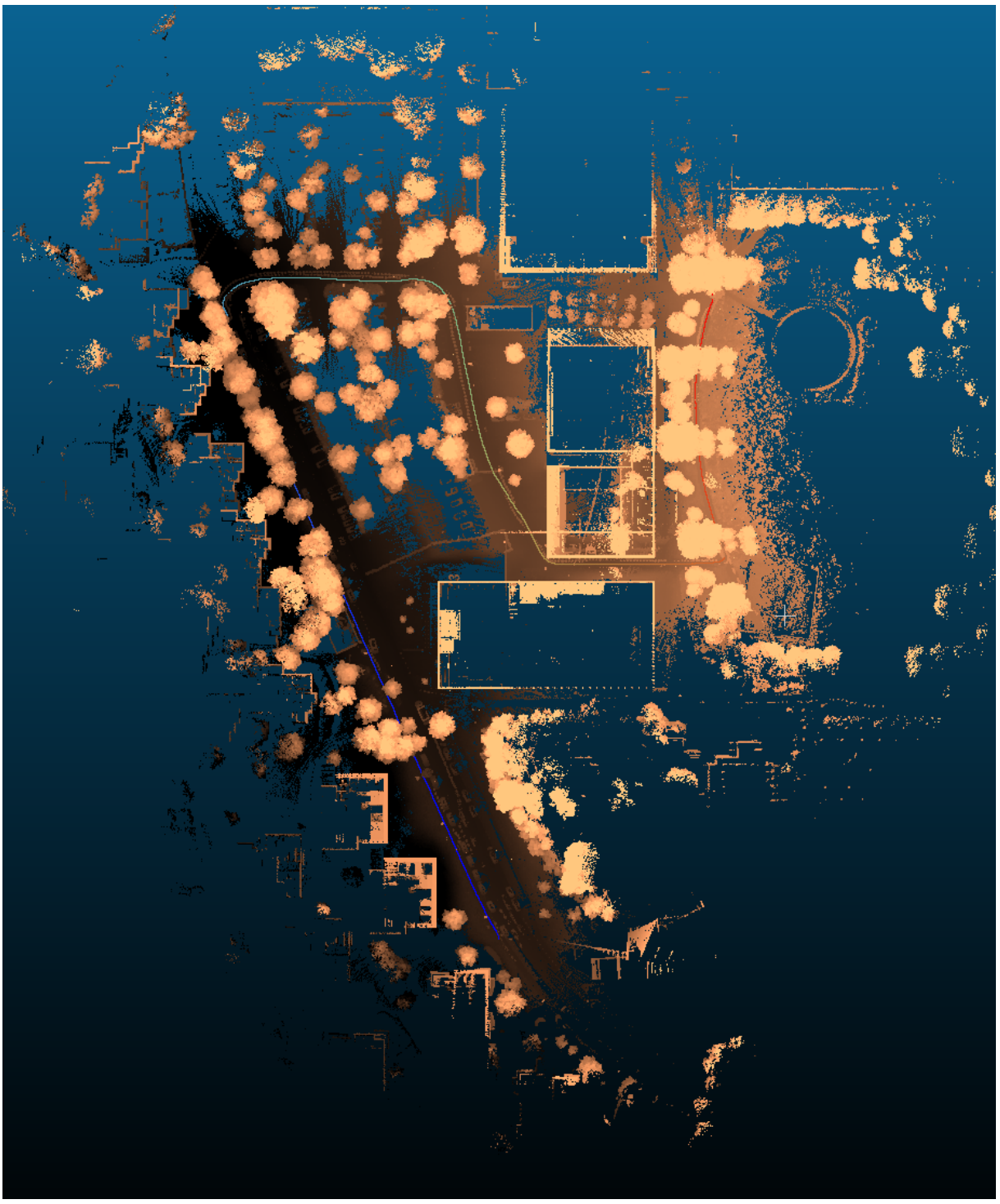

Fig 2.7 The point clouds and whole trajectory of WP 6 (the single line)

As is shown in Fig 2.7, the scanning part that is close to the Hysolar building vanished and the trajectory by the scanner is incomplete. The probable cause for such a break may be related to the instrument, likewise the connection between the scanner and data logger is unstable. But

the exact reason for the broken trajectory is impossible to verify and we should be aware that the scan can fail sometimes.

The continuous silhouette of human are also captured as a “ghost” in the view of scanner as follows,

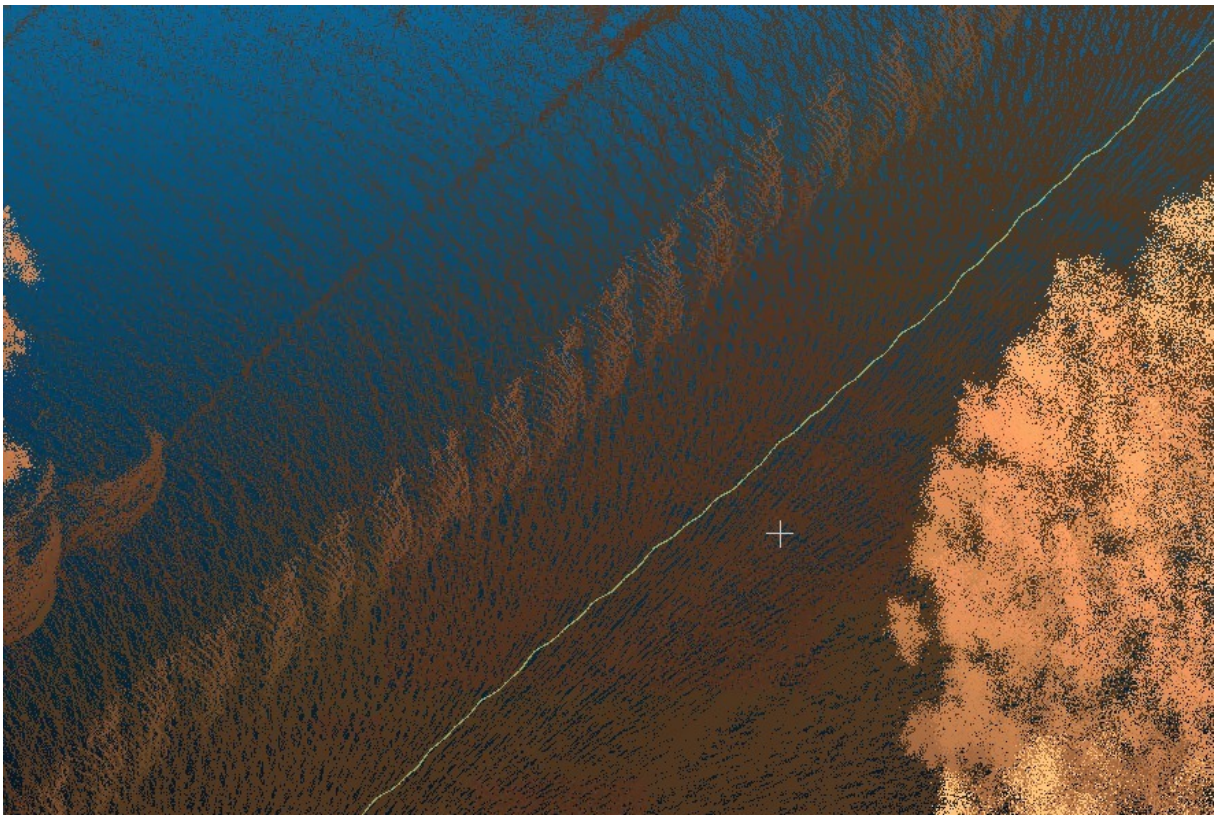

Fig 2.8 The “ghost” in the captured view (the green line represents the trajectory)

3. Visualization with Cesium

The point clouds are then uploaded on Cesium ion server to get an identity number, which can be embedded (by this visualised) on our website.

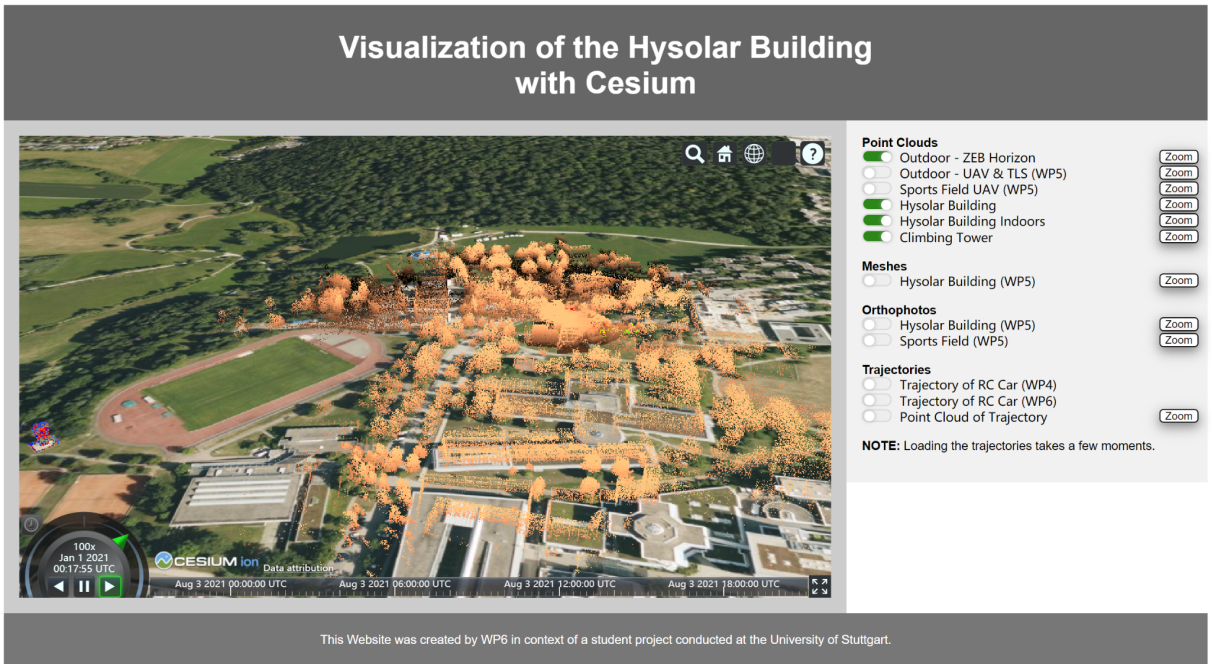

Fig 3.1 The overall display for the website

On the website, the products including point clouds, meshes, orthophotos, and scanning trajectory are available for display. The switch buttons for display of each data are set on the right side of the website page.

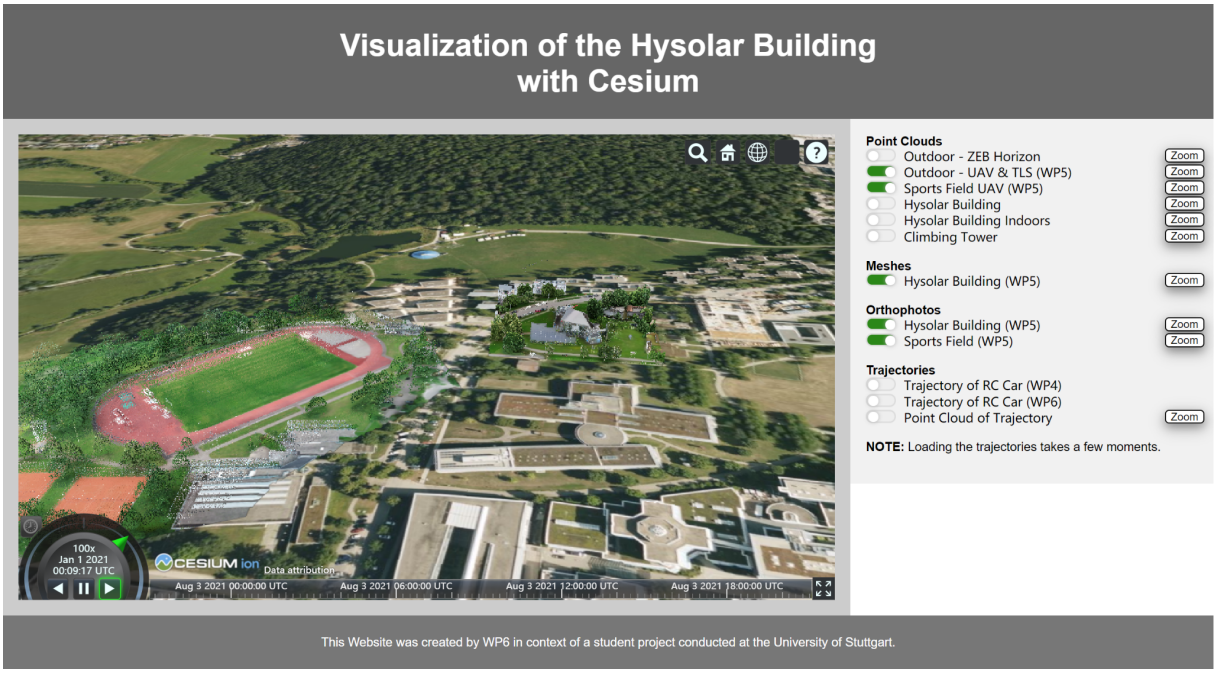

Fig 3.2 The display for all products from WP5 on the website

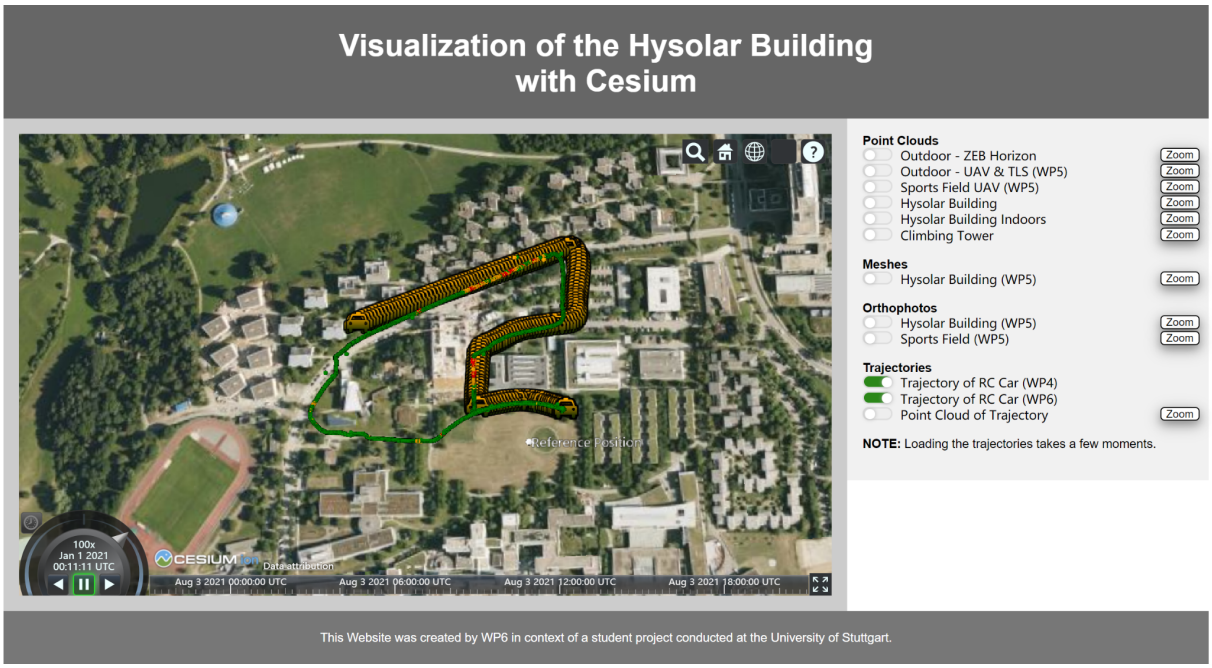

Fig 3.3 The trajectories from WP 4 (green) and 6 (orange car pattern)

Fig 3.4, Fig 3.5 and Fig 3.6 The trajectories from both WPs (zoomed in)

One of the aims is to compare the trajectories measured from WP6 and WP4. The trajectory from WP4 is measured with GNSS while the one from WP6 is collected with the mobile laser scanner. Theoretically the accuracies of two measurements should be different. The two result trajectories should have some difference. The scanning trajectory from WP 6 is accidentally broken, so it is hard to make a complete comparison. But from the trajectory that we still

have, it’s obvious to see that the trajectory of WP 6 is out of the planned path in Fig 3.5, Fig 3.6 and Fig 3.6 shown areas. The trajectory of WP 4 is always on the planned path. If the person who held the scanner was following the remote car from WP 4 as planned, then it can be said that the accuracy from mobile laser scanning is not as good as GNSS in our measurement. One reason is due to the broken scan that the georeferencing of the trajectory of the scanner couldn't be done with a good accuracy.

4. Summary

Overall, most of the point clouds generated from the scanner remain complete and clear. In the measurements that we took, the accuracy of mobile laser scanning is not as good as GNSS. But because our trajectory from WP 6 is broken, some part is missing and was georeferenced manually. So it’s not enough to draw a general conclusion about the accuracy. Learning from this situation, it’s significant to measure repeatedly. Besides, visualization with Cesium provides a direct view of the photogrammetric and navigation products.

Integrated Fieldwork 2021

WP7 – GNSS Availability Check

Supervisor:

M.Sc. Tomke Hobiger

Group Member:

Sylvia Ackermann, Laura Helber,

Aaron Ruof, Alicia Stahl, Yuke Xie

Contents

1 Introduction

With the development of GNSS technology, we are able to determine the position of the user with sub-meter accuracy at any location in real time, especially when using differential positioning, such as RTK mode, to obtain higher positioning accuracy. However, it is obvious that the accuracy of satellite positioning depends on many factors, such as the number of visible satellites, the geometric relationship between satellites and receivers, signal delay and multipath effects. How these factors affect the accuracy of GNSS positioning has always been an interesting topic.

Figure 1: Interfering factors

In order to investigate the availability of GNSS, we will conduct a test with a GNSS antenna next to the Hysolar building in Vaihingen campus of Stuttgart University, which is a complex environment and will be interesting to this experiment. There are solar panels and buildings next to the test field. Therefore, we will focus on the performance of GNSS equipment under solar panels and the visibility next to the buildings. There will be about 50 points distributed at the test site with orange point marks (see figure below) measured by WP 2 using a total station. An adjustment process will be carried out to these points by WP 2. We will use the measured and adjusted coordinates from WP 2 as a reference and compare the measurement accuracy of GNSS devices in the interfered environment to these reference coordinates.

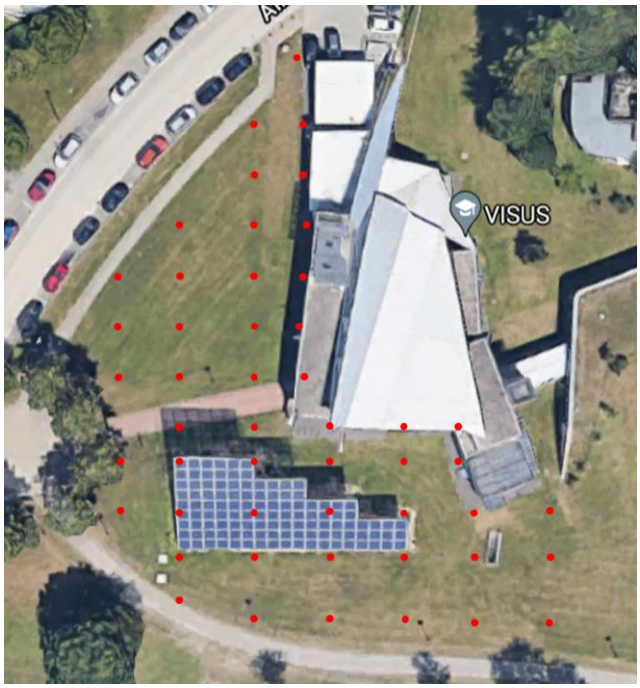

Figure 2: Area of interest

Figure 3: Point marks

Regarding to this, our group will deploy a base station in the open area (for example in the middle of the field) and pare the rover with the base station (see manual in the following chapters). All the measurements of those marked points will be obtained using RTK mode. The post processing and analysis will be done by our group using RTKLIB.

For the equipment, we will use 2 GNSS antenna from EMLID (https://emlid.com/reachrs2/) (rover & base station), and GPS, GLONASS, GALILEO constellations will be used during the measurement.

Figure 4: Base station (left) and rover (right) (Reach-RS2)

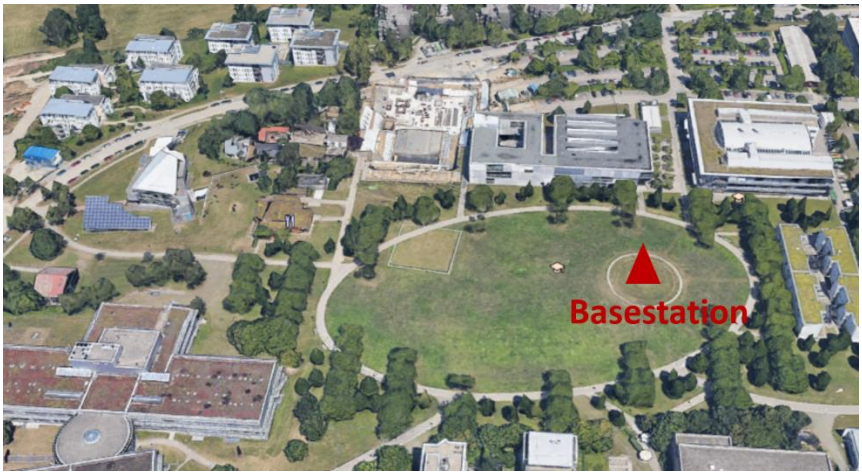

Figure 5: Ideal base station and measurements

1.1 Expected result

As a result, the UTM-coordinates of the marked points and its stochastic properties shall be derived by the measurements (in RTK mode) which are collected during the fieldwork. Furthermore, the e.g. dilution of precision (DOP), the signal-to-noise ratio or the actual obtained formal errors are expected. Finally, the coordinates and stochastic properties shall be compared against the coordinates derived from the total station measurements (WP 2). Taking the local surroundings into account, some statements on how, where and why the satellite visibility, the partial blockage of direct signals and multipath have a negative impact on the GNSS measurements and its stochastics. The results will be visualized in a heatmap where the properties of the measurements in dependence of the surroundings are presented. Our expectation is a high reflection of the GNSS-Signals by the solar panel and the walls of the Hysolar building. Therefore, multipath effects will strongly minimize the accuracy close to those elements. With increasing distance, it is likely that the accuracy of the position will be better. Tools like RTKLIB, Matlab, QGIS will be used for Analysis and visualization.

2 Post-processing

2.1 Measured GNSS-Data

During the Integrated Fieldwork all 50 points were measured by each of the nine measurement-teams with the RTK-Rover.

As a result every group delivered the following files:

- *.csv – file including the point names and measurement times
- RINEX – data of the rover (observation- and navigation-data)
- RINEX – data of the base (observation- and navigation-data)

The groups measured in the following schedule:

Date	**9 – 12 am**	**1 – 5 pm**
21. July 2021		Team H
22. July 2021	Team D	Team C
23. July 2021	Team A	Team B
26. July 2021	Team I	Team E
27. July 2021	Team G	Team F

2.2 Post-processing workflow

To receive the GNSS-coordinates of each measured point, a Matlab-code with connection to RTKLIB was used. The task of the code is to separate the point names, as well as start and end time of each measurement from the csv-file. The information is used to extract this timeslot from the RINEX-data of the rover to calculate its position. To define the processing-settings in RTKLIB a configuration-file is imported. This includes for instance information about the positioning mode (static). Furthermore, it defines, that the coordinates of the base station are read out of the RINEX-header, which have been calculated before as mean value of all base station positions.

Since every point is measured with an update-rate of 1Hz for 60s, we receive a file containing 60 positions for each point. After that all point-files of a group are imported into a second Matlab-code in order to analyze the results. Here the mean value of each GNSS-point-coordinate is calculated. This can be used to compare the GNSS-point-measurements to the reference-coordinates measured by total station. The difference between measurements and reference-coordinates is visualized in two different ways:

1. Visualization of the **coordinate-differences** in an **interpolated heatmap in Matlab**
2. Export of the **coordinate-differences** to a **kml-file** and **visualization in GoogleEarth**
   A color-scale is introduced according to the coordinate-differences, which influences the color of the pin-needles in GoogleEarth.

In addition to that we analyzed the satellite-availability. This is evaluated by calculating the difference of the number of satellites seen by the base and the number of satellites seen by the rover. This is also visualized in a **kml-Map**, where different colors symbolize the **number of satellites which are "lost" by the rover.**

Since every point is measured several times, we calculated the satellite difference for every single measurement. Each point then gets a mean satellite difference that is made of all 60 calculated differences. The result is visualized in GoogleEarth. The pin color indicates how big the satellite difference is for every point.

3 Results

3.1 GNSS-Point Quality

The quality of the measured GNSS-points is evaluated by building the difference between the GNSS-coordinates and the total station-reference-coordinates. Theoretically differences until 70 meters appeared at a few points. In order to exclude these outliers, in both visualizations only differences lower than 5 m are shown. The differences are splitted into equally spaced intervals, all differences higher than that value are set to 5 m. Finally, the heatmaps show GNSS-point quality at linear interpolated points in the area around the Hysolar buildings; in the Google Earth visualization, point differences of our measured 50 points can be analyzed separately.

3.1.1 Heatmap of the coordinate-differences

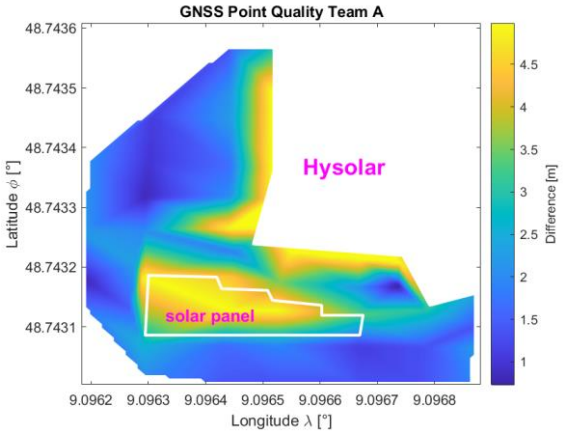

Figure 6.1:Heatmap Group A

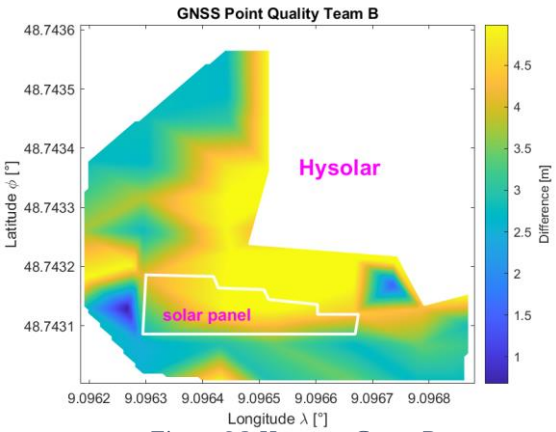

Figure 6.2:Heatmap Group B

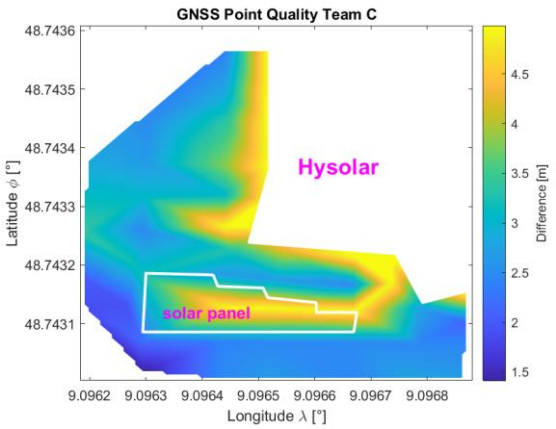

Figure 6.3:Heatmap Group C

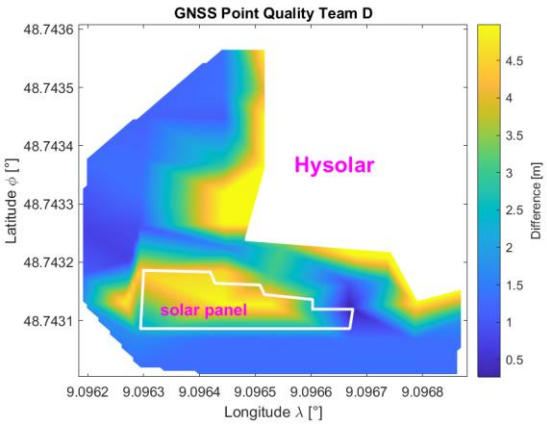

Figure 6.4:Heatmap Group D

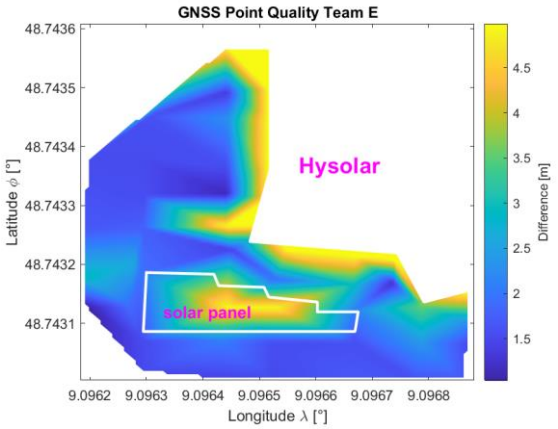

Figure 6.5:Heatmap Group E

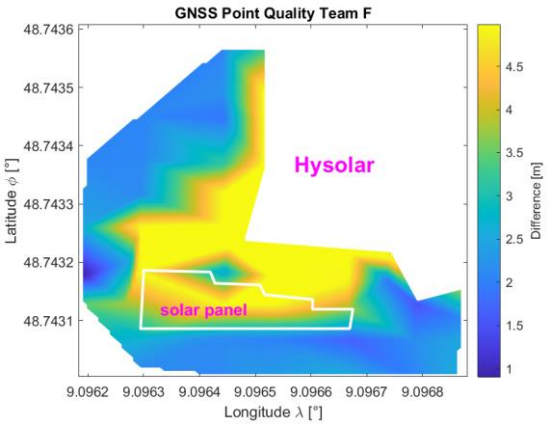

Figure 6.6:Heatmap Group F

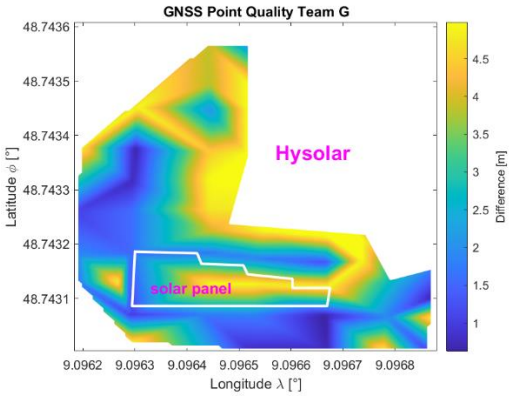

Figure 6.7:Heatmap Group G

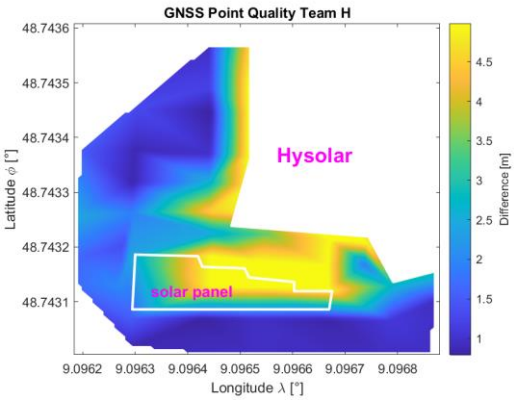

Figure 6.8:Heatmap Group H

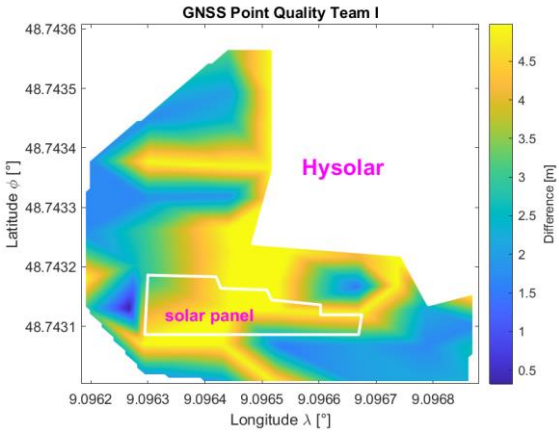

Figure 6.9:Heatmap Group I

As expected all maps show high coordinate-differences near the Hysolar-building and underneath the solar panel. These elements lead to a loss in the number of satellites, which is visualized in 3.2. Additionally here strong multipath effects appear and many signals are blocked. This way the ambiguities can not be solved and a float or single position is possible, which leads to lower accuracies.

3.1.2 Google Earth visualization of coordinate-differences

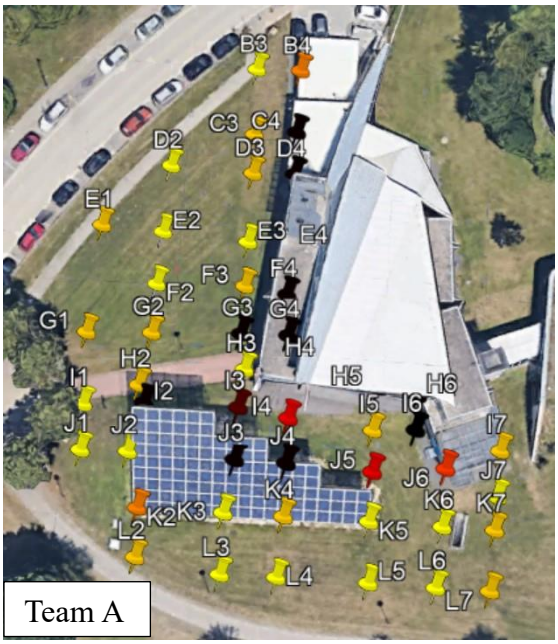

Figure 7.1 Google Earth visualization A

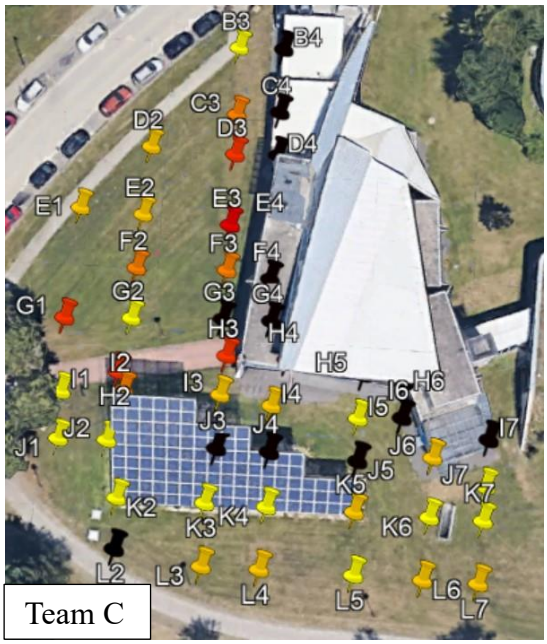

Figure 7.2 Google Earth visualization C

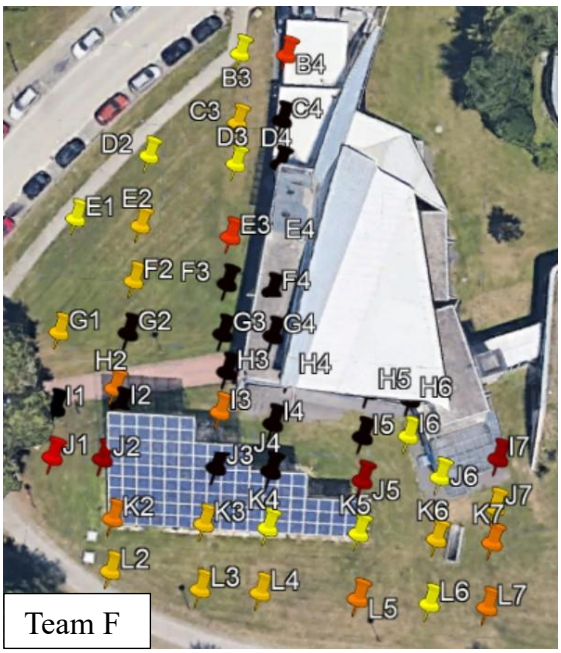

Figure 7.3 Google Earth visualization F

Figure 7.4 Legend of the Google Earth visualizations (the borders of the intervals are the result of creating 10 equal parts between Δ_{min} and 5m)

The Google Earth visualization proofs the results of the heatmap. Here single point differences can be analyzed separately. The difference to the reference-coordinates is especially high under the solar panel and next to the building (black color).

3D-View of the point quality:

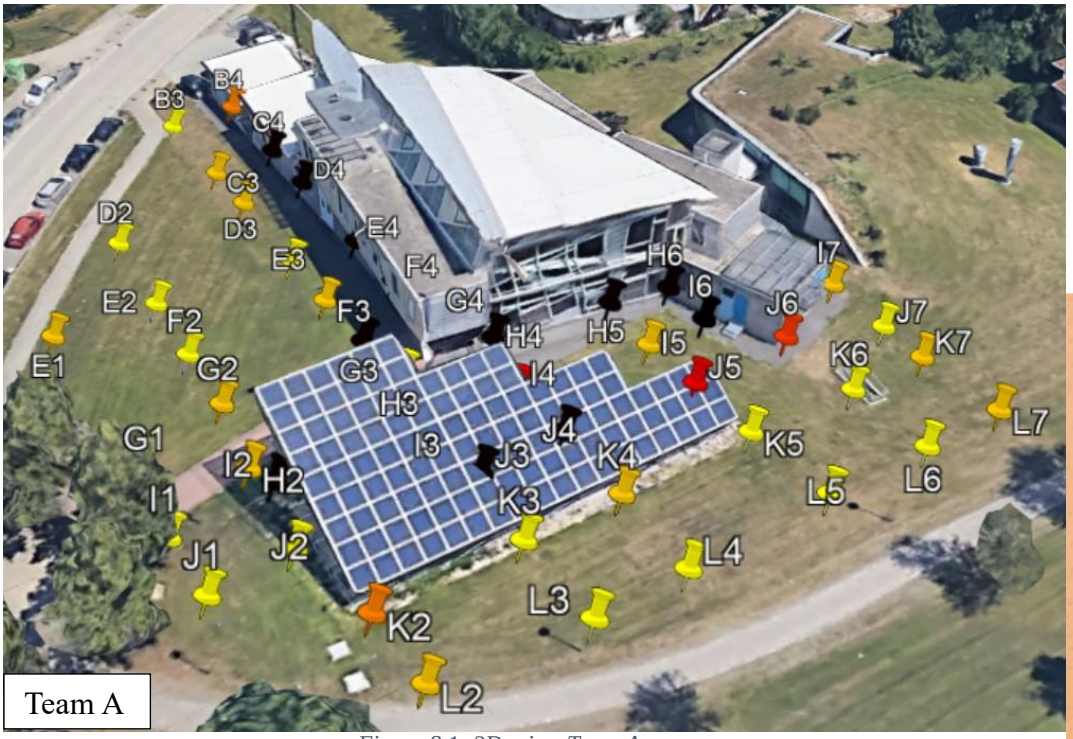

Figure 8.1: 3D- view Team A

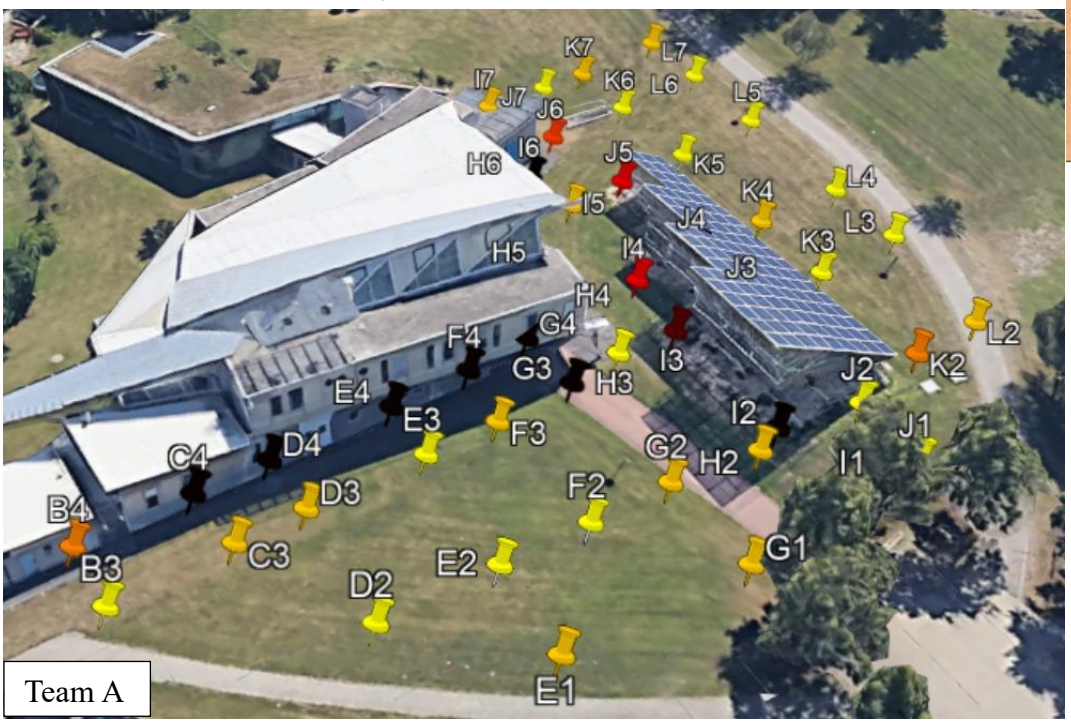

Figure 8.2: 3D- view Team A

3.2 GNSS-Satellite Availability

The satellite availability is made by comparing the number of satellites the rover and the base station can see at the same time. The number of satellites that are not visible at the rover are converted to a percentage to show the relative number of lost satellites.

Since every point measurement consists of 60 individual measurements, the mean value is calculated for every point.

For an overall value, the measurements from all groups are taken and combined to a single result. This is made of the mean over all group measurements.

The result looks like this:

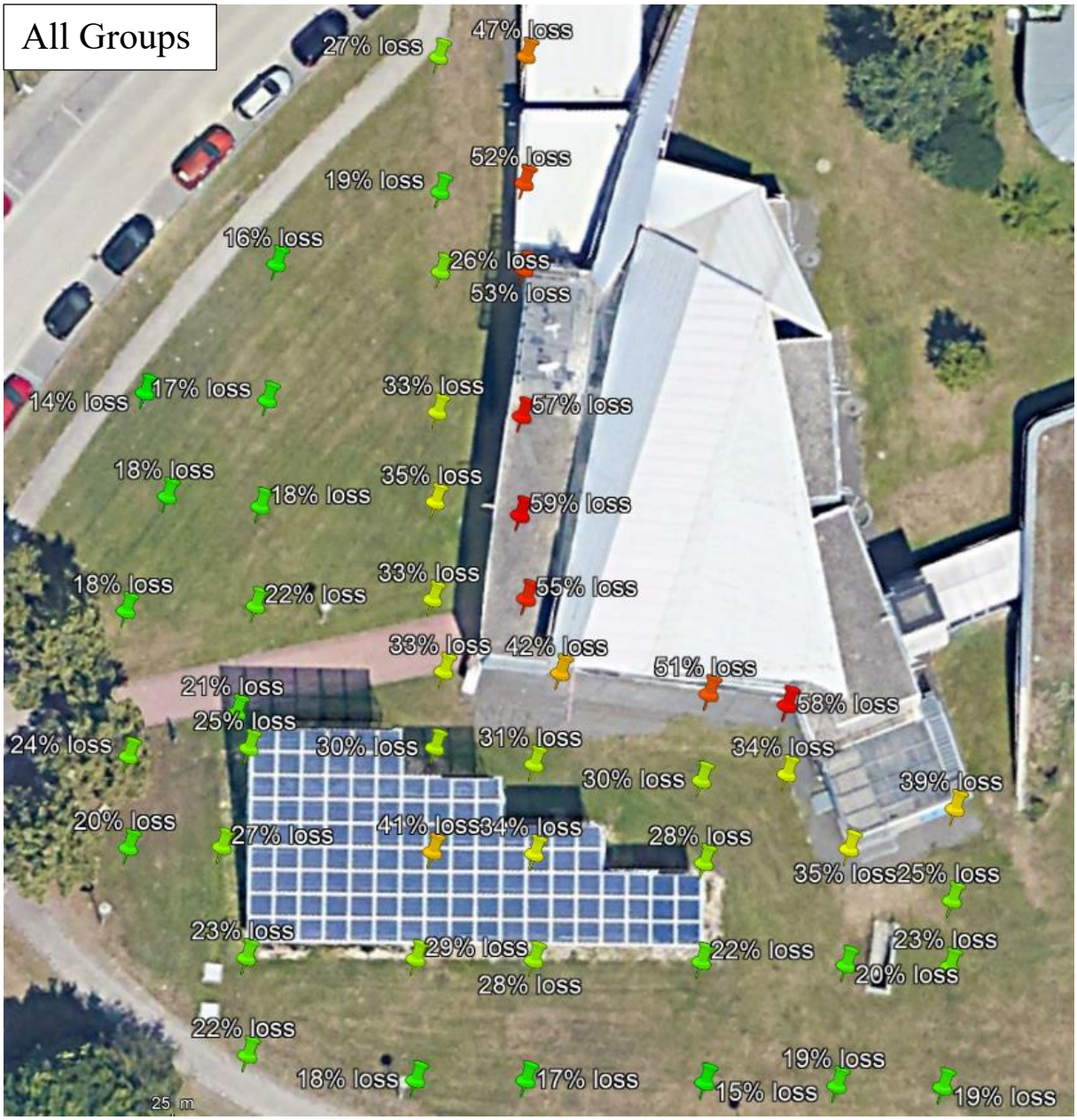

Figure 9.1: satellite availability of all groups – percentage is with regard to the number of satellites visible for the base

As supposed, the closer a point is to the building, the worse is the satellite availability. If a point is surrounded by walls on multiple sides, the satellite availability is bad. The influence of the solar panels can be seen, too. The satellite availability for the points near or under the panels is nearly as bad as if the point is close to a wall.

Overall, the map shows the result one would expect at this site: The points in the grass field without surroundings have the best satellite availability. As closer a point is to a disturbing object like trees, buildings, solar panels, the worse the availability gets.

Nevertheless, the difference between the groups is huge. While some groups have points with zero lost satellites, other groups have no point below 40% lost satellites. Corresponding, their maximum of lost satellites is over 80% while others don't get over 56% lost satellites.

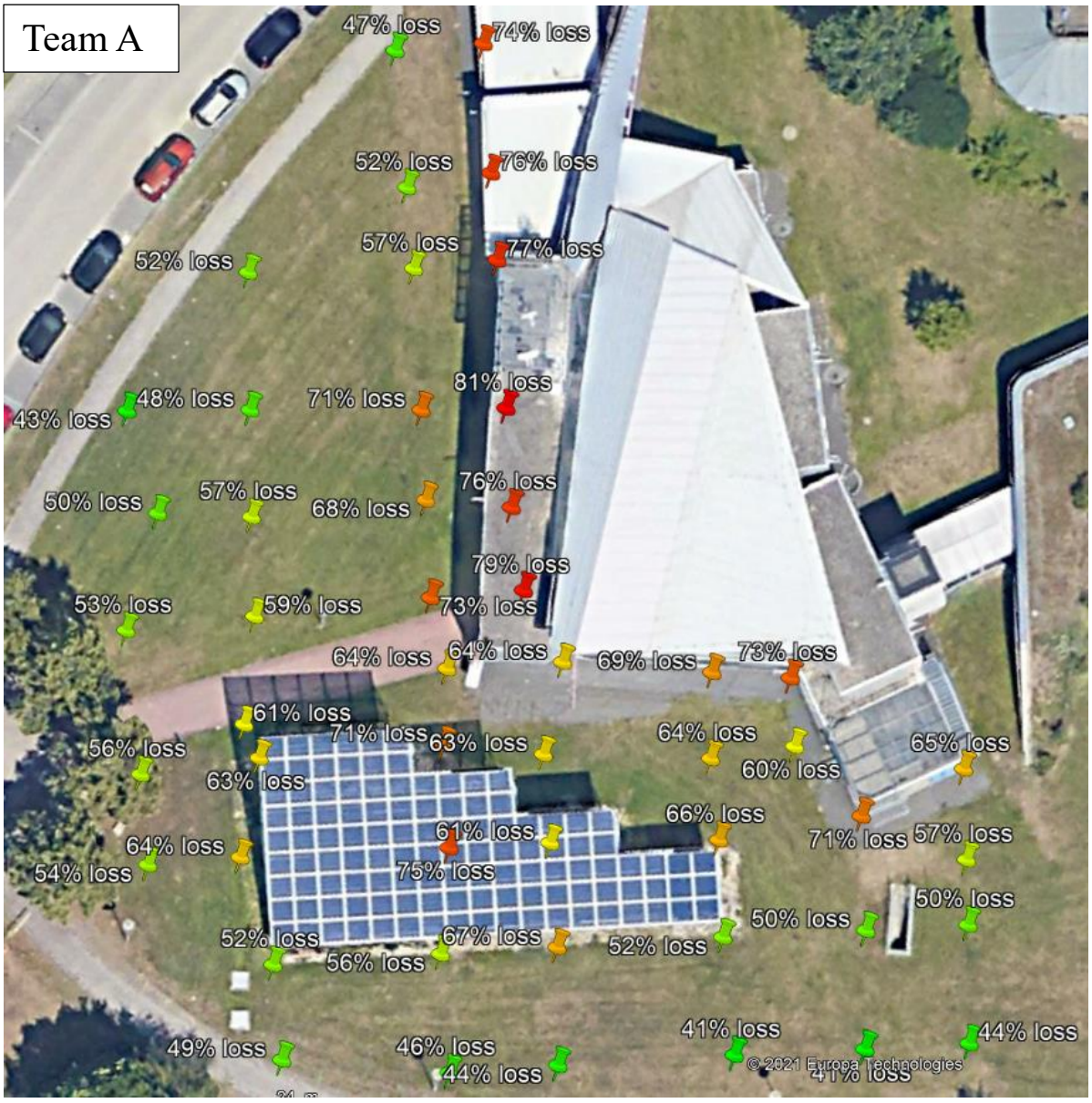

Figure 9.2: satellite availability group A

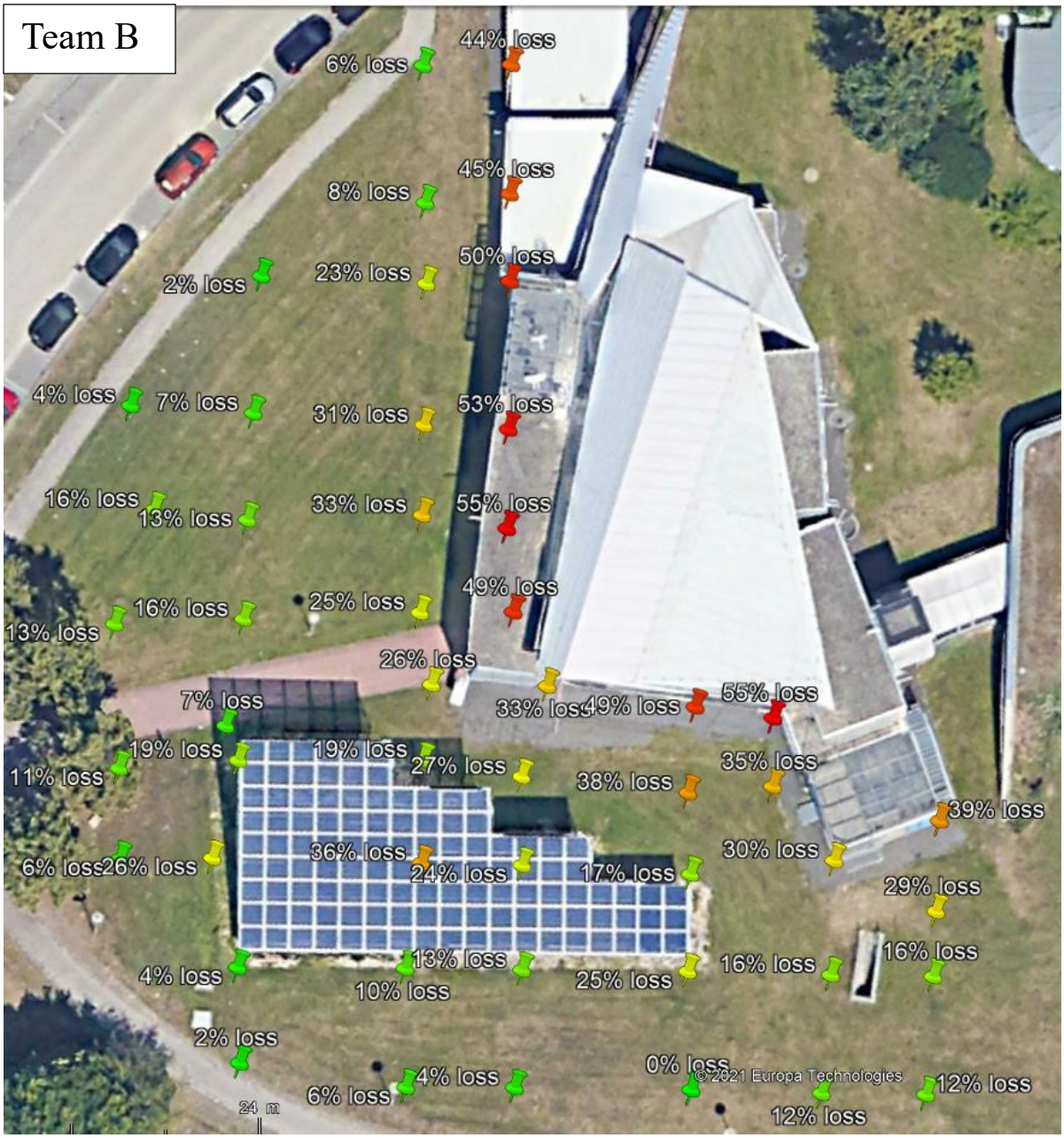

Figure 9.3: satellite availability group B

By Comparing the satellite availability with the coordinate differences, one could see they correlate in a negative way: The less satellites are available, the worse the coordinate differences become. However, this is only true within one group measurement. Comparing Group A and B, while the overall satellite availability from Group A is worse than from Group B, their point differences are actually lower than those from Group B. This can be explained with the satellite configuration. If the satellite signals are close to the horizon, they can be seen by the base station, but not at the rover. Therefore, the rover has a bad satellite availability, but not necessarily a bad measurement. Multipath effects are much more important, as they make bad measurements without being visible in the satellite availability.

3.3 Conclusion

During the integrated fieldwork, our working package set up 50 points around the Hysolor building in the campus, and 9 measuring groups measured all these 50 points using RTK mode on several days. Our working package did the post-processing and analyzed the quality of all the 50 points. We compared the distance difference between the GNSS measurement and the true coordinates measured by WP2, and compared the visible number of satellites between the rover and the base station for the measurement of every second.
In conclusion, as the visualization shows, the positioning accuracy of GNSS measurement depends on a lot of factors, e.g. multipath effect, satellite visibility and atmospheric influence etc. The positioning accuracy using RTK method (cut-off angle: 15 degrees) can reach the accuracy of tens of centimeters, but sometimes can go up to 70 meters depend on the surrounding.
Generally, the points in the open air area have better satellite visibilities and also better accuracies. However, due to the multipath effect from the glass building and the low satellite visibility at some certain positions (the corner of the building, the points under the solar panel and the eaves), the positioning becomes relatively inaccurate.
Through the integrated fieldwork, we understood how to setup the base station and how to do quick measurements using RTK mode. And through post-processing, we learned how to process GNSS data using software and scripts, interesting visualizations were also generated on the map. And last but not the least, we understood the importance of choosing the correct surroundings to do the measurement through investigating the influence of multipath effect and the blockage.
Special thanks should go to supervisors and all the measurement groups.

Figure 10.1: Low accuracies and number of satellites due to strong multipath effects and high signal blockage near the Hysolar building.

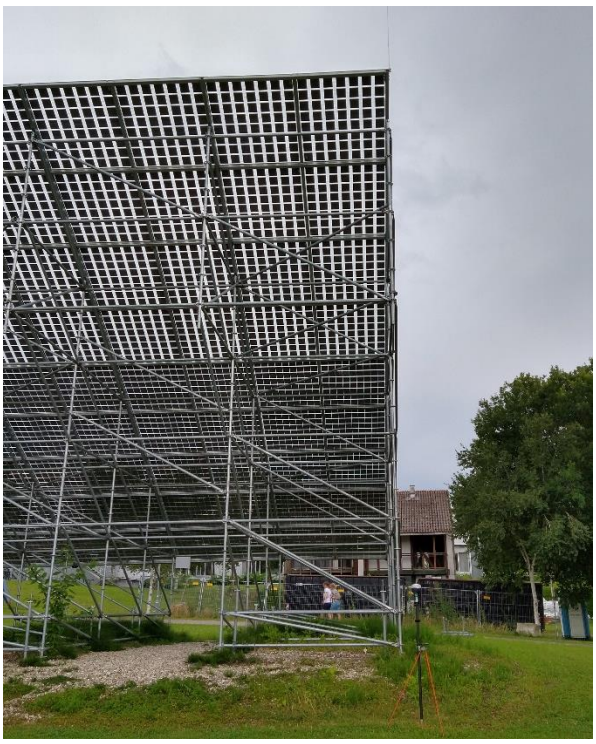

Figure 10.2: Signal blockage underneath the solar panel

Figure 10.3: Base station receives undisturbed signals in a free field with no blockage

Integrated Fieldwork 2021

WP 8:
Profile Measurement by Gravimetry

Supervisor:
Dipl.-Ing. Ron Schlesinger

Team Members:
Florian Josephowitz
Tim Kassulat
Edward Necsulescu
Frieder Schmid

August 2021

Table of contents

1. Introduction

1.1. WP8 aim

This work package deals with gravity observations. The aim is to get an overview about the absolute gravity, gravity anomalies and the gravity gradient in the work area (sports field) for ILA (*Institute of Aircraft Propulsion Systems*). ILA is planning on conducting a high precise pressure sensors which also requires the following prerequisites: map of absolute gravity values (a grid of measured points-relative gravimetry, connection of the grid to the national survey-net of gravimetry). Figure 1 shows the study area:

Figure 1. Study area of the working package 8.

1.2. Instrument - Gravimeter Scrintrex CG5

The instrument was used to measure the relative gravity values with a time resolution of 6 Hz. When the gravity values were determined in the field, different corrections were applied to these. There is an automatic tilt compensation working with an electronic tilt sensor. Exact time and location were used for a tide correction directly inside the instrument.

For our task each point was determined in 3 sessions with a duration of 1 minute over every point. The instrument calculates the mean of 57 seconds and takes 3 seconds for saving.

2. Data Acquisition

The grid points were staked out previously to the starting date of the working package. For the final map with absolute gravity values, one reference point with known gravity was used, and a regular grid with a distance of 8 meters between the points was measured. Surrounding two special points of the grid, measurements were densified (2 meters between points instead of 8).

At these two points an exact measurement of the gravity gradient was conducted. During the gravity gradient measurements, determinations were performed at different heights over the same special point.

The final shape of the grid is presented in Figure 2:

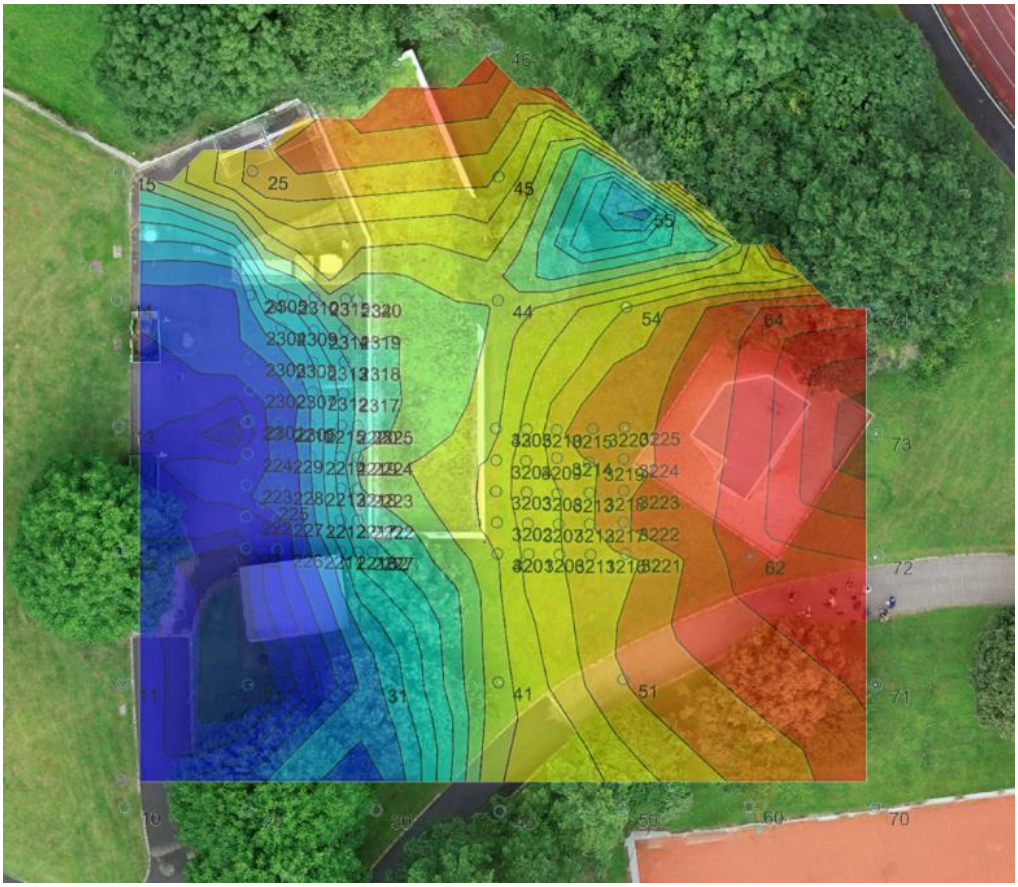

Figure 2. Measured grid points

Besides the measurements with the gravimeter, for each point it was necessary to fill in the specific information in the provided field-book: point ID, instrument height, time of acquisition. The atmospheric pressure was measured at the beginning of each session once. Most of them were necessary in the processing of the data in the later steps.

3. Preprocessing

The preprocessing part consisted in the actual transformation of the field-book data into digital data (*Microsoft Excel Table*). These tables are a necessary input for the *Matlab* function. Moreover, it was also important to organize the data per measurement sessions and to correlate them with the output files from the instrument.

The final result of the preprocessing was a general output file from the instrument with all the measured points of the working package, and also the corresponding points in the Excel tables (converted field-book). The whole workflow of the preprocessing section can be seen in Figure 3:

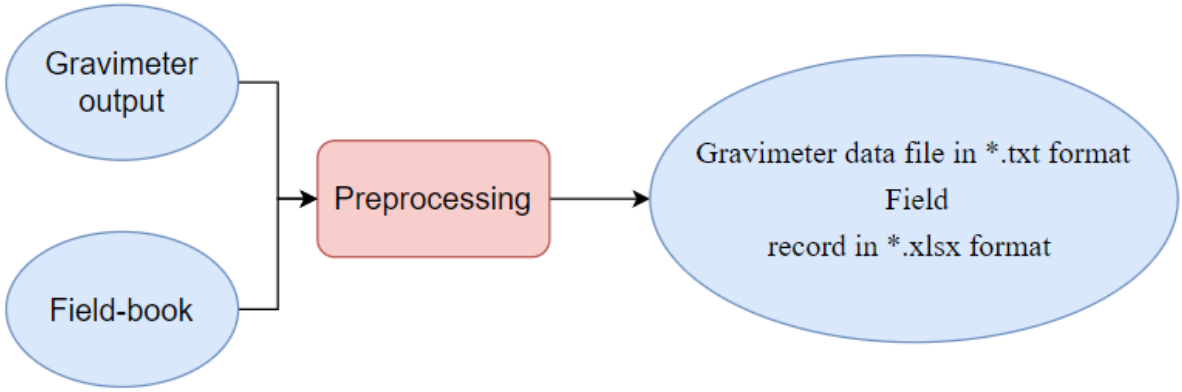

Figure 3. Preprocessing workflow.

The toolbox has five main functions: data selection, adjustment, gravity gradient computation, gravity visualization and calibration. To realize these functions, two files are needed:

- Gravimeter data file in **.txt* format (produced from gravimeter)
- Field record in **.xlsx* format with specific content, based on field book (optional), presented in Figure 4:

PtID	Line	Point Type	Instrument Height [m]	pressure [mbar]	absGrav [mGal]	FAgrad [mGal/m]	DHHN [m]	stdDHHN [m]	X [m]	Y [m]	lattitude [degree]
1000	1	0	0.459	931		-0.308	800		NaN	NaN	48
701	1	0	0.474	931		-0.308	717.696		3521777.977	5372312	48
702	1	0	0.513	931		-0.308	717.919		3521776.93	5372308	
703	1	0	0.514	931		-0.308	718.071		3521775.398	5372303	
704	1	0	0.518	931		-0.308	718.311		3521773.861	5372298	
705	1	0	0.517	931		-0.308	718.322		3521771.905	5372294	

Figure 4. Example of field-book data.

where:

PtID: Point identification (if identical points have different heights, they should have different "*Line*" numbers)

Line: Line number of the measurement, the same "*PtID*" with different "*Line*" indicates the movement of gravimeter, not continuously measuring

Point Type: 0 means common measurement, other positive integers specify the gradient

measurement on that identical point but with different instrument height (the same "*PtID*" with the same positive integer of "*Point Type*")

dh [m]: The height from the top of the gravimeter to the ground

pressure [mbar]: Air pressure

absGrav [mGal]: Absolute gravity of the point (on the ground)

FAgrad [mGal/m]: Free air gradient

DHHN [m]: Height of the point (on the ground) above sea level, height system does not matter

stdDHHN [m]: Standard deviation of "*DHHN*", if nothing filled in, the default value is 0.02 m

X [m]: Horizontal coordinate of the point, used for gravity visualization (Gauss-Kruger coordinates are preferable, but also local coordinates are possible)

Y [m]: Horizontal coordinate of the point, used for gravity visualization (Gauss-Kruger coordinates are preferable, but also local coordinates are possible)

Latitude [degree]: Latitude of the point, used for visualization of Bouguer anomaly

4. Processing

The flowchart of the processing part is illustrated in Figure 5, where all the performed steps of the MATLAB Gravimeter Toolbox are presented.

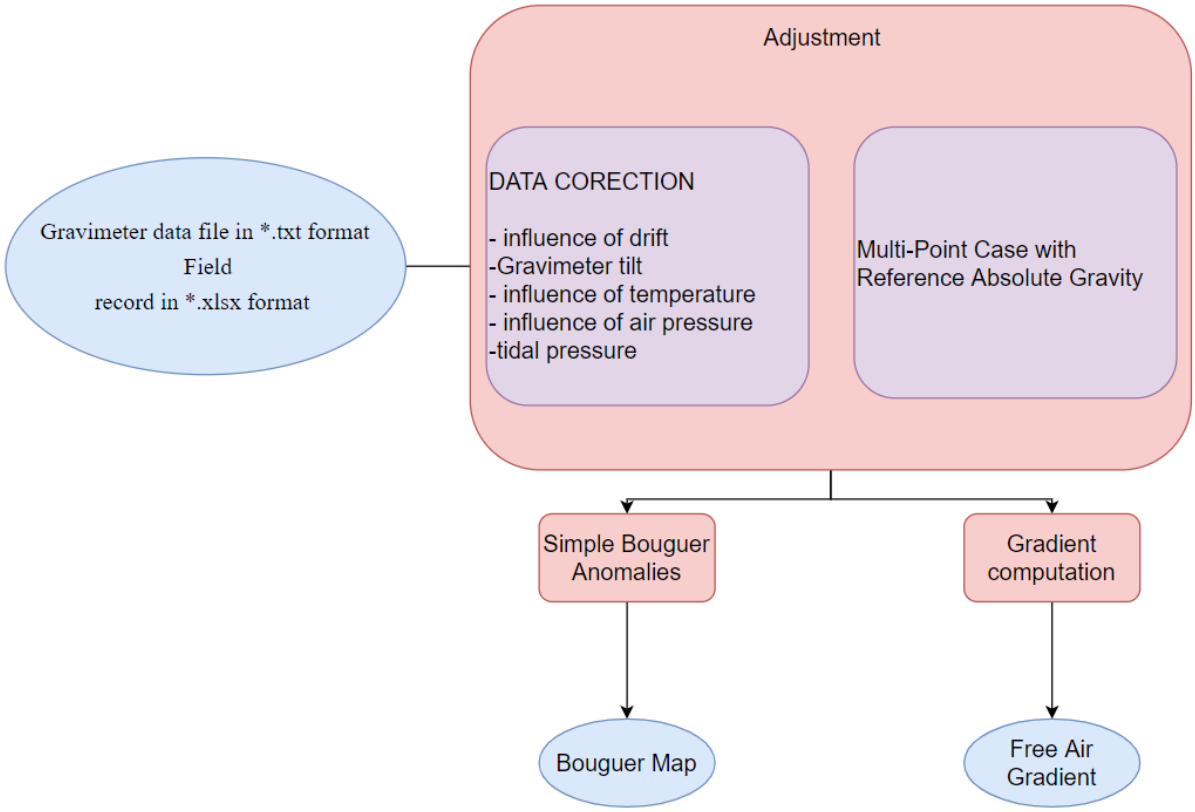

Figure 5 Processing part work flow.

4.1. Multi-Point Case with Reference Absolute Gravity

In this case, the measurements are performed on more than one point and the user has the reference absolute gravity of one or more points. There are several parameters (e.g. the drift and its precision) estimated via least squares adjustment with constraints.

4.2. Simple Bouguer Anomaly

For gravity visualization, the user can choose to obtain a figure of Bouguer anomalies if the required data are in the field record. Bouguer anomaly is a gravity anomaly, which reflects the density contrast of the anomalous masses with respect to normal density (*Blakely, 1996*). It is the gravitational attraction remaining after correcting the measured vertical component of of that point for: (a)normal gravity of the latitude of the point; (b) the free-air correction; (c) the Bouguer correction; and (d) the terrain correction (Encyclopedia.com, 2017, [3]). In this toolbox, as we cannot obtain the terrain model for the real measurement site, we determine only the simple Bouguer anomalies, which ignores the shape of the topography, regard it as a homogeneous slab.

Here is the equation of simple Bouguer anomalies:

$$\Delta g_{sb} = g_{obs} - g_0 - g_{fa} - g_{sb}, \tag{4.2.1}$$

where:

g_{obs} = gravity measurement
g_0 = theoretical gravity
g_{fa} = free air correction
g_{sb} = simple Bouguer correction

4.3. Gradient Computation Method

The gradient is computed as the difference of the absolute gravity values determined for the same point but at different heights over the point, divided by the height differences. The equation to calculate the gradient of two point P1 and P2 is:

$$grad = \frac{g_1 - g_2}{h_1 - h_2}, \tag{4.3.1}$$

where:

g_1, g_2= the absolute gravity value for the determined point
h_1, h_2= the height of the instrument

5. Results and conclusions

5.1. Bouguer Anomaly map

The Bouguer anomaly is a gravity anomaly, which reflects the density contrast of the anomalous masses with respect to normal density (*Blakely, 1996*). Therefore, the map reflects the density contrast of the anomalous masses in the study area compared to the normal density.

The obtained Bouguer anomaly map is presented in Figure 6.

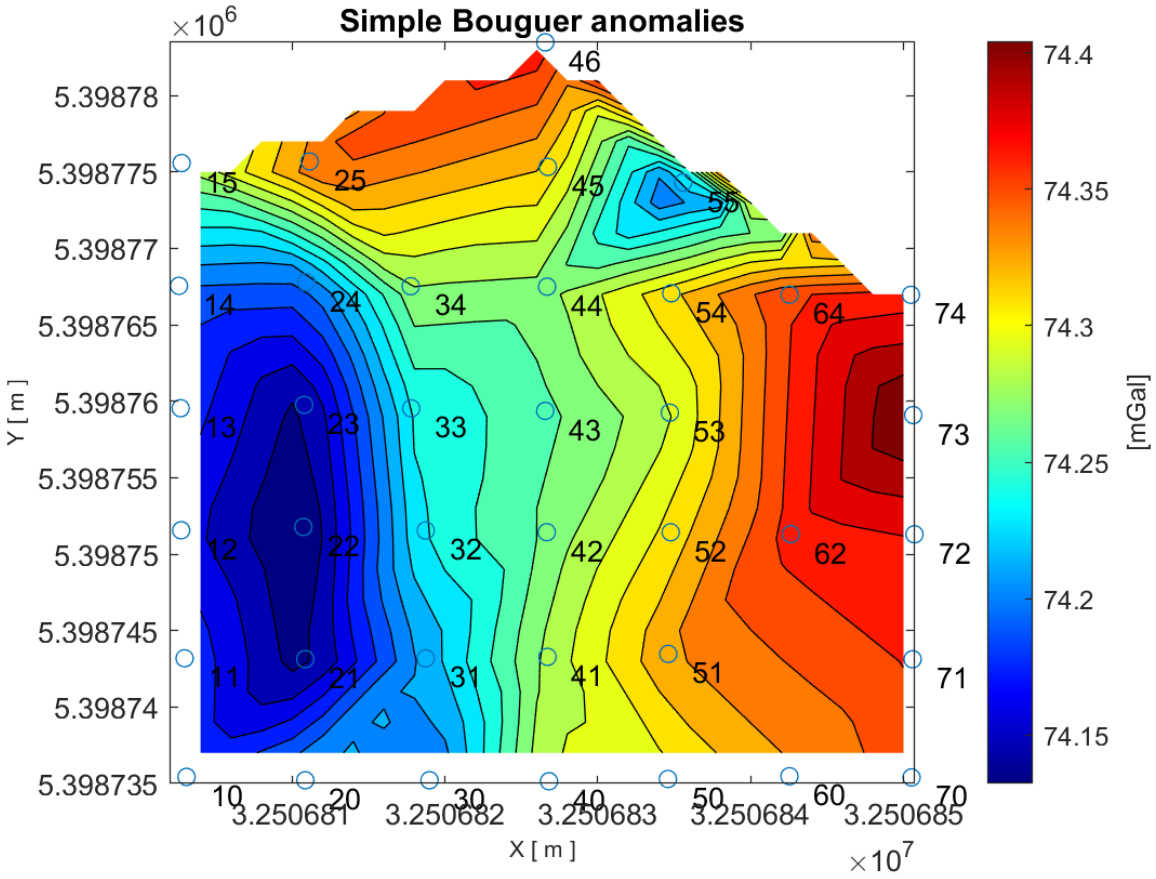

Figure 6. Bouguer anomaly map of the study area.

In order to interpret the results shown in Figure 6, we would like to start from the following known statements: the garage lies between the alignment 32-33-34-25 and 42-43-44, the climbing tower is situated in the area enclosed by points 52-53-54-64-62-52, the area enclosed by points 11-12-13-14-24-23-22-21-11 represents the zone where the drainage and sewage pipes are located.

We can see that the smallest values are registered in the area where the drainage and sewage pipes are located, in this parts there are many voids occupied by the hollow parts of the pipes. This thing is reflected in the lack of masses which is shown in the Bouguer map. Moreover, on the alignment 31-32-33-34 we can observe that the values increase a little due to the fact that the underlying layers do not contain pipes anymore and we approach the foundation of the garage.

In the zone occupied by the garage the anomaly values are higher than in the previously mentioned drainage and sewage pipe zone. This can be accounted to the masses of concrete and metal in the foundation and structure of the building. An important thing to be mentioned here is that the building itself has many hollow parts (rooms), this is the reason why the difference compared to the area where the pipes are, is not that big. We need to mention the fact that these are just interpretations and guesses because we do not have measurements over the garage.

If we move more towards the climbing tower we notice that the anomaly values will increase and we also reach the area where the maximum values are reached. The reason behind this is that we move uphill (we are at a higher point then the garage or the pipes area and we

have an extra layer of masses which represents this height difference) and the nature of material changes. We have compact soil and also gravel which would increase the amount of masses. It could also be that the density values used in the Bouguer corrections were not representative enough for the masses in this area.

The lower anomaly values from the rectangle composed by points 44-45-55-54 could be due to a cavity which belongs to the building (small storage room or small drainage basin), or an error in the measurements.

In two special areas the grid was densified (2x2 m), and the Bouguer anomalies in the densified areas are presented in Figure 7 and Figure 8.

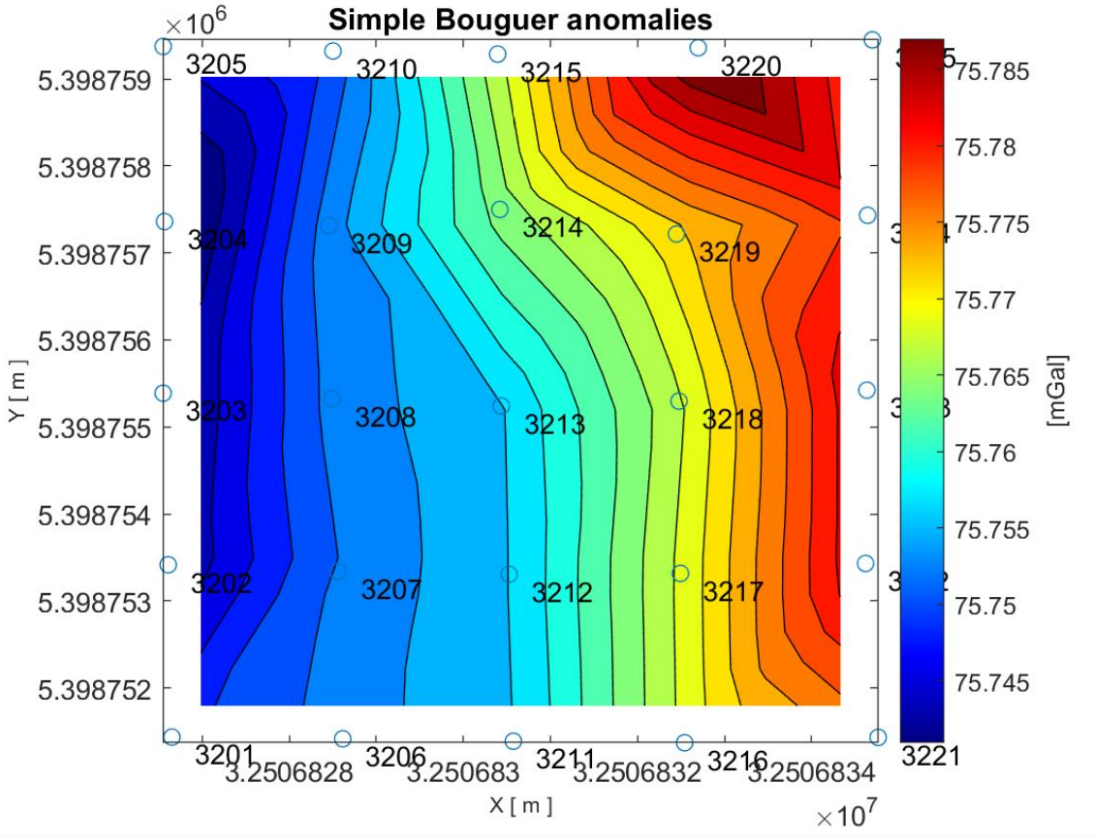

Figure 7. Bouguer anomalies in the densified area right behind the garage.

This densified grid represents the crossing from the garage to the climbing tower and is marked by intermediary anomaly values, this could be due to the fact that some lighter materials were used right in the surrounding of the building in order to prevent water infiltration. Therefore, here we see a stepwise transition from lighter materials to a heavier soil and gravel. Furthermore, the garage is filled with air, this means that there are less masses pulling down.

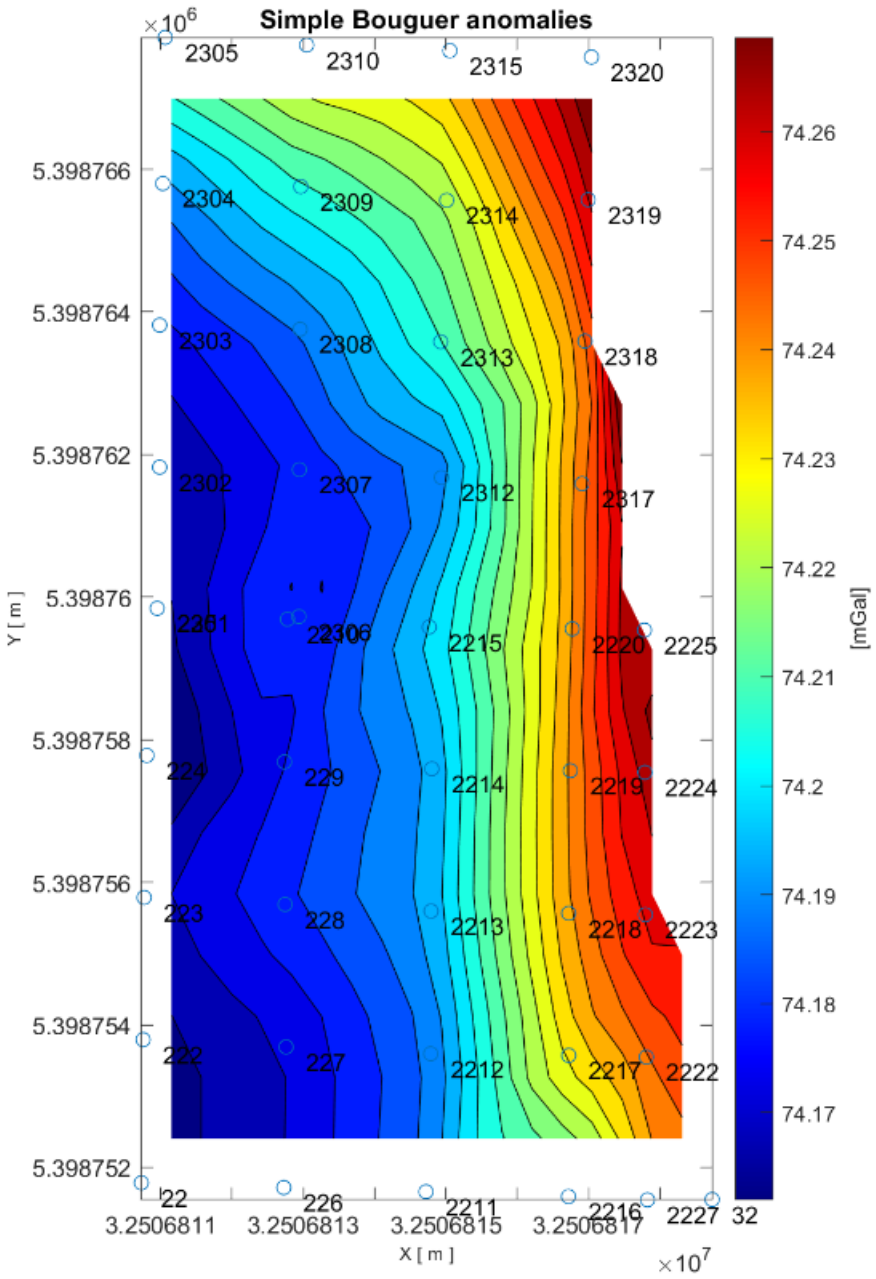

Figure 8. Bouguer anomalies in the densified area in front of the garage.

In Figure 8 we can distinguish the building shape, the straight red lines which also follow a leftwards twist (a real twist in the building) in the upper part of the map. This anomaly map also confirms the fact that the concrete and metal used in the foundation and structure do account for higher anomaly values than for the surroundings in the front part of the garage.

One of the finalities, which is related to the Bouguer anomalies, is the obtained absolute gravity values for the study area. Results are presented in Figure 9.

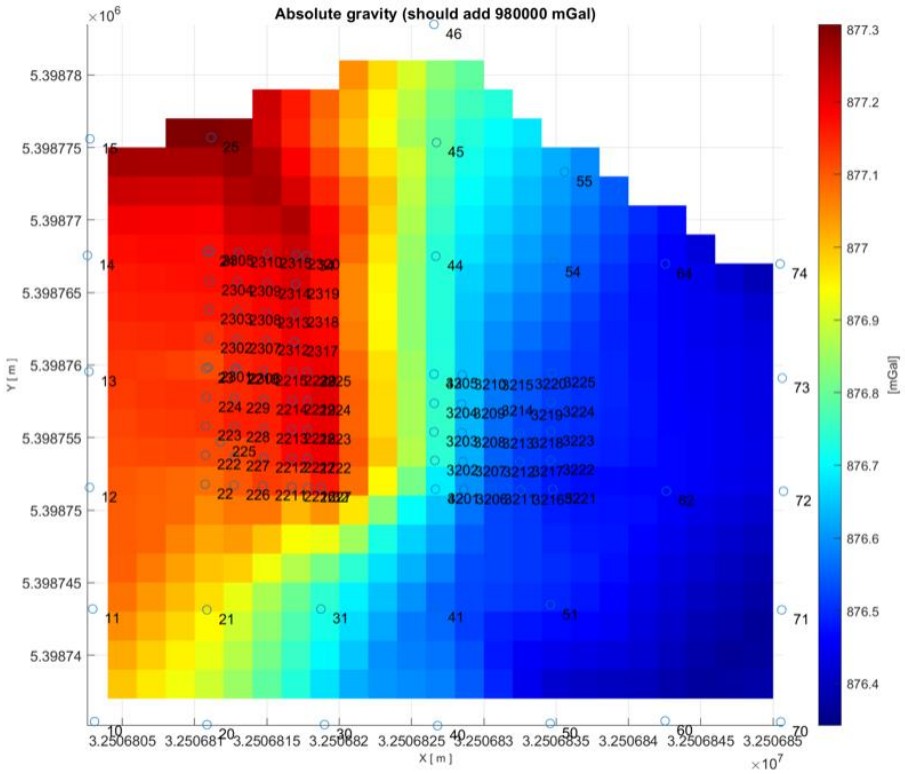

Figure 9. Absolute gravity map of the study area

5.2. Gravity gradient determination

The gravity gradients were determined over two points, each one from different densification grid. Namely, we have 2213 and 3213. The obtained gravity gradients are presented in Table 1 (each value is a result of many adjusted observations), while Figure 10, Figure 11 and Figure 12 present the adjustment errors and standard deviation for each component measurement in particular.

Table 1. Determined gravity gradients.

Point ID	Measurement day	Position [up/down]	Gravity gradient [mGal/m]	Precision [mGal/m]
2213	1	down	-0.27	0.02
		up	-0.24	0.01
3213	2	down	-0.35	0.02
		up	-0.30	0.03

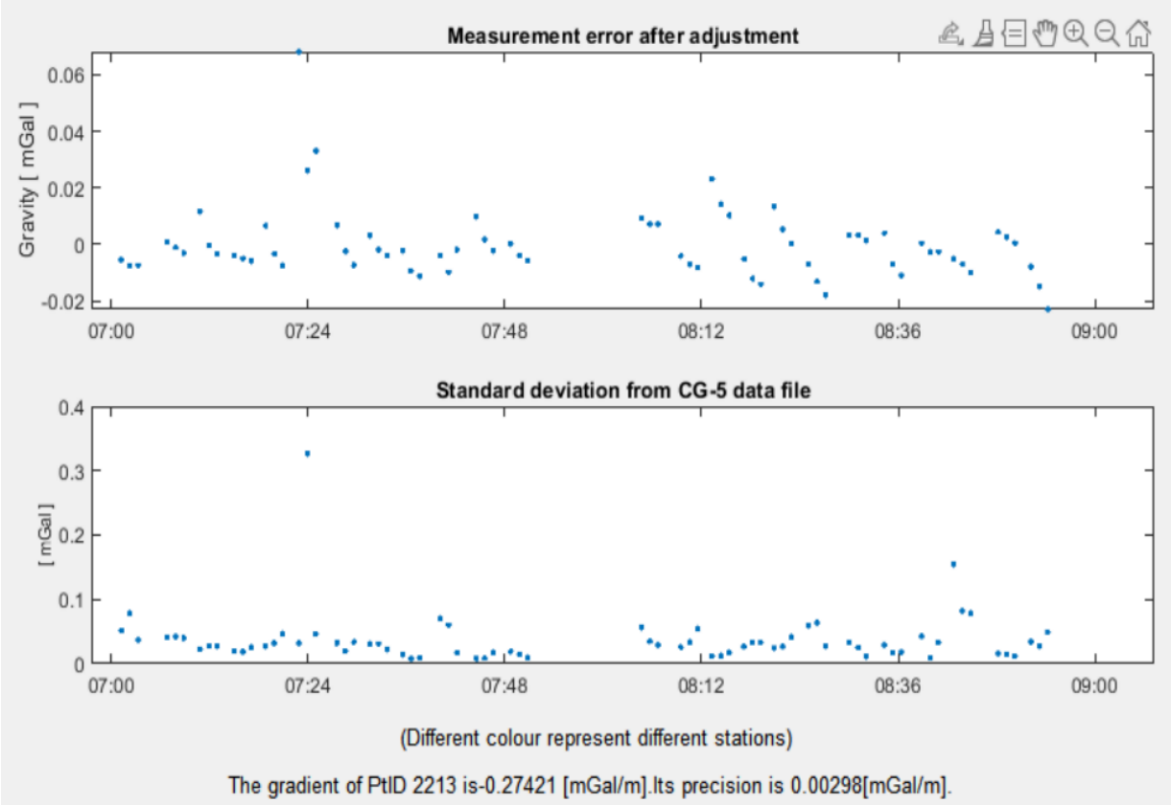

Figure 10. Gravity gradient determined over point 2213 – lower pair.

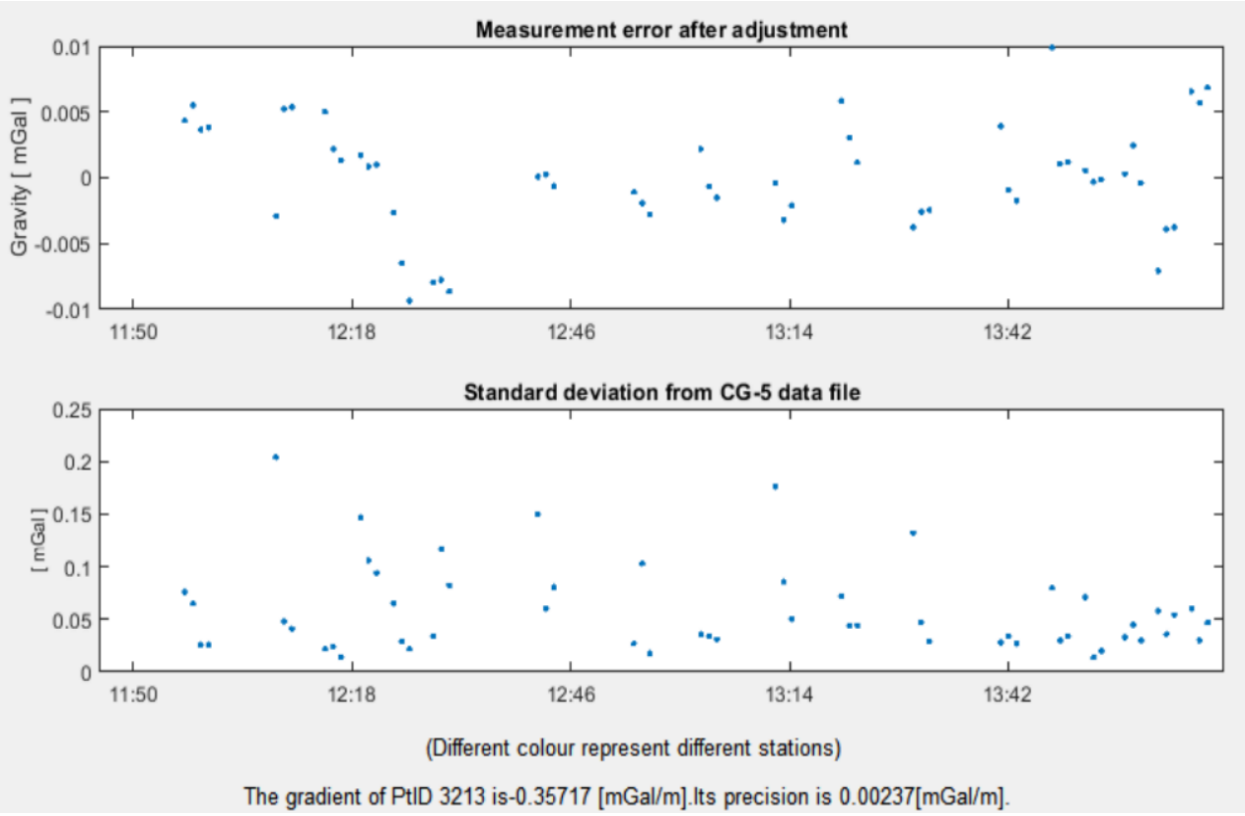

Figure 11. Gravity gradient determined over point 3213 – lower pair.

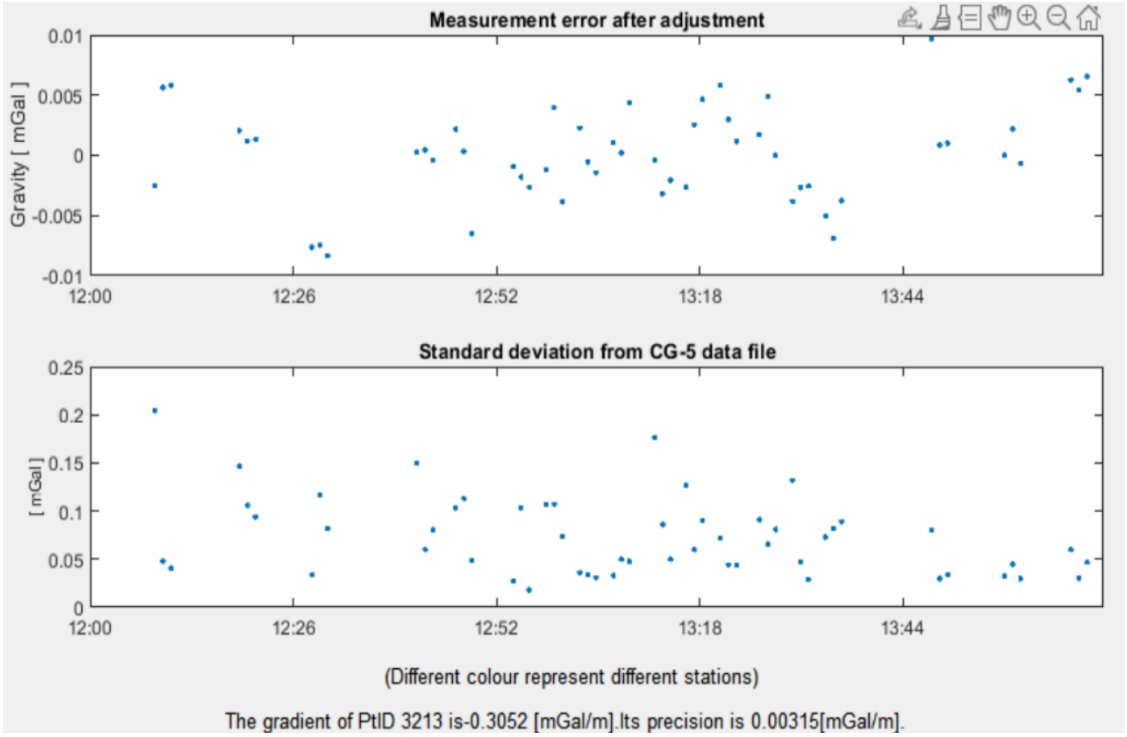

Figure 12. Gravity gradient determined over point 3213 – upper pair.

If we take a closer look to the precisions that correspond to the obtained values, which are in the range of 0.03-0.05 mGal/m, we can conclude that the actual differences between the lower and upper pairs are not reliable due to the fact that they are out of our range of detection.

Therefore, the only assumption that we can make, which is also sustained by the obtained data, is that the gravity gradient changes with the height. Actually we can see that it is decreasing with the height.

We could also argue, on a hypothetical level that in these observed values the differences occur due to the influence of the masses in between the observation points (i.e. garage, climbing tower).

6. References

[1] – Siyun, G. (2017), *A MATLAB toolbox for the Scintrex CG-5 Gravimeter at GIS.* Abschlussarbeit (Master), XI, 45, http://dx.doi.org/10.18419/opus-9162.

[2] – Blakely, R. (1995). *Potential Theory in Gravity and Magnetic Applications*. Cambridge: Cambridge University Press. doi:10.1017/CBO9780511549816.

[3] - https://www.encyclopedia.com/